PERIDYNAMICS FOR DOMAIN AGNOSTIC ANALYSIS

Erdogan Madenci

Aerospace and Mechanical Engineering

University of Arizona, Tucson AZ

The Institute of Fundamental Technological Research

Polish Academy of Sciences in Warsaw

November 21, 2022

Outline

- Peridynamics
- Peridynamic differential operator
- Multi-physics modeling
- Multi-scale modeling
- Material failure
- Solution to PDEs
- Discovery of PDEs
- Data manipulation
- Final remarks

Peridynamics

- Unifies the mechanics of continuous and discontinuous media.
- Continuum approach without spatial derivatives.
    - Removes mathematical singularities.
- Restores nonlocal interactions.
- Introduces an internal length parameter.
- Links different length scales.
- Enables autonomous damage initiation and growth.
    - Damage nucleation in unspecified locations
    - Damage propagation along unguided paths
    - Emergence of multiple damage sites and their complex interactions

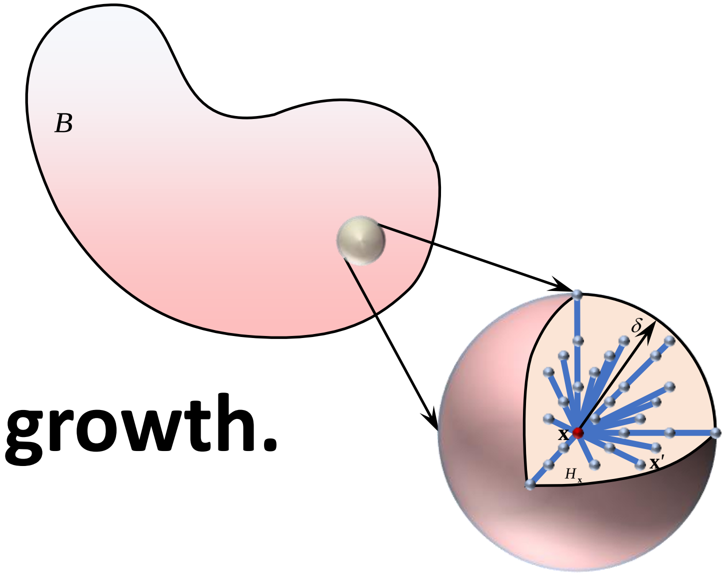

Silling S. A., 2000, “Reformulation of elasticity theory for discontinuities and long-range forces,” JMPS, 48:175-209.
Silling et al. , 2007, “Peridynamics states and constitutive modeling,” J. Elasticity, 88:151-184.

Peridynamic differential operator

- Enables differentiation through integration.

$$\frac{\partial^{p_1+p_2+\cdots+p_M} f(\mathbf{x})}{\partial x_1^{p_1} \partial x_2^{p_2} \cdots \partial x_M^{p_M}} = \int_{H_{\mathbf{x}}} f(\mathbf{x}+\boldsymbol{\xi})\, g_N^{p_1 p_2 \cdots p_M}(\boldsymbol{\xi}) d\xi_1 d\xi_2 \cdots d\xi_M$$

$$p_1 + p_2 + \cdots + p_M \leq N$$

Peridynamic functions

  - M variables and Nth order
  - Mathematically it never blows up – always valid.
- PDDO provides nonlocal form of local differential equations in space and time.

Madenci et al. , 2016, Peridynamic differential operator and its applications, CMAME, 304:408–451

Peridynamic functions

- Orthogonal to each term in Taylor Series Expansion except for the term involving the desired derivative.

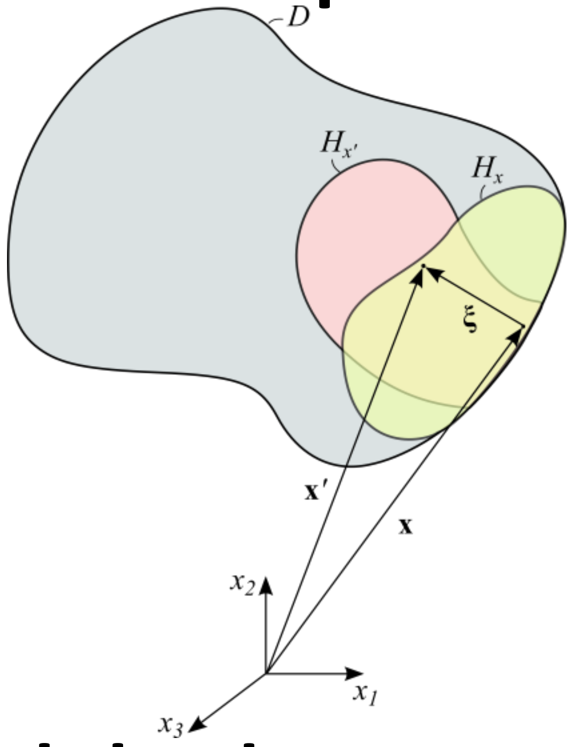

Orthogonality condition

$$\int_{H_{\mathbf{x}}} \xi_1^{n_1}\xi_2^{n_2}\cdots\xi_M^{n_N}\; g_N^{p_1p_2\cdots p_N}(\boldsymbol{\xi})dV_{\mathbf{x}'} = n_1!n_2!\cdots n_N!\;\delta_{n_1p_1}\delta_{n_2p_2}\cdots\delta_{n_{N-1}p_{N-1}}\delta_{n_Np_N}$$

- Although arbitrary in form, complete polynomials lead to analytical expressions.

Madenci et al. , 2016, Peridynamic differential operator and its applications, CMAME, 304:408–451

PDDO for 2D analysis

Taylor series expansion

$$f(\mathbf{x}+\boldsymbol{\xi}) = f(\mathbf{x}) + \xi_1 \frac{\partial f(\mathbf{x})}{\partial x_1} + \xi_2 \frac{\partial f(\mathbf{x})}{\partial x_2} + \frac{1}{2!}\xi_1^2 \frac{\partial^2 f(\mathbf{x})}{\partial x_1^2} + \frac{1}{2!}\xi_2^2 \frac{\partial^2 f(\mathbf{x})}{\partial x_2^2} + \xi_1 \xi_2 \frac{\partial^2 f(\mathbf{x})}{\partial x_1 \partial x_2} + R(2,\mathbf{x})$$

Multiply each term with PD functions and integrate over family

$$\int_{H_{\mathbf{x}}} f(\mathbf{x}+\boldsymbol{\xi})\, g_2^{p_1 p_2}(\boldsymbol{\xi}) dV_{\mathbf{x}'} = f(\mathbf{x}) \int_{H_{\mathbf{x}}} g_2^{p_1 p_2}(\boldsymbol{\xi}) dV_{\mathbf{x}'} + \frac{\partial f(\mathbf{x})}{\partial x_1} \int_{H_{\mathbf{x}}} \xi_1\, g_2^{p_1 p_2}(\boldsymbol{\xi}) dV_{\mathbf{x}'} + \frac{\partial f(\mathbf{x})}{\partial x_2} \int_{H_{\mathbf{x}}} \xi_2\, g_2^{p_1 p_2}(\boldsymbol{\xi}) dV_{\mathbf{x}'}$$
$$+ \frac{\partial^2 f(\mathbf{x})}{\partial x_1^2} \int_{H_{\mathbf{x}}} \frac{1}{2!}\xi_1^2\, g_2^{p_1 p_2}(\boldsymbol{\xi}) dV_{\mathbf{x}'} + \frac{\partial^2 f(\mathbf{x})}{\partial x_2^2} \int_{H_{\mathbf{x}}} \frac{1}{2!}\xi_2^2\, g_2^{p_1 p_2}(\boldsymbol{\xi}) dV_{\mathbf{x}'} + \frac{\partial^2 f(\mathbf{x})}{\partial x_1 \partial x_2} \int_{H_{\mathbf{x}}} \xi_1 \xi_2\, g_2^{p_1 p_2}(\boldsymbol{\xi}) dV_{\mathbf{x}'}$$

Orthogonality condition

$$\frac{1}{n_1! n_2!} \int_{H_{\mathbf{x}}} \xi_1^{n_1} \xi_2^{n_2}\, g_2^{p_1 p_2}(\boldsymbol{\xi}) dA_{\mathbf{x}'} = \delta_{n_1 p_1} \delta_{n_2 p_2} \qquad n_1, n_2, p_1, p_2 = 0,1,2$$

$$\frac{\partial^{p_1+p_2} f(\mathbf{x})}{\partial x_1^{p_1} \partial x_2^{p_2}} = \int_{H_{\mathbf{x}}} f(\mathbf{x}+\boldsymbol{\xi})\, g_2^{p_1 p_2}(\boldsymbol{\xi})\, dV_{\mathbf{x}'} \quad \text{for } p_1 + p_2 \le 2$$

PD derivatives

Madenci et al. , 2016, Peridynamic differential operator and its applications, CMAME, 304:408–451

PD functions

$$g_2^{p_1 p_2}(\boldsymbol{\xi}) = a_{10}^{p_1 p_2}\, w_1(|\boldsymbol{\xi}|)\xi_1 + a_{01}^{p_1 p_2}\, w_1(|\boldsymbol{\xi}|)\xi_2 + a_{20}^{p_1 p_2}\, w_2(|\boldsymbol{\xi}|)\xi_1^2 + a_{02}^{p_1 p_2}\, w_2(|\boldsymbol{\xi}|)\xi_2^2 + a_{11}^{p_1 p_2}\, w_2(|\boldsymbol{\xi}|)\xi_1\, \xi_2$$

Degree of interactions

$$w_1(|\boldsymbol{\xi}|) = w_2(|\boldsymbol{\xi}|)$$

Orthogonality condition

$$\mathbf{Aa} = \mathbf{b}$$

$$\mathbf{A} = \int_{H_{\mathbf{x}}} w(|\boldsymbol{\xi}|) \begin{bmatrix} 1 & \xi_1 & \xi_2 & \xi_1^2 & \xi_2^2 & \xi_1\xi_2 \\ \xi_1 & \xi_1^2 & \xi_1\xi_2 & \xi_1^3 & \xi_1\xi_2^2 & \xi_1^2\xi_2 \\ \xi_2 & \xi_1\xi_2 & \xi_2^2 & \xi_1^2\xi_2 & \xi_2^3 & \xi_1\xi_2^2 \\ \xi_1^2 & \xi_1^3 & \xi_1^2\xi_2 & \xi_1^4 & \xi_1^2\xi_2^2 & \xi_1^3\xi_2 \\ \xi_2^2 & \xi_1\xi_2^2 & \xi_2^3 & \xi_1^2\xi_2^2 & \xi_2^4 & \xi_1\xi_2^3 \\ \xi_1\xi_2 & \xi_1^2\xi_2 & \xi_1\xi_2^2 & \xi_1^3\xi_2 & \xi_1\xi_2^3 & \xi_1^2\xi_2^2 \end{bmatrix} dV_{\mathbf{x}'}$$

$$\mathbf{a} = \begin{bmatrix} a_{00}^{00} & a_{00}^{10} & a_{00}^{01} & a_{00}^{20} & a_{00}^{02} & a_{00}^{11} \\ a_{10}^{00} & a_{10}^{10} & a_{10}^{01} & a_{10}^{20} & a_{10}^{02} & a_{10}^{11} \\ a_{01}^{00} & a_{01}^{10} & a_{01}^{01} & a_{01}^{20} & a_{01}^{02} & a_{01}^{11} \\ a_{20}^{00} & a_{20}^{10} & a_{20}^{01} & a_{20}^{20} & a_{20}^{02} & a_{20}^{11} \\ a_{02}^{00} & a_{02}^{10} & a_{02}^{01} & a_{02}^{20} & a_{02}^{02} & a_{02}^{11} \\ a_{11}^{00} & a_{11}^{10} & a_{11}^{01} & a_{11}^{20} & a_{11}^{02} & a_{11}^{11} \end{bmatrix}$$

$$\mathbf{b} = \begin{bmatrix} 1 & 0 & 0 & 0 & 0 & 0 \\ 0 & 1 & 0 & 0 & 0 & 0 \\ 0 & 0 & 1 & 0 & 0 & 0 \\ 0 & 0 & 0 & 2 & 0 & 0 \\ 0 & 0 & 0 & 0 & 2 & 0 \\ 0 & 0 & 0 & 0 & 0 & 1 \end{bmatrix}$$

Shape matrix

Coef. of PD functions

Madenci et al. , 2016, Peridynamic differential operator and its applications, CMAME, 304:408–451

PD discretization

The family is nonsymmetric near the boundaries

PD discretization in 1D

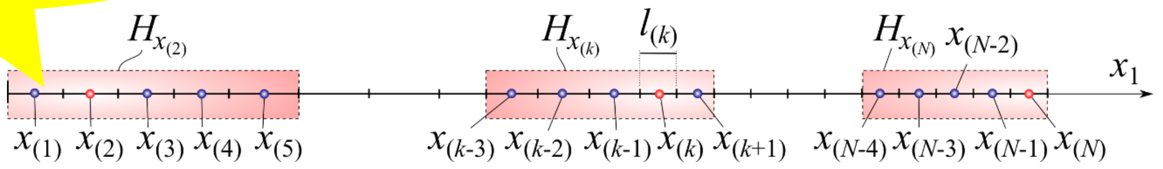

PD discretization of domain

The family is nonsymmetric near the boundaries

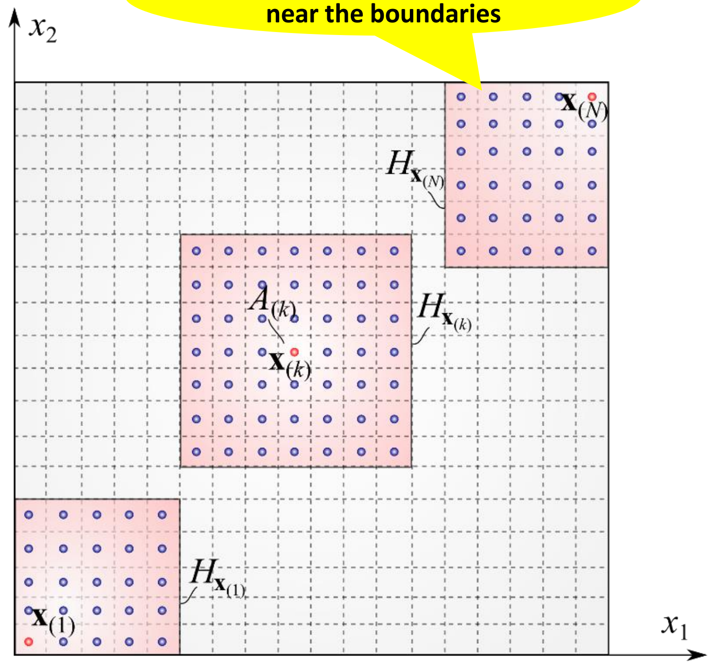

PD discretization of space-time domain

The family is always nonsymmetric

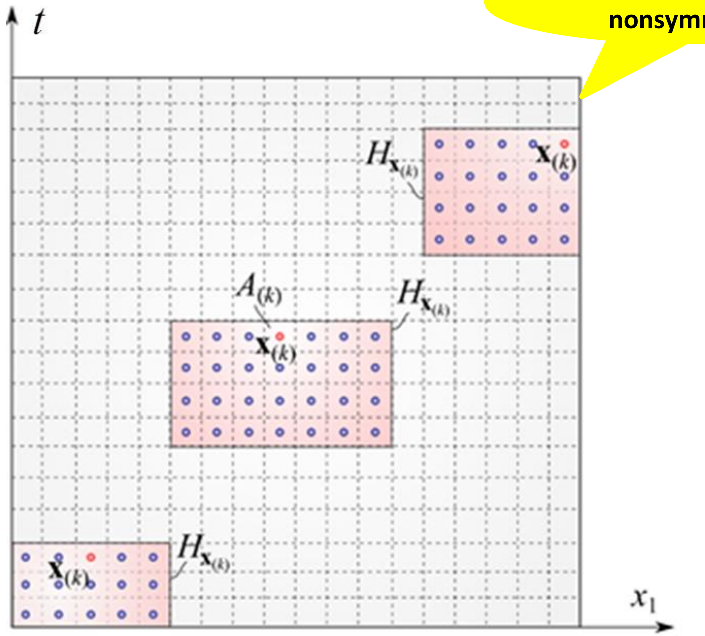

Numerical implementation

$$\left(\frac{\partial^2}{\partial x_1^2}+\frac{\partial^2}{\partial x_2^2}\right)\Phi(x_1,x_2)=Q(x_1,x_2)\ \text{ with } 0\le x_1\le \ell_1,\ 0\le x_2\le \ell_2$$

$$\frac{\partial}{\partial x_1}\Phi\left(x_1=0,x_2\right)=p(x_2),\ \frac{\partial}{\partial x_1}\Phi\left(x_1=\ell_1,x_2\right)=q(x_2)$$

$$\Phi\left(x_1,x_2=0\right)=r(x_1),\ \Phi\left(x_1,x_2=\ell_2\right)=s(x_1)$$

$$\sum_j\left[g_2^{20}(x_{1(j)}-x_{1(k)},x_{2(j)}-x_{2(k)})+g_2^{02}(x_{1(j)}-x_{1(k)},x_{2(j)}-x_{2(k)})\right]A_{(j)}\Phi(x_{1(j)},x_{2(j)})=Q(x_{1(k)},x_{2(k)})$$

$$\sum_{j=1}\Phi(x_{1(j)},x_{2(j)})\,g_2^{10}(x_{1(j)}-x_{1(k)},x_{2(j)}-x_{2(k)})A_{(j)}=p(x_{2(k)})\ \text{ for }\ x_{1(k)}=0+\Delta x_1/2\ ,$$

$$\sum_{j=1}\Phi(x_{1(j)},x_{2(j)})\,g_2^{10}(x_{1(j)}-x_{1(k)},x_{2(j)}-x_{2(k)})A_{(j)}=q(x_{2(k)})\ \text{ for }\ x_{1(k)}=\ell_1-\Delta x_1/2\ ,$$

$$\sum_{j=1}\Phi(x_{1(j)},x_{2(j)})\,g_2^{00}(x_{1(j)}-x_{1(k)},x_{2(j)}-x_{2(k)})A_{(j)}=r(x_{1(k)})\ \text{ for }\ x_{2(k)}=0+\Delta x_2/2\ ,$$

$$\sum_{j=1}\Phi(x_{1(j)},x_{2(j)})\,g_2^{00}(x_{1(j)}-x_{1(k)},x_{2(j)}-x_{2(k)})A_{(j)}=s(x_{1(k)})\ \text{ for }\ x_{2(k)}=\ell_2-\Delta x_2/2.$$

$$\begin{bmatrix}\mathbf{L} & \mathbf{c}^T\\ \mathbf{c} & \mathbf{0}\end{bmatrix}\begin{Bmatrix}\mathbf{u}\\ \boldsymbol{\lambda}\end{Bmatrix}=\begin{Bmatrix}\mathbf{b}\\ \mathbf{d}\end{Bmatrix}$$

Convergence

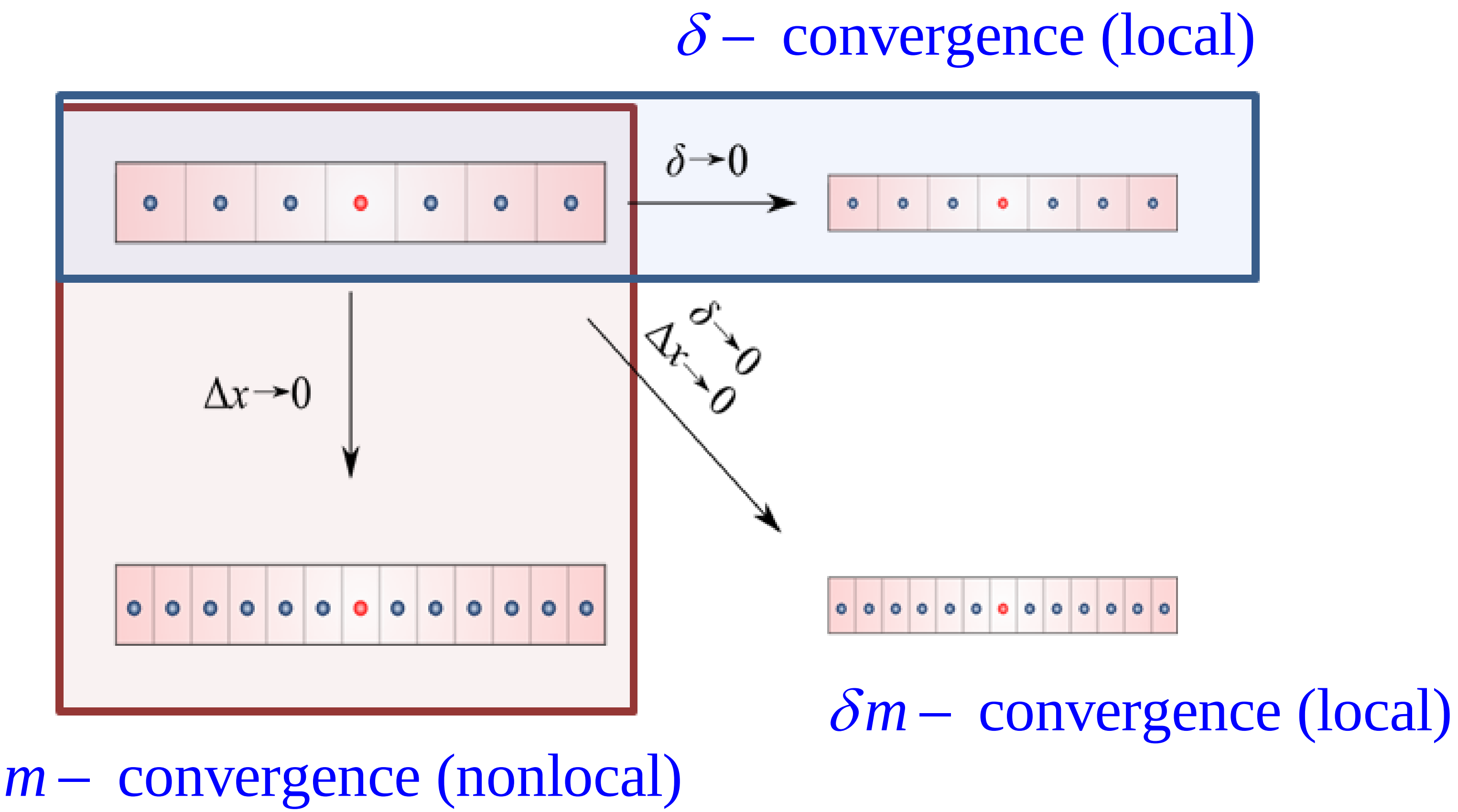

Bobaru etal., 2009, Convergence, adaptive refinement, and scaling in 1D peridynamics. IJNME, 77, 852–877.

Numerical error

$$e = e(\delta, m, \Delta x, w, R, N, Q)$$

- N is dictated by the highest order of differentiation
- Interaction domain (number of family members)

$$\left.\begin{array}{l} \delta = m\Delta x \\ N \leq m \leq N+2 \end{array}\right\} \Rightarrow \delta = (N+1)\Delta x$$

- Weight function, $w(\xi) = e^{-(2\xi/\delta)^2}$
- Integration error, Q
- Remainder error, R

Differentiation of a step function

$$u(x) = H(x - x_0) \text{ with } x_0 = 0$$
$$\text{in } -0.05 \le x \le 0.05$$

$$\frac{du}{dx} = \sum_{j=1} u(x)\left[g_2^1(x_{(j)} - x_{(k)}) \right] \ell_{(j)}$$

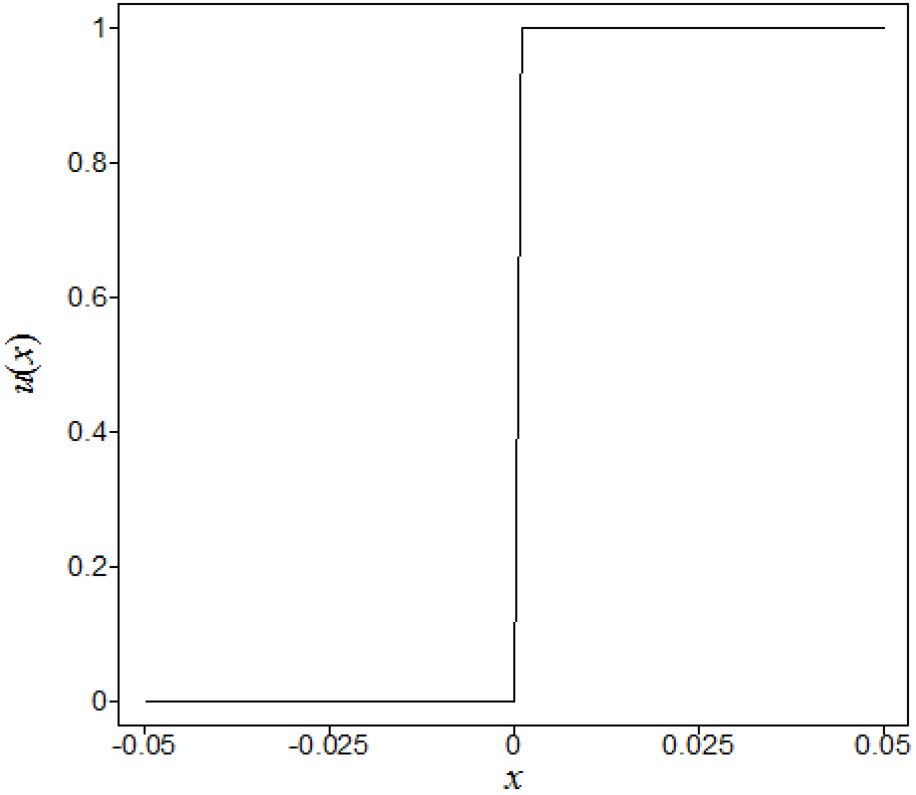

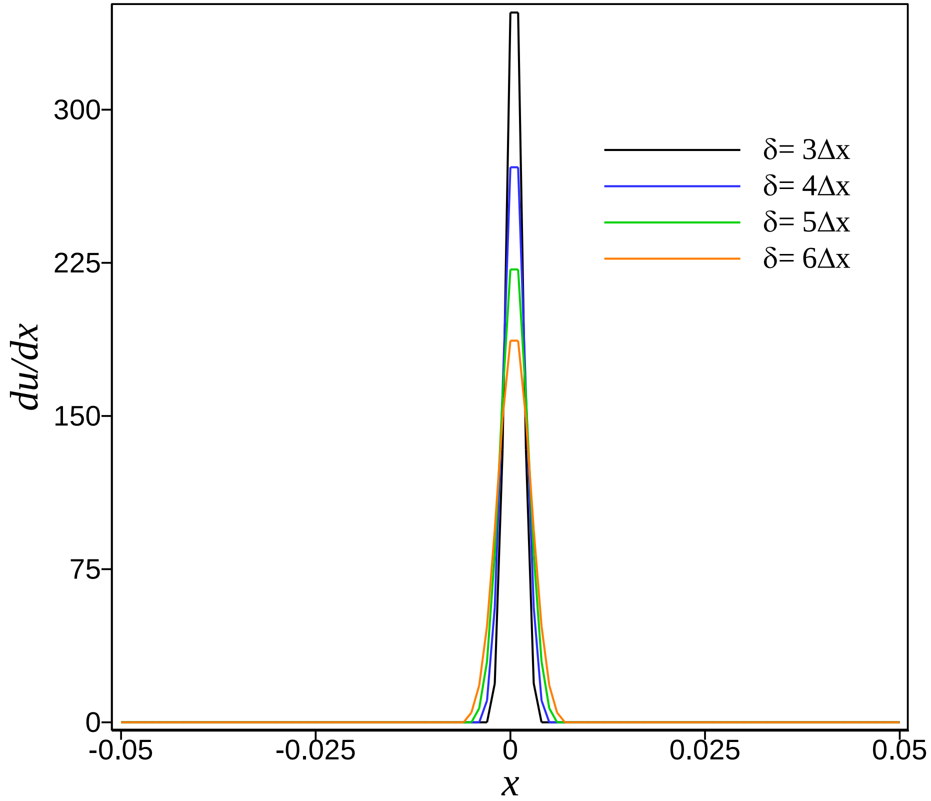

Differentiation of discrete data

$$f(x_{1(k)}, x_{2(k)}) = \left(2 - (2x_{1(k)} - 1)^2\right)^2 \sin(4x_{2(k)})$$

$$\frac{\partial^{p_1+p_2}}{\partial x^{p_1} \partial y^{p_2}} f(x_{1(k)}, x_{2(k)}) = \sum_{j=1} f(x_{1(j)}, x_{2(j)}) g_4^{p_1 p_2}\left((x_{1(j)} - x_{1(k)}), (x_{2(j)} - x_{2(k)})\right) A_{(j)}$$

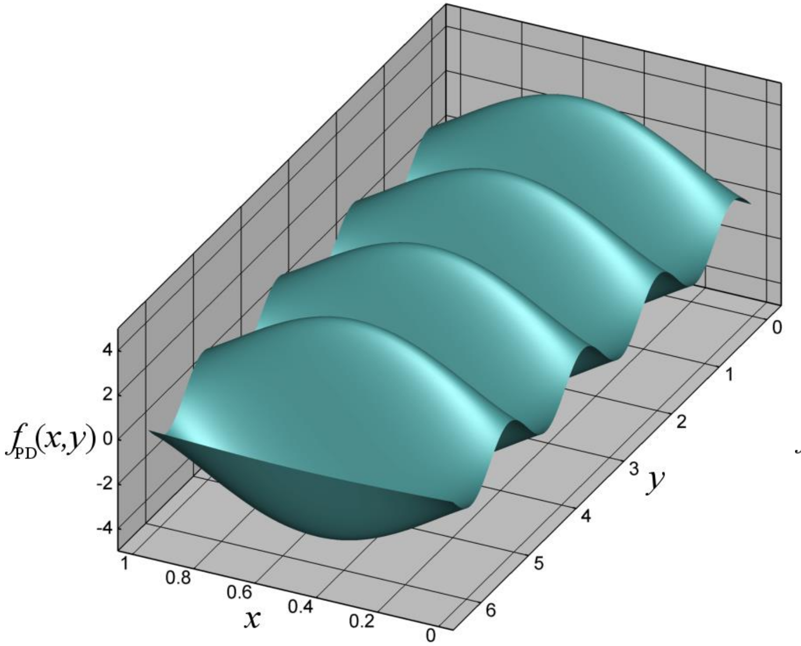

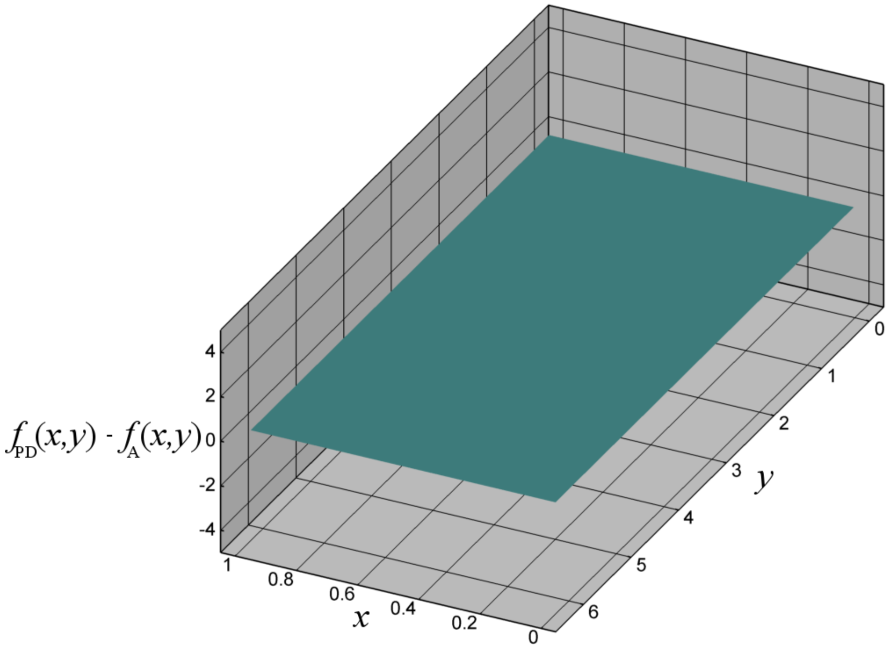

Nakamura et al. , 2008. Numerical differentiation for the second order derivative of functions with several variables, J. of Comp. and App. Math., http://www. researchgate.net/publication/228972292

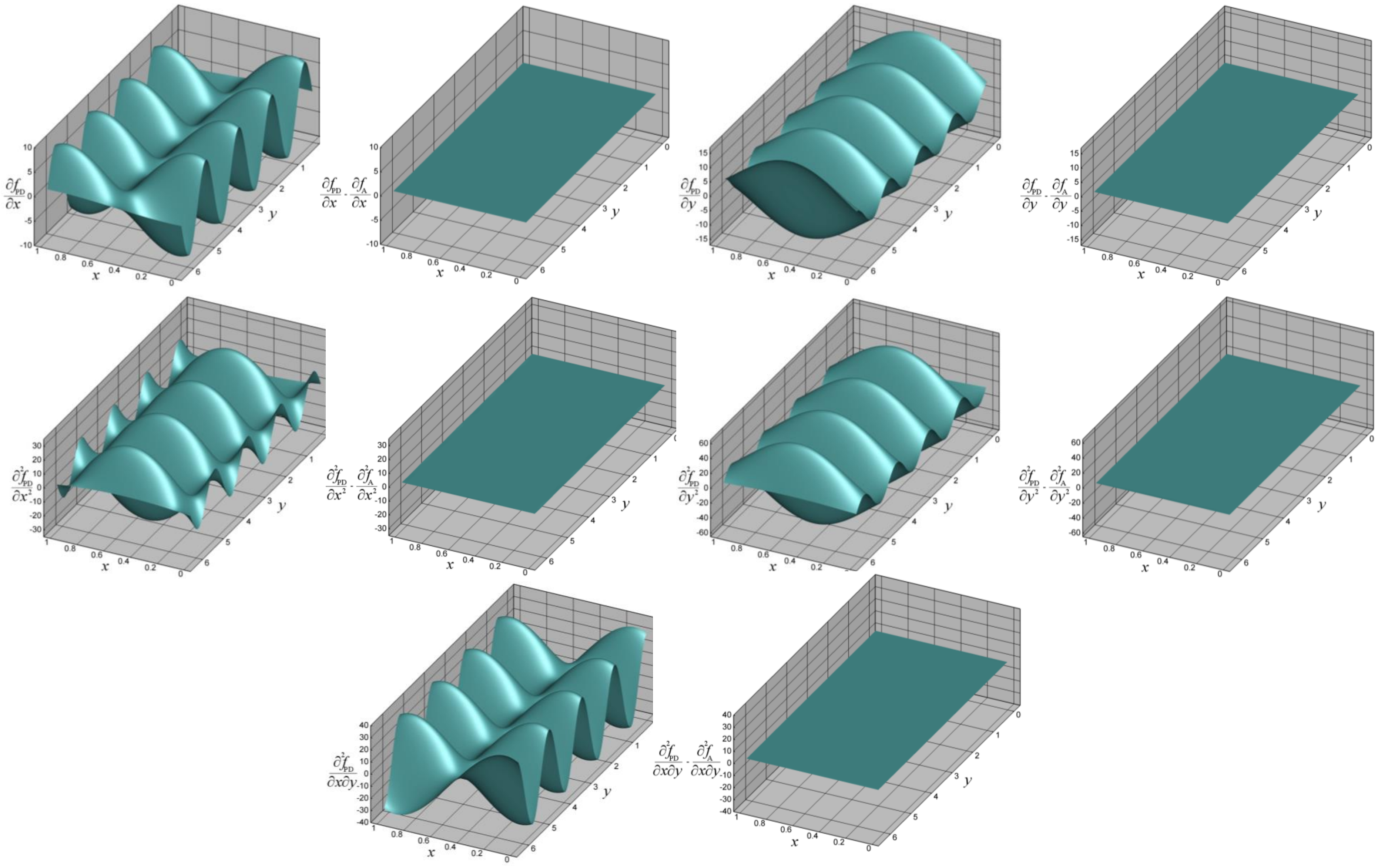

Madenci et al., 2016, Peridynamic differential operator and its applications, CMAME, 304 : 408–451

PD Failure/damage

When the elastic bond stretch reaches its critical value, bond breakage occurs

$$\hat{\mu}(\mathbf{x},\mathbf{x}',t)=\begin{cases}1, & s(\mathbf{x},\mathbf{x}',t)<s_c\\ 0, & s(\mathbf{x},\mathbf{x}',t)\geq s_c\end{cases}$$

$$s_c=\sqrt{\frac{G_{IC}}{3\mu\delta}}$$

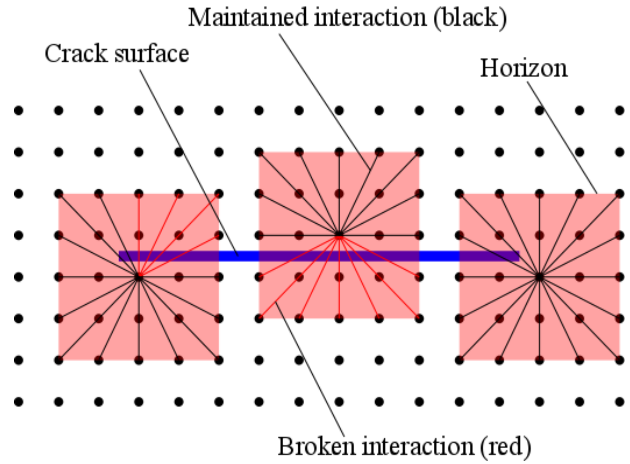

$$\phi(\mathbf{x},t)=1-\frac{\int_{H_{\mathbf{x}}}\hat{\mu}(\mathbf{x},\mathbf{x}',t)dV_{\mathbf{x}'}}{\int_{H_{\mathbf{x}}}dV_{\mathbf{x}'}}$$

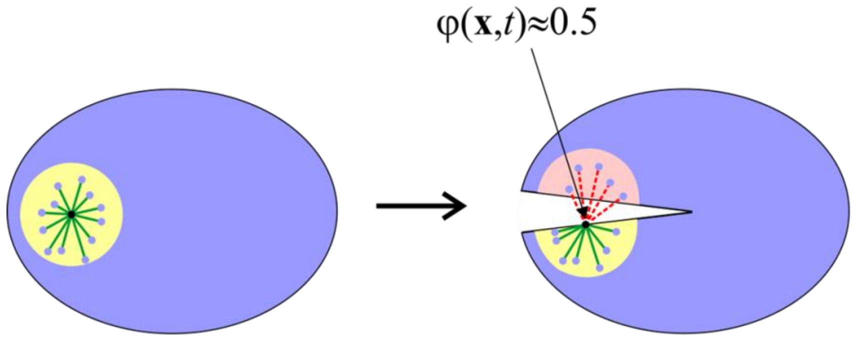

Local damage is the ratio of number of broken bonds to total number of bonds

Silling, S. and Askari, E.,2005, A Meshfree Method Based on the Peridynamic Model of Solid Mechanics," Computers and Struct., 83, 1526-1535.

Multi-physics modeling

- Cracking in charring materials during ablation
- Corrosion
- Electrodeposition
- Electromigration
- Fuel pellet cracking

Charring Process

- Heat conduction in TPS
  - Internal decomposition of material
  - Decomposition of material to char
  - Formation of pyrolysis gas
  - Gases in the boundary react with char
  - Surface recession- chemical reactions, erosion and combustion

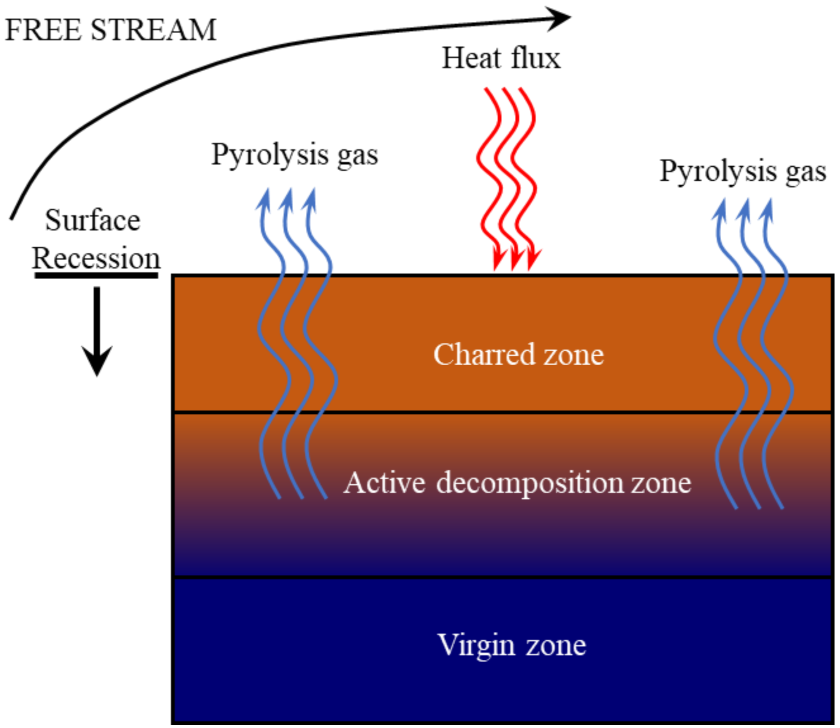

Virgin material decomposes to char. Char at surface has better insulation properties than virgin material.

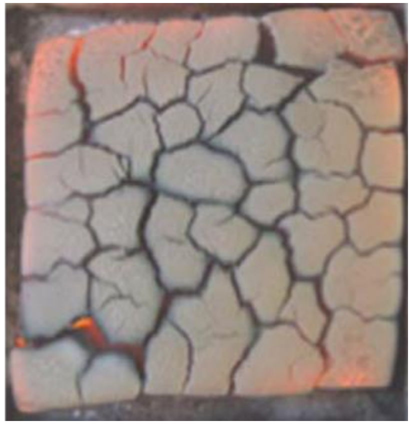

Amar, A., Calvert, N., & Kirk, B. (2011, January). Development and verification of the charring ablating thermal protection implicit system solver. In 49th AIAA Aerospace Sciences Meeting including the New Horizons Forum and Aerospace Exposition (p. 144).

Governing equations for ablation

- Conservation of mass
  - Equation for decomposition
- Conservation of energy
  - PD form of nonlinear heat equation with surface recession
- Conservation of linear momentum
  - Peridynamic equilibrium equation with shrinkage and expansion

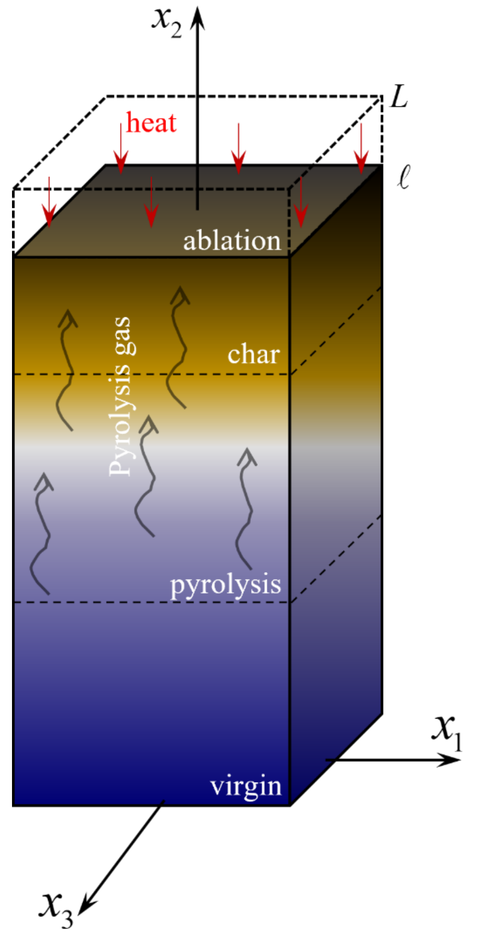

Decomposition of material

- **Virgin material decomposes to char and releases pyrolysis gas upon combustion due to heating**

Virgin material $\longrightarrow$ **Char + pyrolysis gas**

- **Density of decomposed components governed through Arrhenius law**

A: **pre- exponential factor**
r: **order of reaction**
R: **universal gas constant**
E: **activation energy**

$$\dot{\rho}(\mathbf{x},t) = -A\rho_v \left(\frac{\rho(\mathbf{x},t) - \rho_c}{\rho_v} \right)^r \exp\left(-\frac{E}{RT(\mathbf{x},t)} \right)$$

Material decomposition leads to loss of mass; thus, shrinkage and degradation of material properties

PD form of nonlinear heat conduction

- **Classical equation**

$$\underbrace{\frac{\partial\big(\rho(\mathbf{x},t)h(\mathbf{x},t)\big)}{\partial t}}_{\text{Rate of energy storage}} = \underbrace{\nabla\bullet\big(k(\mathbf{x},t)\nabla T(\mathbf{x},t)\big)}_{\text{Rate of heat flux}} - \underbrace{\nabla\bullet\big(h_g(\mathbf{x},t)\dot{\mathbf{m}}_g(\mathbf{x},t)\big)}_{\text{Convection of pyrolysis gases}} - \underbrace{Q\dot{\rho}(\mathbf{x},t)}_{\text{Rate of energy consumption due to decomposition}}$$

- **PD heat equation**

$$\rho(\mathbf{x},t)C_p(\mathbf{x},t)\dot{T}(\mathbf{x},t) = k(\mathbf{x},t)\left(\frac{6}{\pi\delta^4}\int_{H_{\mathbf{x}}}\frac{T(\mathbf{x}',t)-T(\mathbf{x},t)}{|\boldsymbol{\xi}|}dV_{\mathbf{x}'}\right)$$
$$+\left(\frac{9}{4\pi\delta^3}\int_{H_{\mathbf{x}}}\frac{k(\mathbf{x}',t)-k(\mathbf{x},t)}{|\boldsymbol{\xi}|}dV_{\mathbf{x}'}\right)\left(\frac{9}{4\pi\delta^3}\int_{H_{\mathbf{x}}}\frac{T(\mathbf{x}',t)-T(\mathbf{x},t)}{|\boldsymbol{\xi}|}dV_{\mathbf{x}'}\right)$$
$$-C_{pg}(\mathbf{x},t)\big(\dot{\mathbf{m}}_g(\mathbf{x},t)\big)\bullet\left(\frac{9}{4\pi\delta^3}\int_{H_{\mathbf{x}}}\frac{T(\mathbf{x}',t)-T(\mathbf{x},t)}{|\boldsymbol{\xi}|}\mathbf{n}(\boldsymbol{\xi})dV_{\mathbf{x}'}\right)-\dot{\rho}(\mathbf{x},t)\big(Q+h(\mathbf{x},t)-h_g(t)\big)$$

The heat equation considers energy convection due pyrolysis gases and energy consumption for decomposition

Nonlinear boundary conditions

- **Classical equation**

$$\underbrace{-k(\mathbf{x},t)\left.\frac{\partial T(\mathbf{x},t)}{\partial x_2}\right|_{x_2=\ell}}_{\text{Heat flux}} = \underbrace{q(\mathbf{x},t)}_{\text{Ext. heat flux}} \underbrace{-\sigma\varepsilon\left(T_s^4(\mathbf{x},t)-T_\infty^4\right)}_{\text{Heat radiation}} \underbrace{-h_{conv}\left(T_s(\mathbf{x},t)-T_\infty\right)}_{\text{Convection}} + \underbrace{\dot{m}_{com}(\mathbf{x},t)h_{com}}_{\text{Combustion}}$$

- **Rate of mass combusted at the surface comes from rate of surface recession**

$$\dot{m}_{com}(\mathbf{x},t)=\rho_c\dot{S}(\mathbf{x},t)$$

- **PD form of BC through PD differential operator**

$$-k(\mathbf{x},t)\left.\left(\int_{H\mathbf{x}} g_2^{010}(\xi)\left(T(\mathbf{x}',t)-T(\mathbf{x},t)\right)dV_{\mathbf{x}'}\right)\right|_{x_2=\ell} = q(\mathbf{x},t)-\sigma\varepsilon\left(T_s^4(\mathbf{x},t)-T_\infty^4\right)$$
$$-h_{conv}\left(T_s(\mathbf{x},t)-T_\infty\right)+h_{com}\dot{m}_{com}(\mathbf{x},t)$$

Balance of energy entering and leaving on material boundary

Madenci et al. 2016,. "Peridynamic differential operator and its applications." , CMAME, 304:408-451.

Peridynamic equilibrium equation

- **Material response is isotropic and elastic**
  - **Deformation due to thermal expansion**
  - **Deformation due to shrinkage from mass loss**

$$\rho(\mathbf{x},t)\ddot{\mathbf{u}}(\mathbf{x},t) = \int_{H_{\mathbf{x}}} \mathbf{f}(\mathbf{u}'-\mathbf{u},\mathbf{x}'-\mathbf{x},t)\,dV_{\mathbf{x}'} + \mathbf{b}(\mathbf{x},t)$$

$$s = \frac{|\mathbf{y}'-\mathbf{y}| - |\mathbf{x}'-\mathbf{x}|}{|\mathbf{x}'-\mathbf{x}|}$$

$$\mathbf{f}(\mathbf{u}'-\mathbf{u},\mathbf{x}'-\mathbf{x},t) = c\left(s(\mathbf{x},\mathbf{x}',t) - \underbrace{\alpha_{avg}(\mathbf{x},\mathbf{x}',t)\,\Theta_{avg}(\mathbf{x},\mathbf{x}',t)}_{\text{Thermal expansion}} - \underbrace{\gamma\,\Omega_{avg}(\mathbf{x},\mathbf{x}',t)}_{\text{Shrinkage stretch}}\right)\frac{\mathbf{y}'-\mathbf{y}}{|\mathbf{y}'-\mathbf{y}|}$$

$$\mathbf{f}(\mathbf{u}'-\mathbf{u},\mathbf{x}'-\mathbf{x},t) = c\left(\left(\mathbf{n}(\xi)\otimes\mathbf{n}(\xi)\right)\frac{\mathbf{u}(\mathbf{x}',t)-\mathbf{u}(\mathbf{x},t)}{|\xi|} - \alpha_{avg}(\mathbf{x},\mathbf{x}',t)\frac{\Theta(\mathbf{x},t)\mathbf{n}(\xi)-\Theta(\mathbf{x}',t)\mathbf{n}(\xi')}{2} - \gamma\frac{\Omega(\mathbf{x},t)\mathbf{n}(\xi)-\Omega(\mathbf{x}',t)\mathbf{n}(\xi')}{2}\right)$$

- **Shrinkage from density change**

$$\Omega(\mathbf{x},t) = \frac{\left(\rho(\mathbf{x},t)-\rho_v\right)}{\rho_v}$$

Degraded material property

- **Material degrades due to ablation**
- **Virgin and char material properties can be measured**
- **Intermediate state is approximated through linear interpolation based on density change**

Thermal conductivity	$k(\mathbf{x},t)=F(\mathbf{x},t)k_v+\left(1-F(\mathbf{x},t)\right)k_c$
Specific heat	$C_p(\mathbf{x},t)=F(\mathbf{x},t)C_{pv}+\left(1-F(\mathbf{x},t)\right)C_{pc}$
Coefficient of thermal expansion	$\alpha(\mathbf{x},t)=F(\mathbf{x},t)\alpha_v+\left(1-F(\mathbf{x},t)\right)\alpha_c$
Volume fraction	$F(\mathbf{x},t)=\dfrac{\rho_v}{\rho_v-\rho_c}\left(1-\dfrac{\rho_c}{\rho(\mathbf{x},t)}\right)$

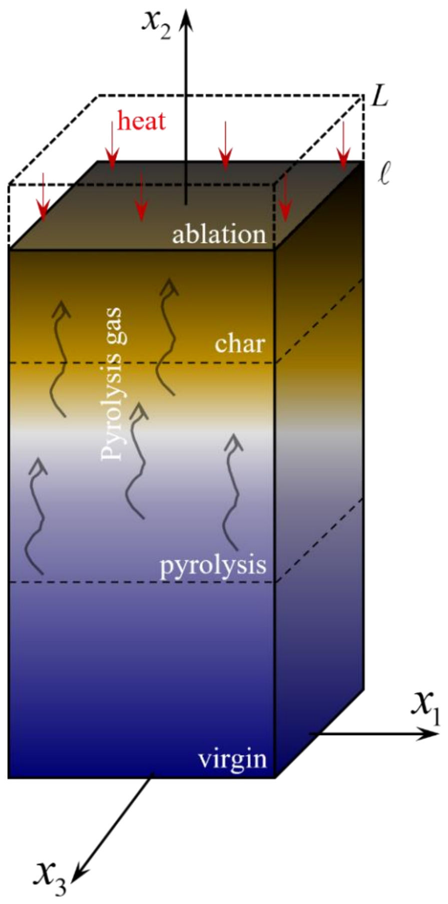

Numerical Implementation

- **3D discretization of the geometry**
- **Explicit update of loss of mass equation**

$$\rho^{n}_{(k)} = \rho^{n-1}_{(k)} + \dot{\rho}^{n-1}_{(k)}\Delta t$$

- **Explicit update for heat equation**

$$T^{n}_{(k)} = T^{n-1}_{(k)} + \dot{T}^{n-1}_{(k)}\Delta t$$

- **Adaptive dynamic relaxation for EOM**
- **Update surface recession**

$$S^{n} = S^{n-1} + \dot{S}^{n-1}\Delta t$$

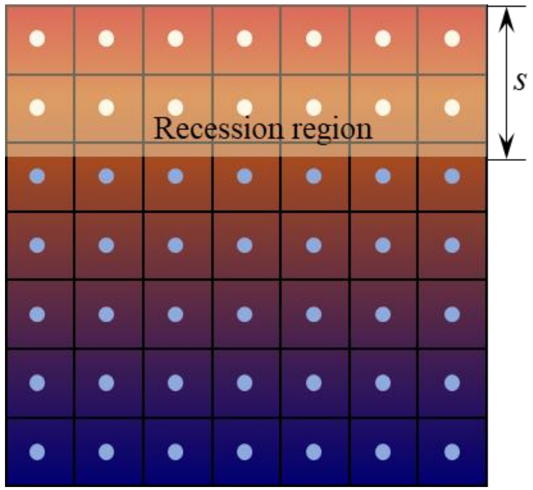

Implicit-Explicit algorithm

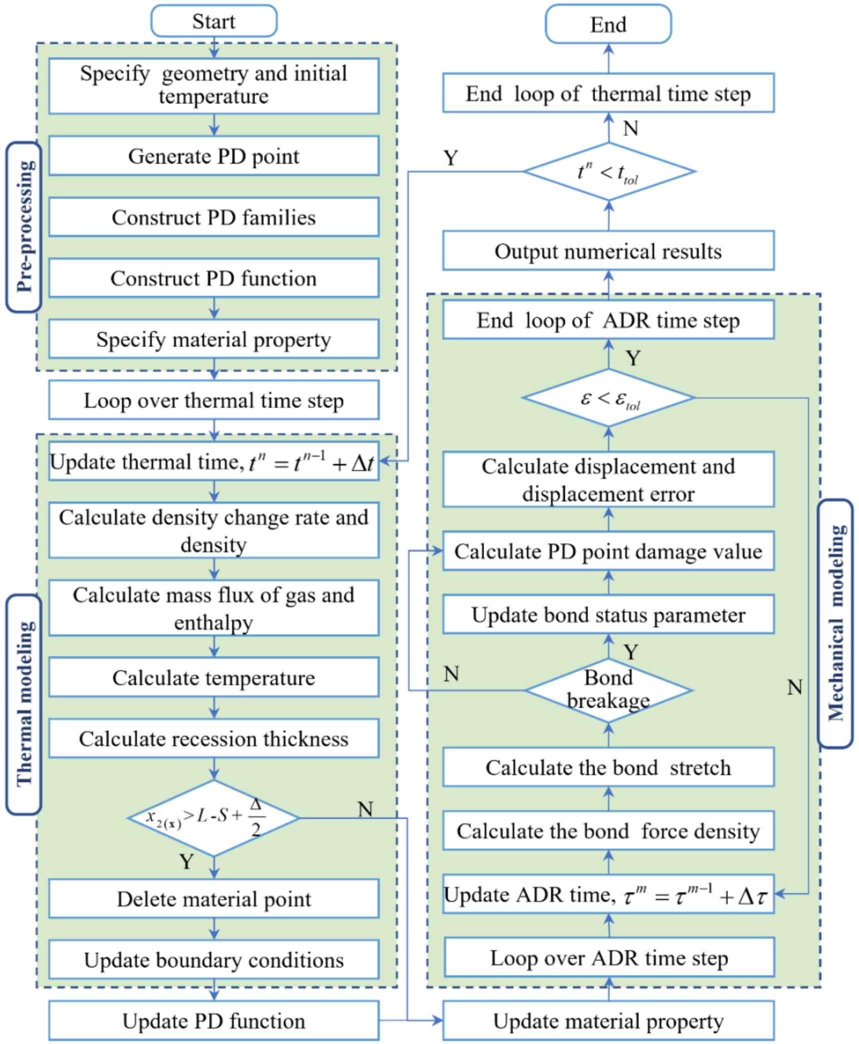

Crack propagation in 3D block

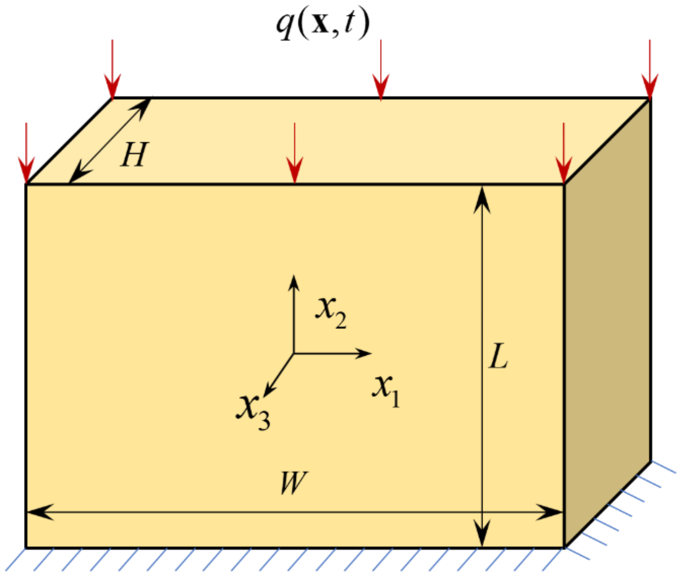

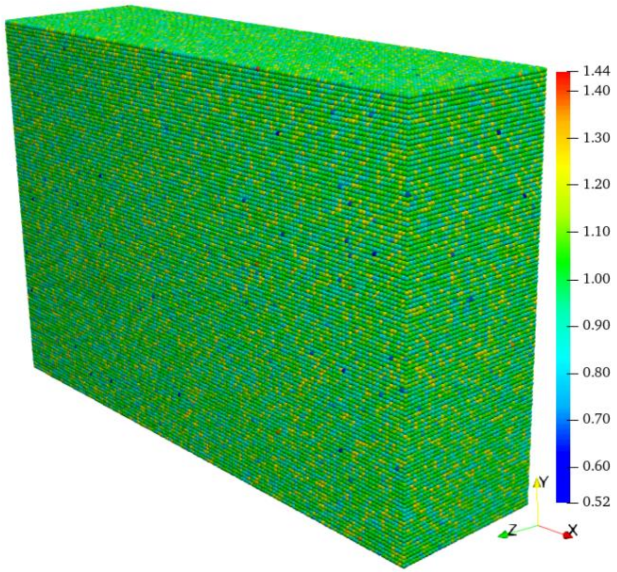

$L = 0.01\text{m} \qquad W = 0.015\text{m} \qquad H = 0.004\text{m}$

$\Delta = 1\times10^{-4}\,\text{m} \qquad \Delta t = 5\times10^{-3}\,\text{s}$

$$q(\mathbf{x},t) = \begin{cases} 279.7\text{kW/m}^2, & x_2 = L/2 \\ 0, & \text{other surfaces} \end{cases}$$

Inhomogeneity through Gaussian distribution with mean 1 and STD 0.1 for material properties

Property	Unit	Value
Fiber Young's modulus, E_f	GPa	72.4
Resin Young's modulus, E_r	GPa	6.0
Energy release rate, G_{IC}	J/m^2	400
Thermal expansion coefficient of fiber and resin, α_f, α_r	K^{-1}	8.59×10^{-5}
Char thermal expansion coefficient α_c	K^{-1}	$-7.42\times10^{-5}, \quad \rho/\rho_0 \geq 0.492$

Cracking due to expansion and shrinkage

At 5s, formation of surface crack due to expansion

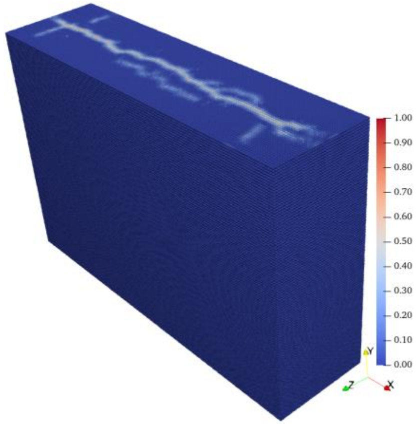

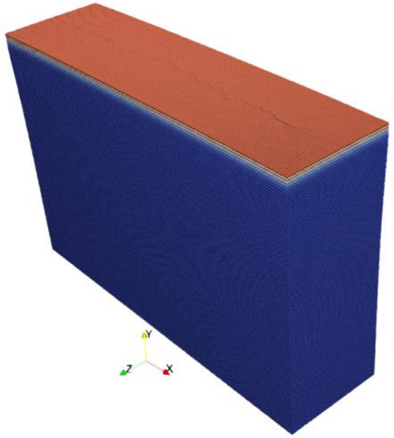

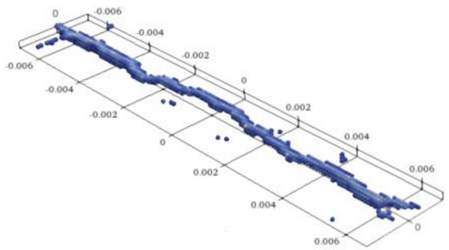

At 15 s, crack branching due to combined expansion and decomposition

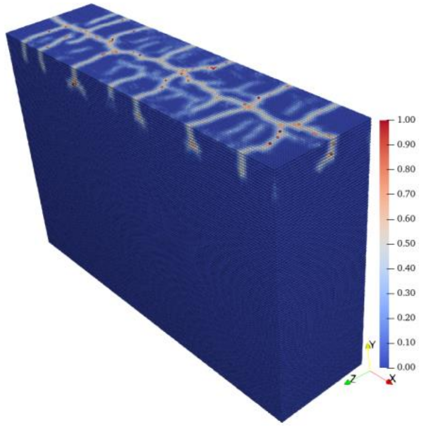

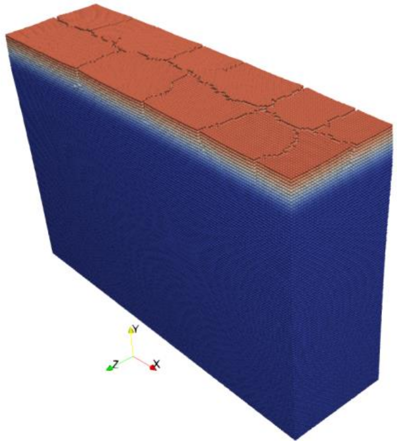

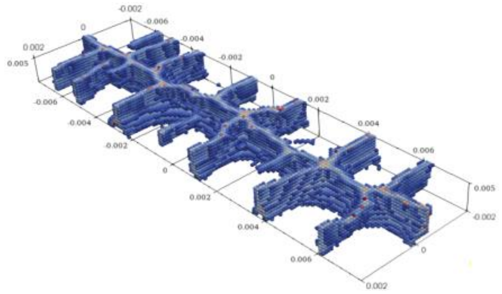

Crack propagation due to shrinkage

In-depth propagation of
crack at 50s and 85 s

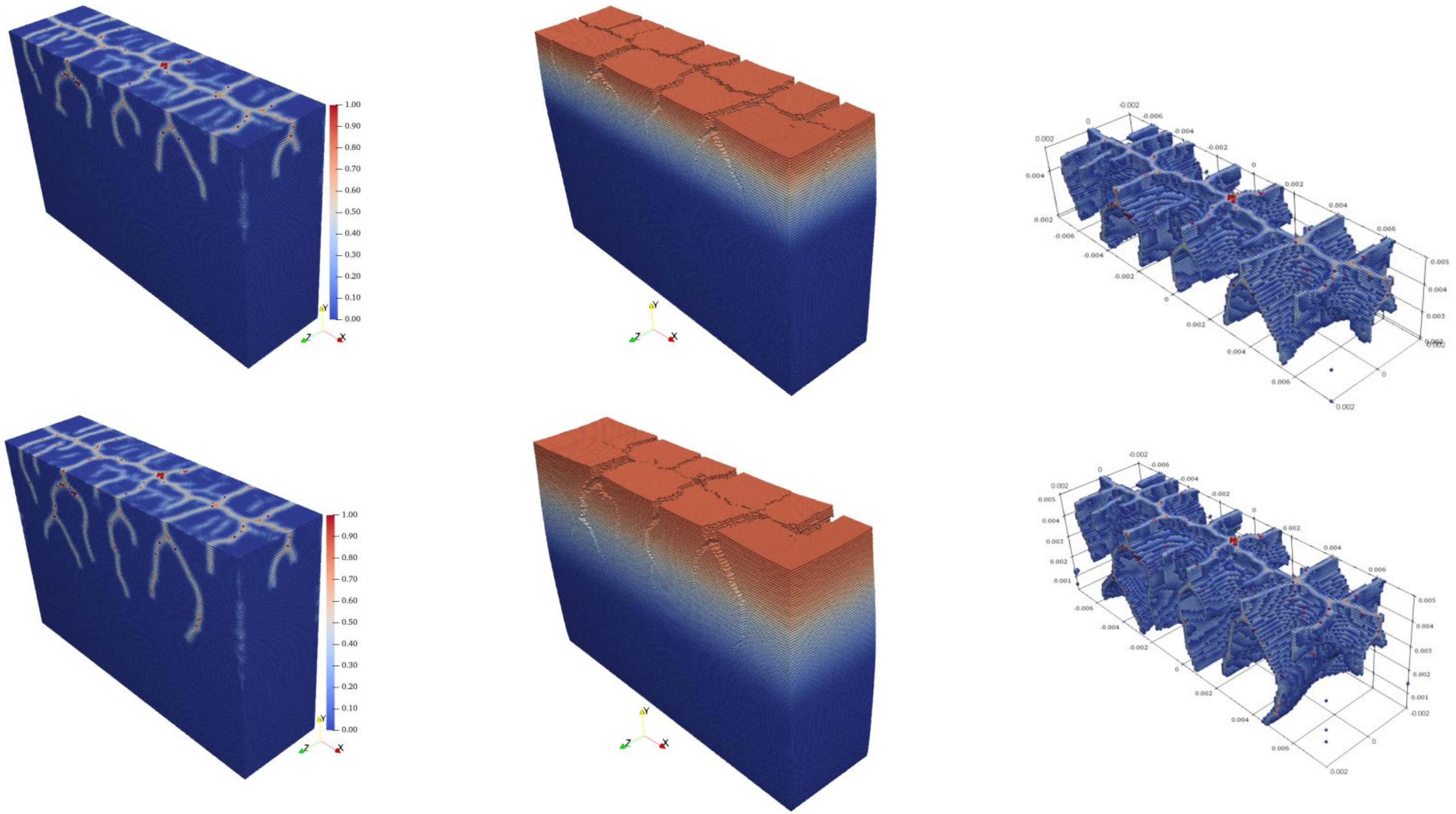

Multi-scale modeling

- Homogenization
- Micro-architected materials
- Design of cement micro-structure

Peridynamics for homogenization

Short-fiber “random” microstructure

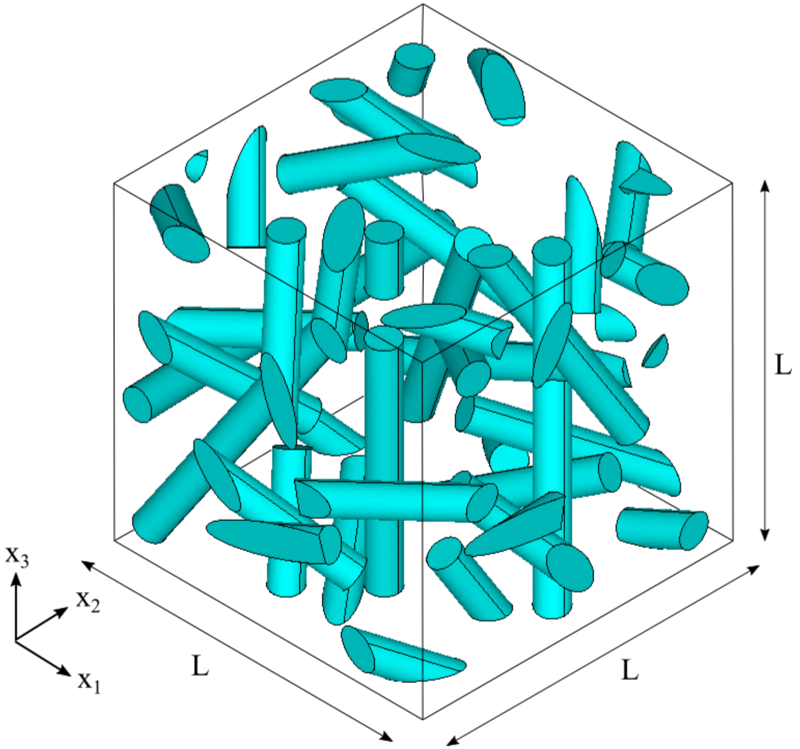

Property	Matrix	Short-fiber
$E\ (GPa)$	45	450
ν	0.18	0.17
$\alpha\ (\mu/°C)$	64.8	-0.4

Sertse et al., 2018, Challenge problems for the benchmarking of micromechanics analysis: Level I initial results, *Journal of Composite Materials*, Vol. 52, pp. 61–80

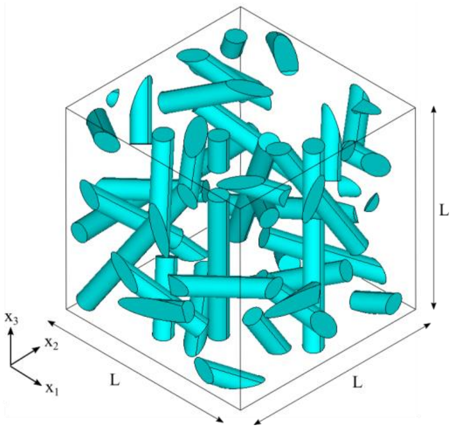

Effective elastic properties

Approach	C_{11}	C_{12}	C_{13}	C_{14}	C_{15}	C_{16}	C_{22}	C_{23}	C_{24}	C_{25}	C_{26}
GMC	52.83	11.53	11.53	0	0	0	53.08	11.53	0	0	0
DIGIMAT-MF/MT	57.15	12.82	12.83	0	0	0	57.15	12.83	0	0	0
DIGIMAT-MF/DI	57.35	12.86	12.88	0	0	0	57.35	12.88	0	0	0
Altair MDS	59.64	13.56	13.36	0.06	-0.58	0.54	61.67	13.37	0.53	-0.27	-0.14
ESI	61.65	14.03	13.85	0.08	-0.64	0.59	63.81	13.85	0.58	-0.30	-0.23
SwiftComp/3D FEA	59.60	13.66	13.47	0.05	-0.60	0.56	61.70	13.47	0.55	-0.27	-0.12
PDUC	**54.83**	**12.38**	**12.43**	**0.02**	**0**	**0**	**54.83**	**12.38**	**0.57**	**0.02**	**0**

Approach	C_{33}	C_{34}	C_{35}	C_{36}	C_{44}	C_{45}	C_{46}	C_{55}	C_{56}	C_{66}
GMC	52.86	0	0	0	20.53	0	0	20.53	0	20.53
DIGIMAT-MF/MT	57.26	0	0	0	22.18	0	0	22.18	0	21.16
DIGIMAT-MF/DI	57.46	0	0	0	22.26	0	0	22.26	0	22.24
Altair MDS	58.83	0.69	-0.09	-0.44	23.32	-0.44	-0.31	23.24	0.08	23.52
ESI	60.93	0.81	-0.06	-0.48	24.06	-0.50	-0.38	23.98	0.10	24.25
SwiftComp/ 3D FEA	58.75	0.70	-0.07	-0.45	23.24	-0.45	-0.32	23.16	0.08	23.45
PDUC	**55.24**	**0.7**	**0**	**0**	**21.35**	**0**	**0**	**22.23**	**0.09**	**22.00**

Micro-architected materials

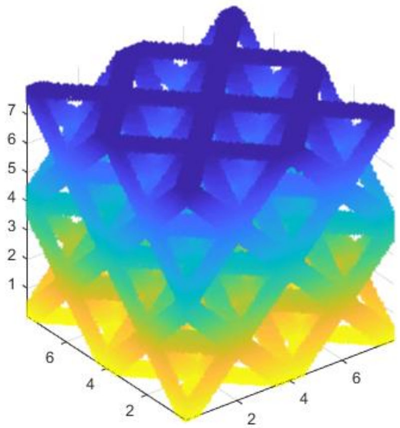

Octet

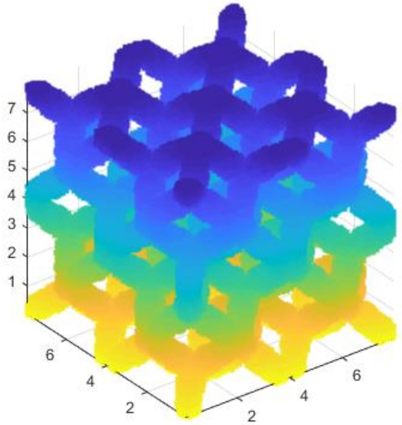

Rhombic

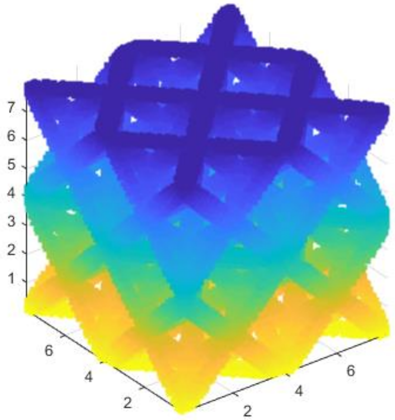

Rhoctan

(GPa)	E_{11}	E_{22}	E_{33}	G_{23}	G_{31}	G_{12}	ν_{23}	ν_{31}	ν_{12}
Octet	7.68	7.69	7.71	3.87	3.86	3.86	0.28	0.28	0.28
Rhombic	7.50	7.48	7.48	3.13	3.15	3.14	0.25	0.25	0.25
Rhoctan	8.66	8.65	8.65	2.74	2.74	2.75	0.23	0.23	0.23

Random cement micro-structures

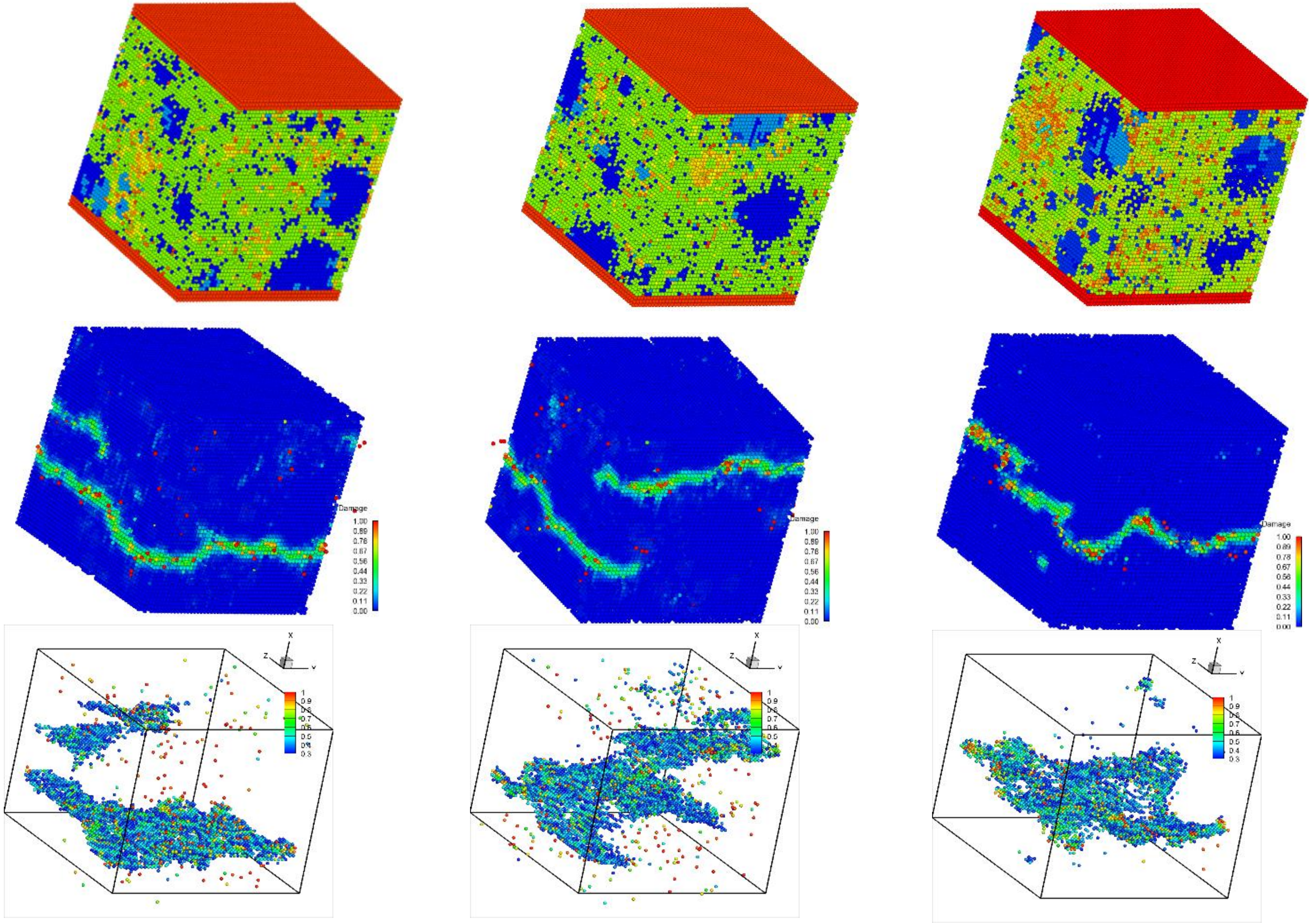

Different material phases
Dynamic loading - 0.06m/s

Final damage

Crack surface

Li et al., 2022, "Effect of water-cement ratio and size on tensile damage in hardened cement paste: Insight from peridynamic simulations," Construction and Building Materials, Vol. 356, 129256

Stress-strain response

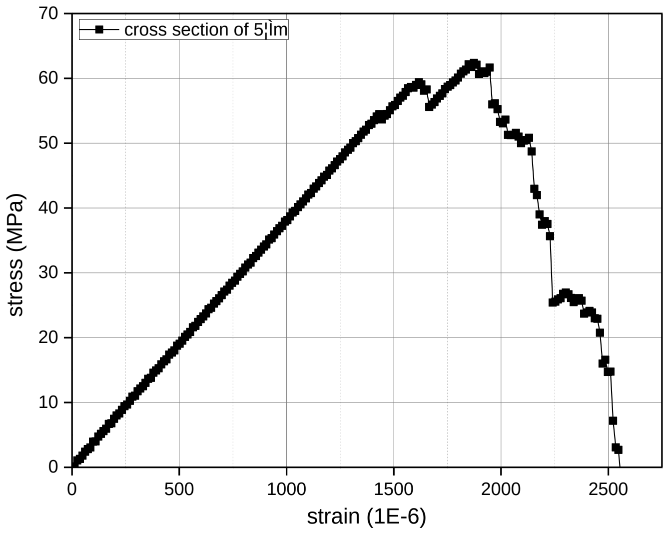

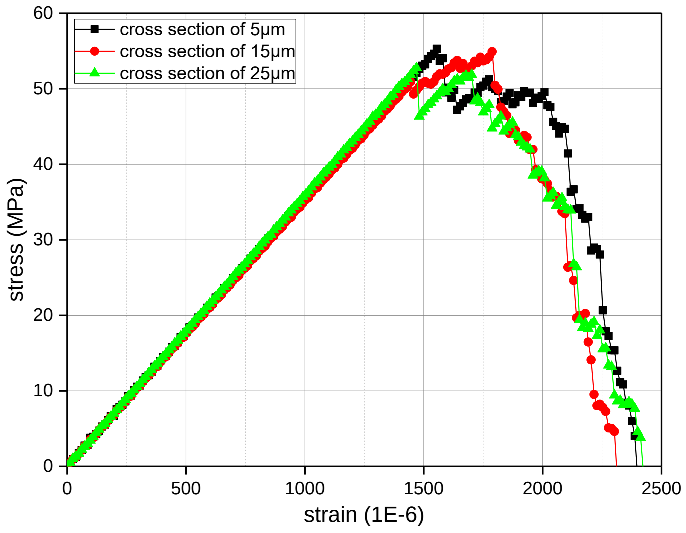

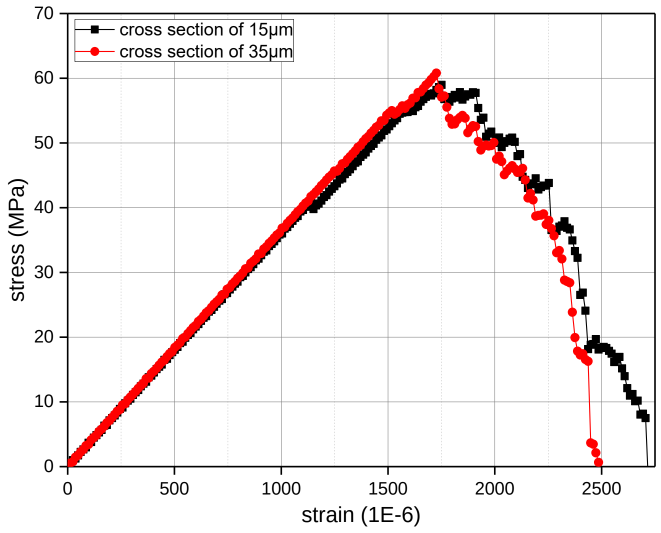

	Peak stress (MPa)	Max. strain	Young's modulus (Gpa)	Energy release rate (J/m²)
No failure	65.97	2.83E-3	39.78	5.67
Failure	58.04	2.57E-3	36.68	4.21

Li et al., 2022, "Effect of water-cement ratio and size on tensile damage in hardened cement paste: Insight from peridynamic simulations," Construction and Building Materials, Vol. 356, 129256

Material failure

- High velocity impact/penetration
- Damage due to sand impact
- Frangibility of glass
- CAI damage in composites
- Fiber steered composites
- Failure in polymers
- Fatigue life
  - Composites
  - Metals

Damage due to sand particle impact

- **Impactor kinetics**
- **Contact model**
- **Multiple damage sites**
- **Material removal**

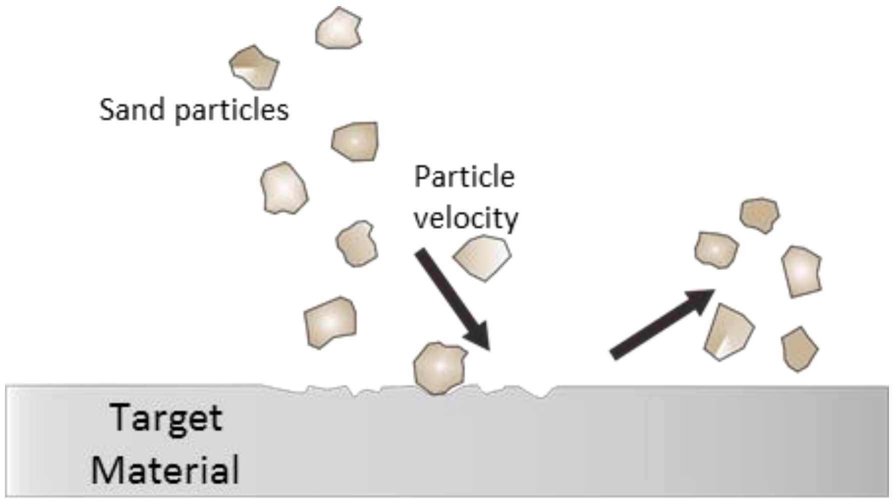

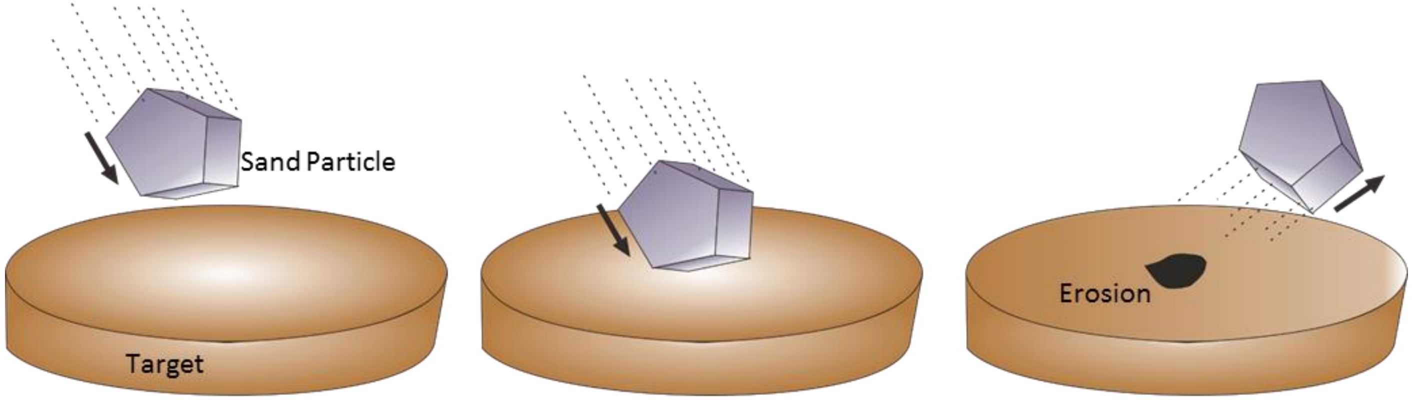

Single particle impact

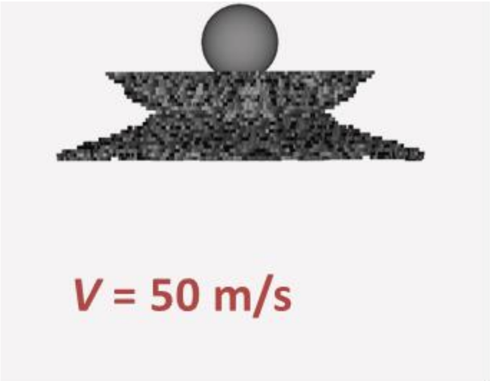

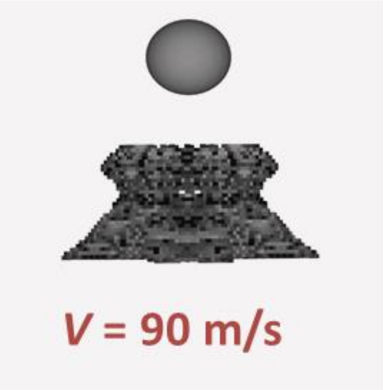

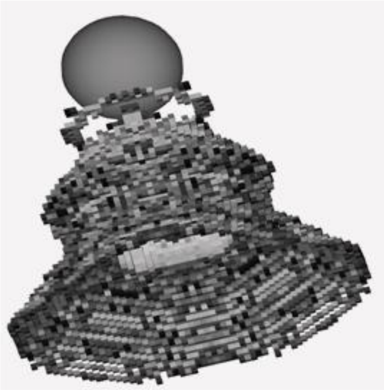

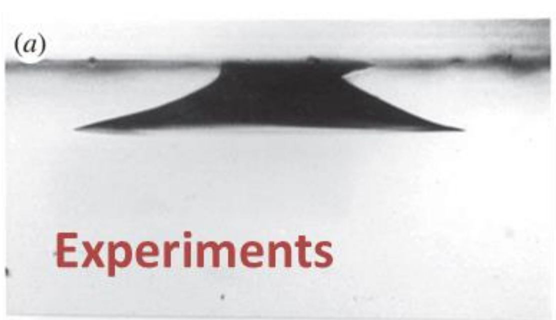

Conical crack profiles

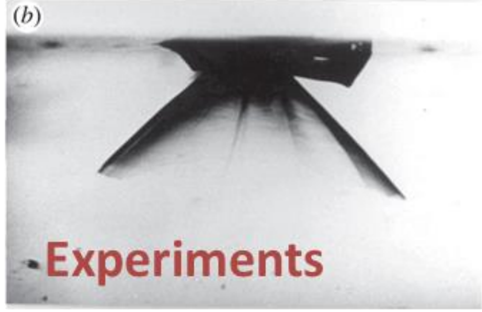

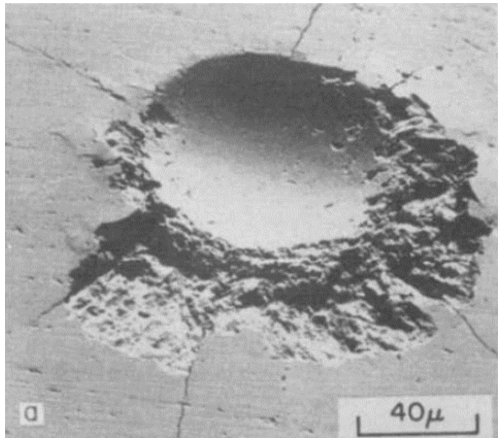

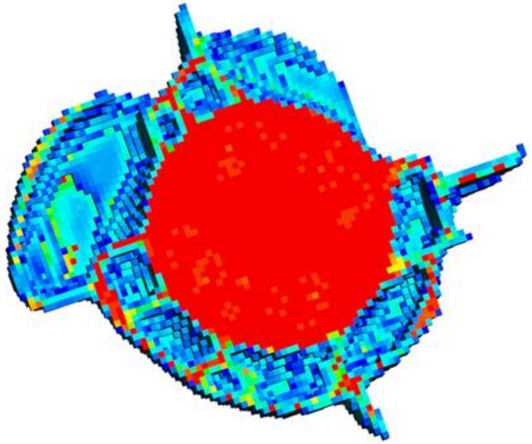

Material removal by lateral cracks on the surface

Anicode et al.2020, “Peridynamic Modeling of Damage due to Multiple Sand Particle Impacts in the Presence of Contact and Friction,” 61th SciTech Conference, Orlando, Florida, AIAA-2020-0968

Multiple sand particles

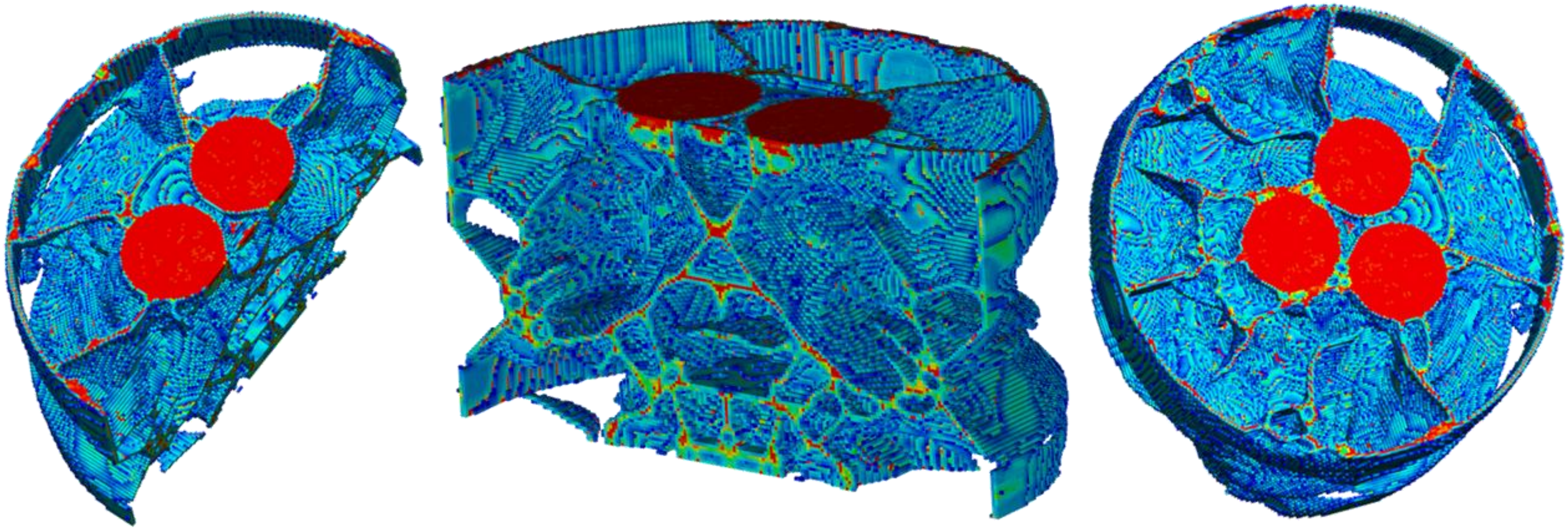

Coalescence of multiple cracks

Anicode et al.2020, "Peridynamic Modeling of Damage due to Multiple Sand Particle Impacts in the Presence of Contact and Friction," 61th SciTech Conference, Orlando, Florida, AIAA-2020-0968

Frangibility in glass

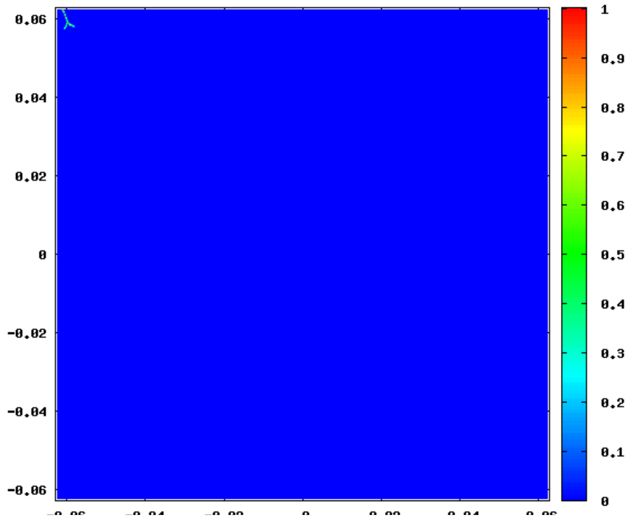

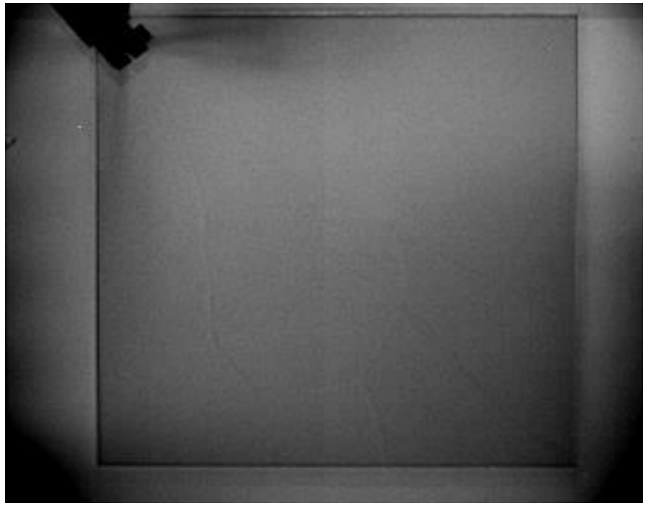

CT=69 MPa

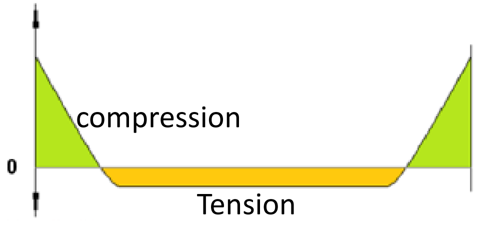

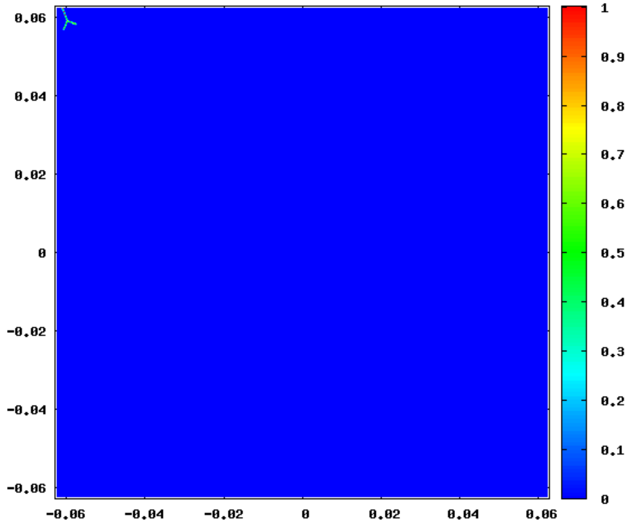

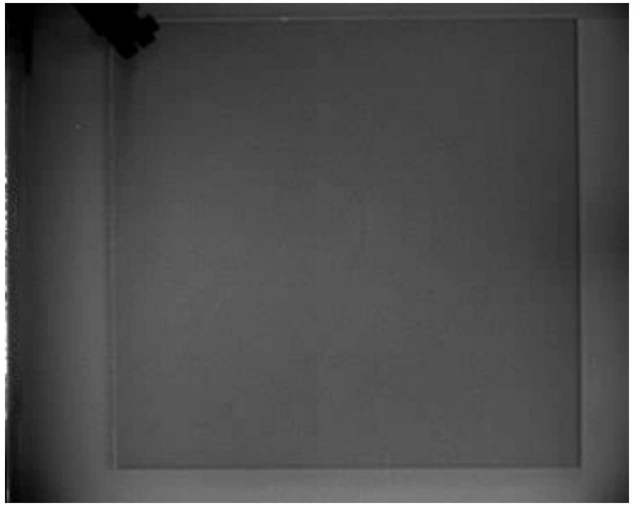

CT=72 MPa

Tang, et al., Appl. Phys. A, 2014. DOI 10.1007/s00339-014-8370-y

Crack initiation and growth in CMC

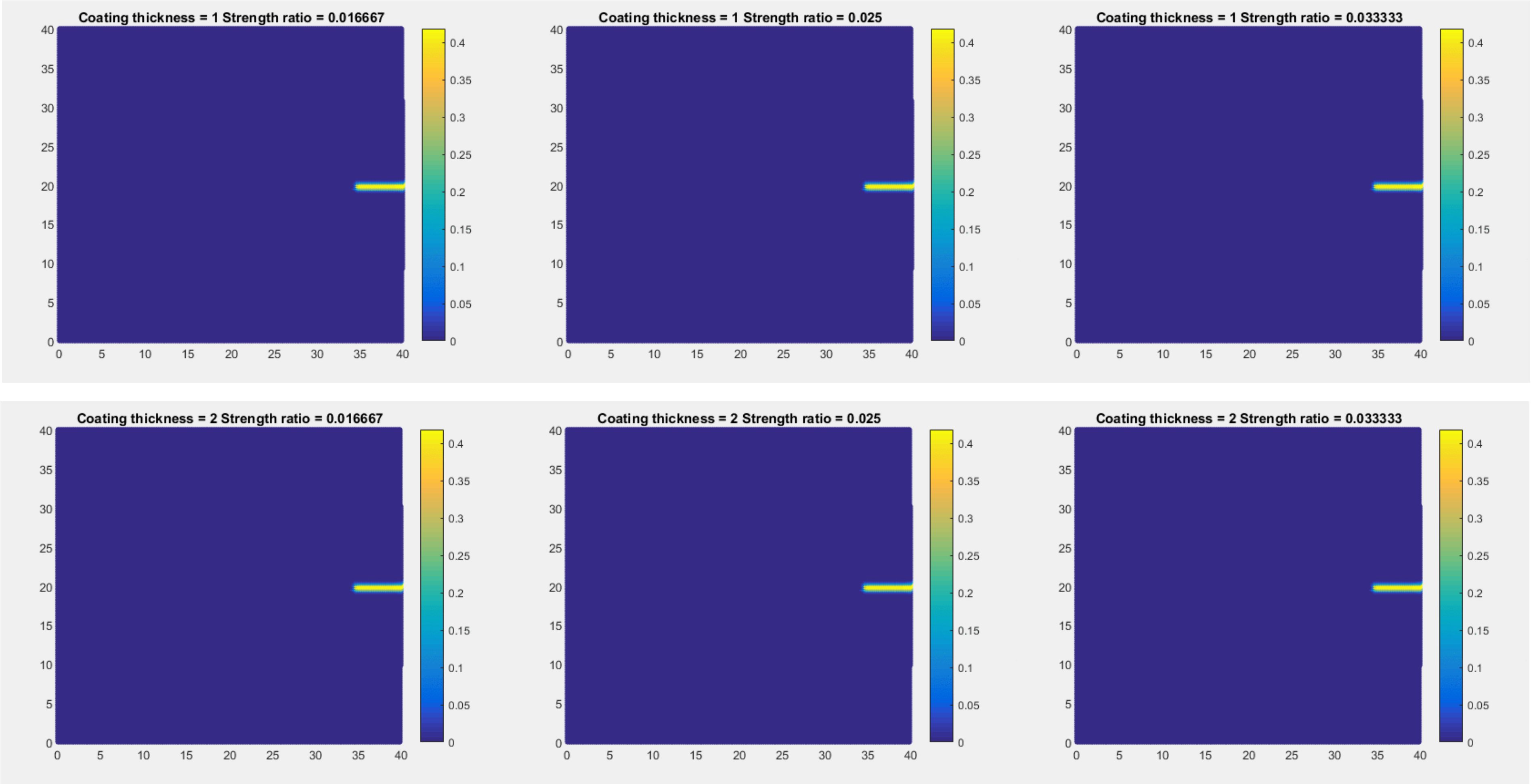

- **As ratio of coating-matrix failure stress decreases, a secondary crack initiates in the coating earlier**
- **As coating thickness increases, a secondary crack initiates when the primary crack is closer to the coating**

Mitts et al., 2020, “Axisymmetric peridynamic analysis of crack deflection in a single strand ceramic matrix composite” Engineering Fracture Mechanics, 107074.

Rubber sheet with double edge cracks

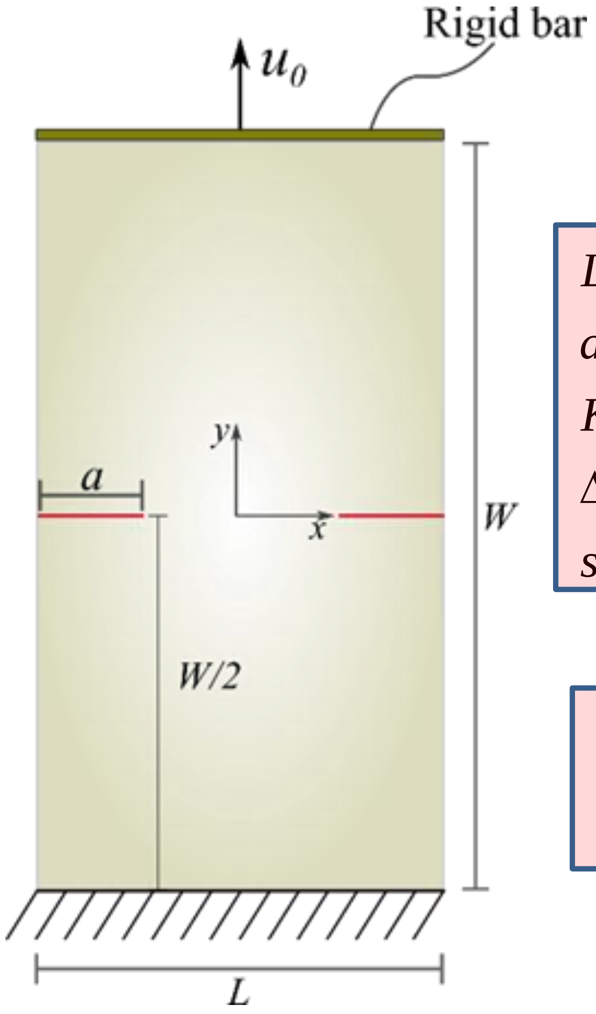

$$L = 80\text{mm}, W = 200\text{mm}, t = 3\text{mm}$$
$$a = 12, 16, 20, 24, 28\text{mm}$$
$$K = 2.68 \text{ MPa}, \quad \mu = 0.268 \text{ MPa}$$
$$\Delta u_0 = 0.25 \text{ mm}$$
$$s_c = 3.1$$

$$A_{(k)} = 1.0 \text{ mm}^2$$
$$\delta = 3.015 \Delta x$$

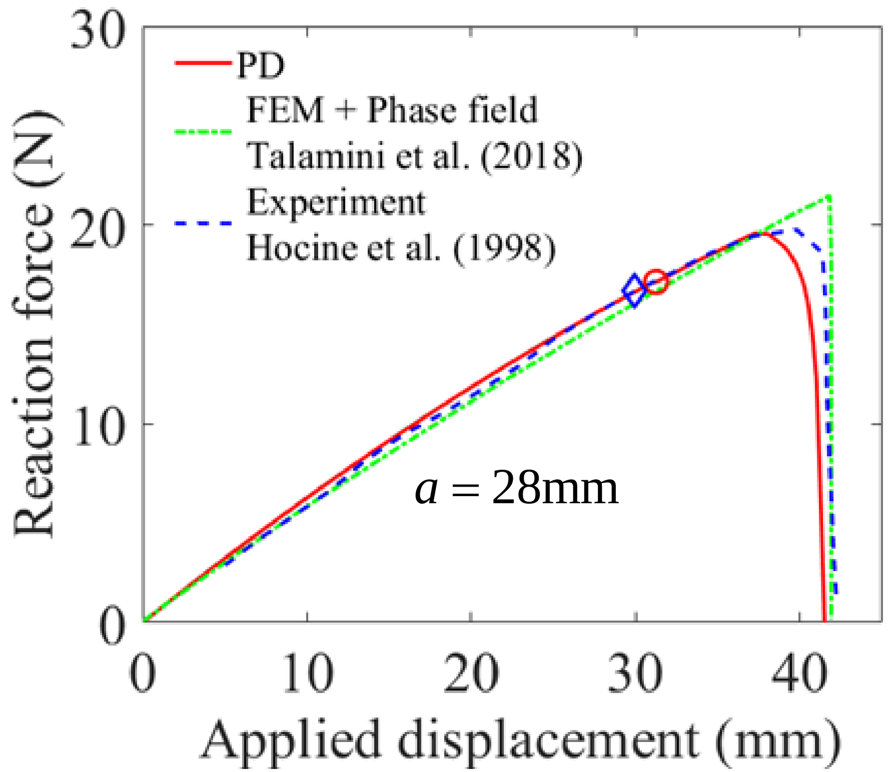

Calibrate critical stretch from load-displacement curve

Hocine NA, Abdelaziz MN and Mesmacque G. Experimental and numerical investigation on single specimen methods of determination of J in rubber materials. Int J Fract 1998; 94: 321–338.

B Talamini, Y Mao, L Anand Progressive damage and rupture in polymers Journal of the Mechanics and Physics of Solids 2018 111, 434-457

Damage initiation, growth and rupture

$a = 28\text{mm}$

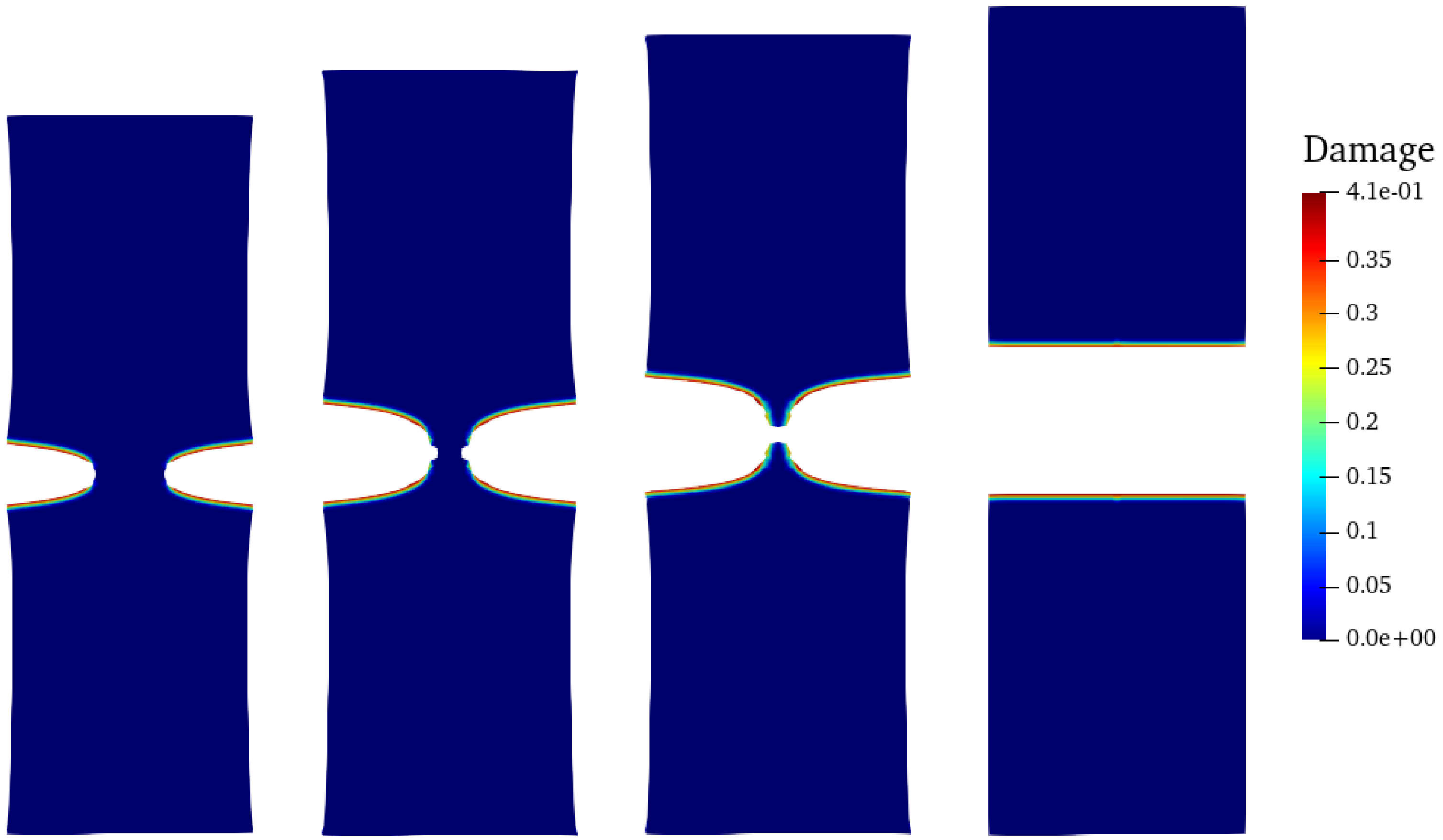

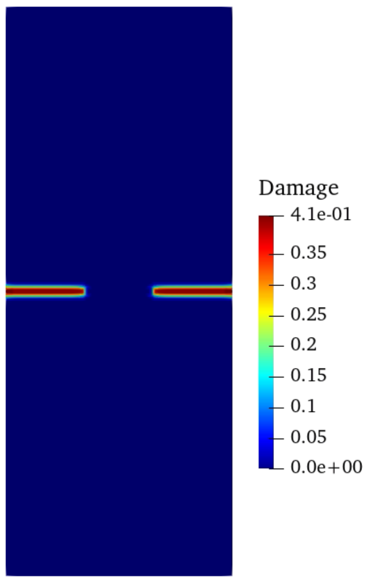

Behera et al., 2020, "Peridynamic simulation of finite elastic deformation and rupture in polymers" Engineering Fracture Mechanics, 236, 107226

Polydimythlsiloxane (PDMS) sheets

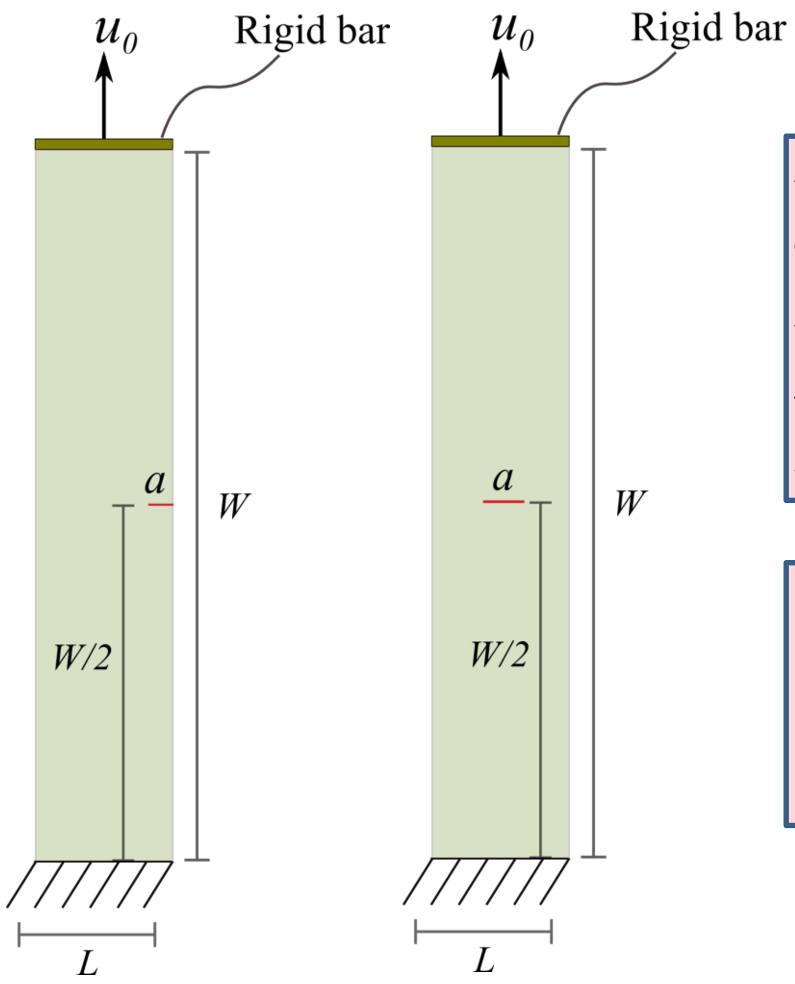

Edge crack **Internal crack**

$L = 12.5\text{mm}, W = 100\text{mm}, t = 1\text{mm}$

$a = 2\text{mm}$

$K = 159.9 \text{ MPa}, \ \mu = 0.32 \text{ MPa}$

$\Delta u_0 = 0.25 \text{mm}$

$s_c = 4.1$

$A_{(k)} = 6.25e-2 \text{ mm}^2$

20000 material points

$\delta = 3.015 \Delta x$

Zhang et al. 2017, Numerical Simulation and Experimental Study of Crack Propagation of Polydimethylsiloxane. Procedia engineering, 214, 59-68.

Polymer sheet with an edge crack

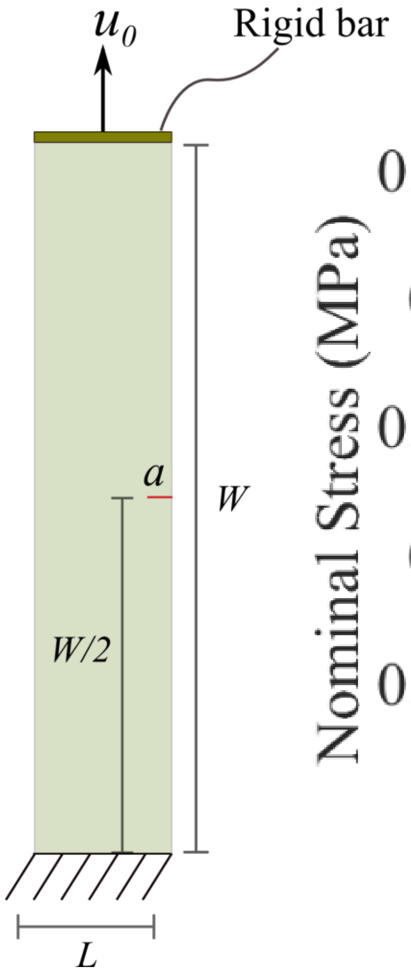

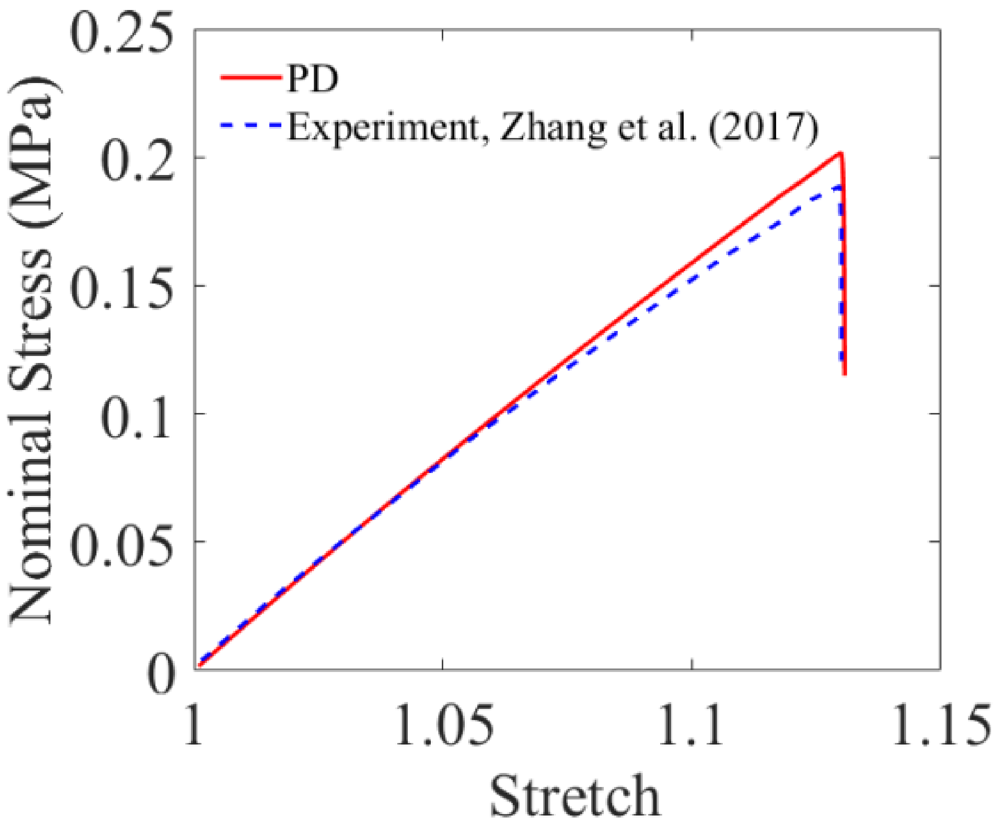

Experimental observation

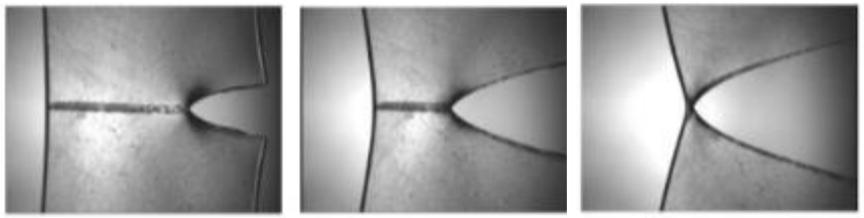

Damage prediction

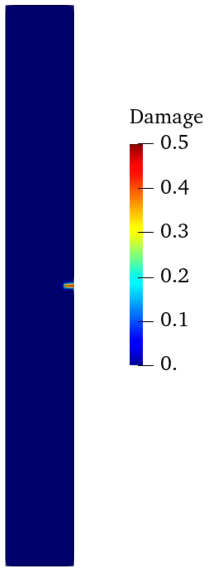

Zhang et al. 2017, Numerical Simulation and Experimental Study of Crack Propagation of Polydimethylsiloxane. Procedia engineering, 214, 59-68.

Behera et al., 2020, "Peridynamic simulation of finite elastic deformation and rupture in polymers" Engineering Fracture Mechanics, 236, 107226

Polymer sheet with an internal crack

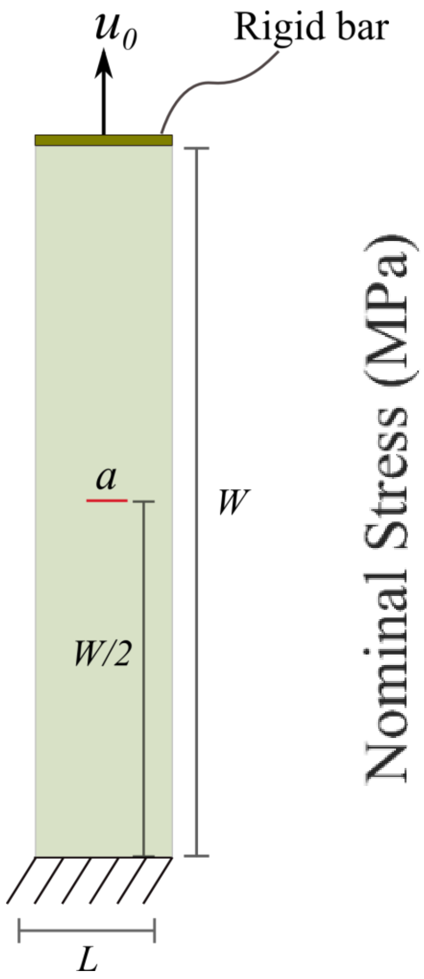

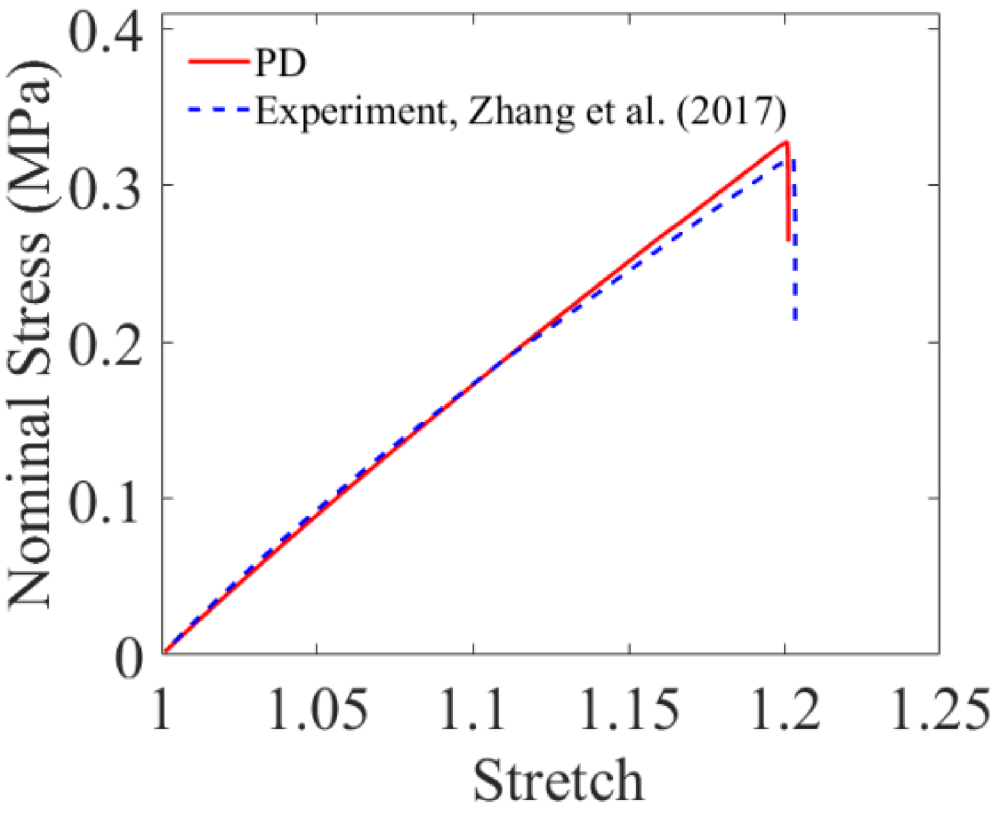

Experimental observation

Damage prediction

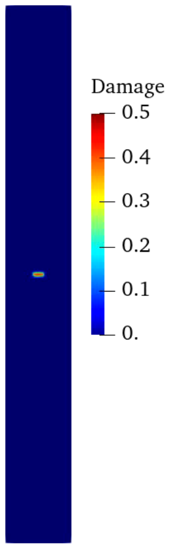

Zhang et al. 2017, Numerical Simulation and Experimental Study of Crack Propagation of Polydimethylsiloxane. Procedia engineering, 214, 59-68.

Behera et al., 2020, "Peridynamic simulation of finite elastic deformation and rupture in polymers" Engineering Fracture Mechanics, 236, 107226

Solution to hyperbolic PDEs

- **Time dependent**
  - **Sod's shock tube**
- **Time independent**
  - **Eikonel equation**

Inherent challenges with hyperbolic equations

$$\frac{\partial u}{\partial t} + \frac{\partial F(u)}{\partial x} = 0$$

Many systems appear as conservation law

$$\left|\nabla T(x,y)\right|^2 = \frac{1}{\upsilon^2(x,y)} \text{ with } T\left(x_s, y_s\right) = 0$$

Steady-state high-frequency wave equation

Solution does not smooth out with time

Discontinuities persist and require accurate approximation

Knowledge of characteristic directions are essential

- **Information travels along characteristics**

Solution should ideally preserve conservation of energy

- **Presence of numerical diffusion (or numerical viscosity) is unavoidable**

Central difference schemes usually break down near discontinuities

Smooth initial conditions do not guarantee smooth solution of NL equations – shock

- **Determination of single valued solution requires numerical dissipation**

Directional nonlocality

Modification of weight function

- Upwinding direction
- Positive and negative advancing fluxes
- Gradient of traveltime

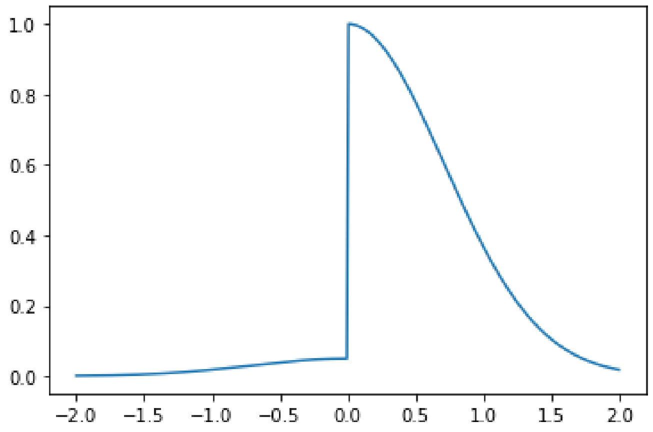

$$w(|\xi|,\kappa;\delta) = \kappa e^{-4(|\xi|/\delta)^2}$$

$$\kappa = \begin{cases} 0.1 & \text{if} \quad \xi < 0 \\ 1.0 & \text{if} \quad \xi \geq 0 \end{cases}$$

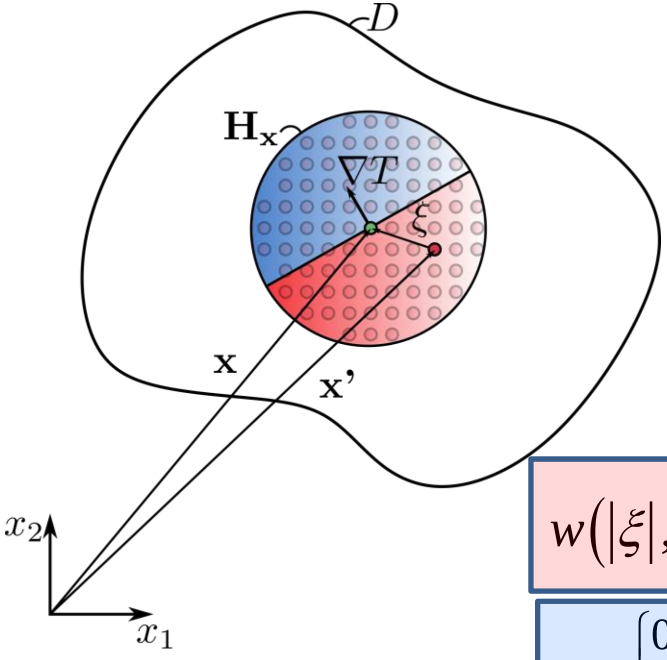

$$w(|\xi|,\kappa;\delta) = \kappa e^{-4(|\xi|/\delta)^2}$$

$$\kappa = \begin{cases} 0.1 & \text{if} \quad \xi \cdot \nabla T < 0 \\ 1.0 & \text{if} \quad \xi \cdot \nabla T \geq 0 \end{cases}$$

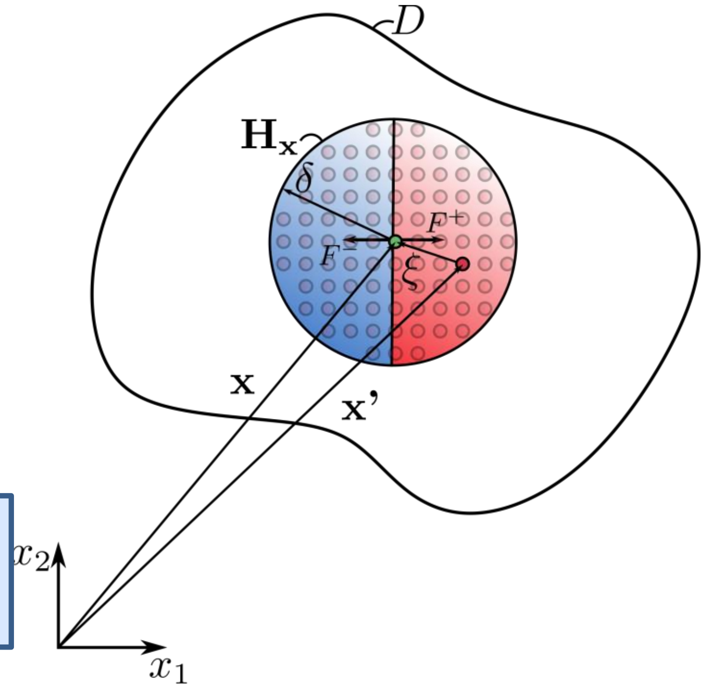

$$w(|\xi|,\kappa^{\pm};\delta) = \kappa^{\pm} e^{-4(|\xi|/\delta)^2}$$

$$F^+ \to \kappa^+ = \begin{cases} 0.1 & \text{if} \quad \xi < 0 \\ 1.0 & \text{else} \quad \xi \geq 0 \end{cases}$$

$$F^- \to \kappa^- = \begin{cases} 1.0 & \text{if} \quad \xi < 0 \\ 0.1 & \text{else} \quad \xi \geq 0 \end{cases}$$

Isotropic Eikonal equation – P waves

$$T_{,x}^2 + T_{,z}^2 = \frac{1}{\upsilon^2} \quad \text{for} \quad (x,z) \in [0, L = 2\text{km}]$$

$$T = T(1.0, 1.0) \text{ - source location}$$

$$T_{\text{initial}}(\mathbf{x}) = \frac{1}{1.5}\cosh^{-1}\left(1 + \frac{1.5^2 \left|\mathbf{x} - \mathbf{x}_s\right|^2}{6\upsilon(\mathbf{x})}\right)$$

$$\left(\sum_{j=1}^{N_{(k)}} T_{(k)(j)} g_1^{10}(\xi_{1(k)(j)}, \xi_{2(k)(j)}) A_{(j)}\right)^2 + \left(\sum_{j=1}^{N_{(k)}} T_{(k)(j)} g_1^{01}(\xi_{1(k)(j)}, \xi_{2(k)(j)}) A_{(j)}\right)^2 = \frac{1}{\upsilon^2}$$

$$\Delta = 0.02 \text{ km}$$

$$\delta = 2\Delta$$

$$K = 101 \times 101$$

$$\text{Convergence } \left\|\mathbf{F}(\mathbf{u})\right\| < 1.8777 \times 10^{-13}$$

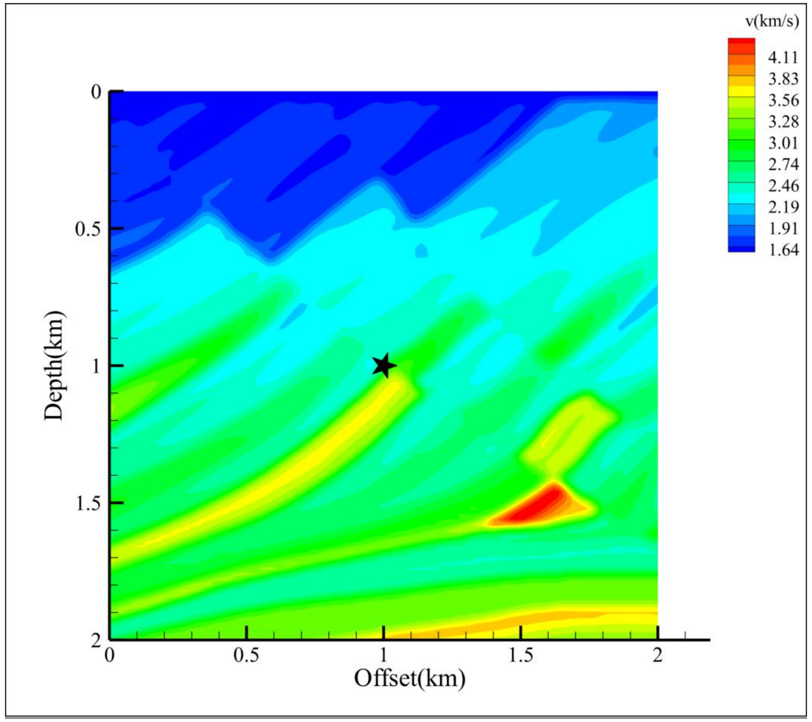

Velocity field - Marmousi

Bekar et al. ,2022, “Solving the Eikonal equation for compressional and shear waves in anisotropic media using peridynamic differential operator,” Geophysical Journal International, Vol. 229, pp. 1942–1963,

Comparison of solutions

Reference: Fast Marching with fine mesh

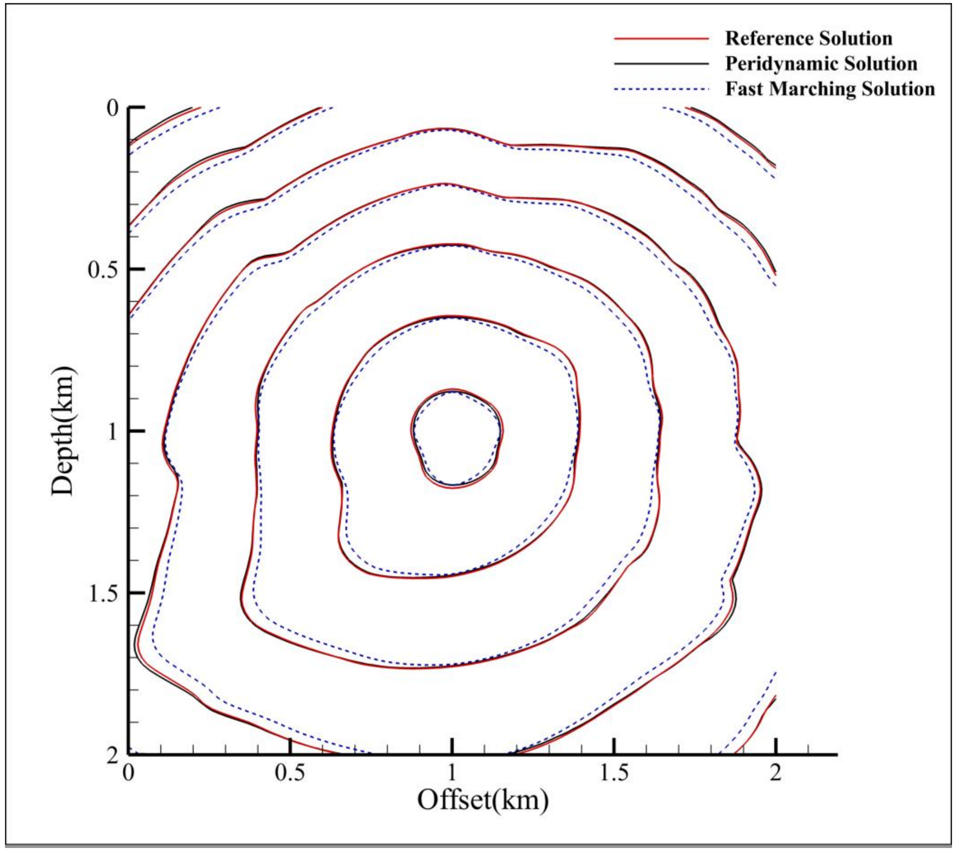

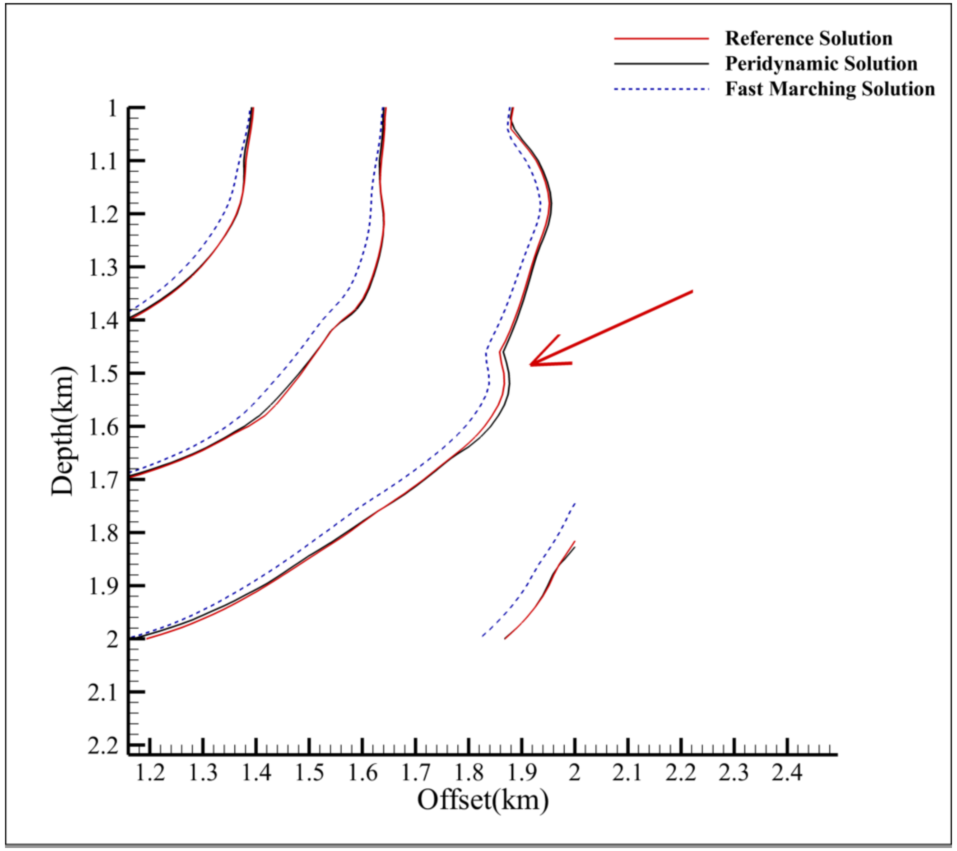

PD captures the sharp change in traveltimes around the region with the highest velocity gradient

Sethian, J. A. (1996). A fast marching level set method for monotonically advancing fronts. Proceedings of the National Academy of Sciences of the USA, 93(4), 1591–1595.

Bekar et al. ,2022, "Solving the Eikonal equation for compressional and shear waves in anisotropic media using peridynamic differential operator," Geophysical Journal International, Vol. 229, pp. 1942–1963,

Error measure against reference solution

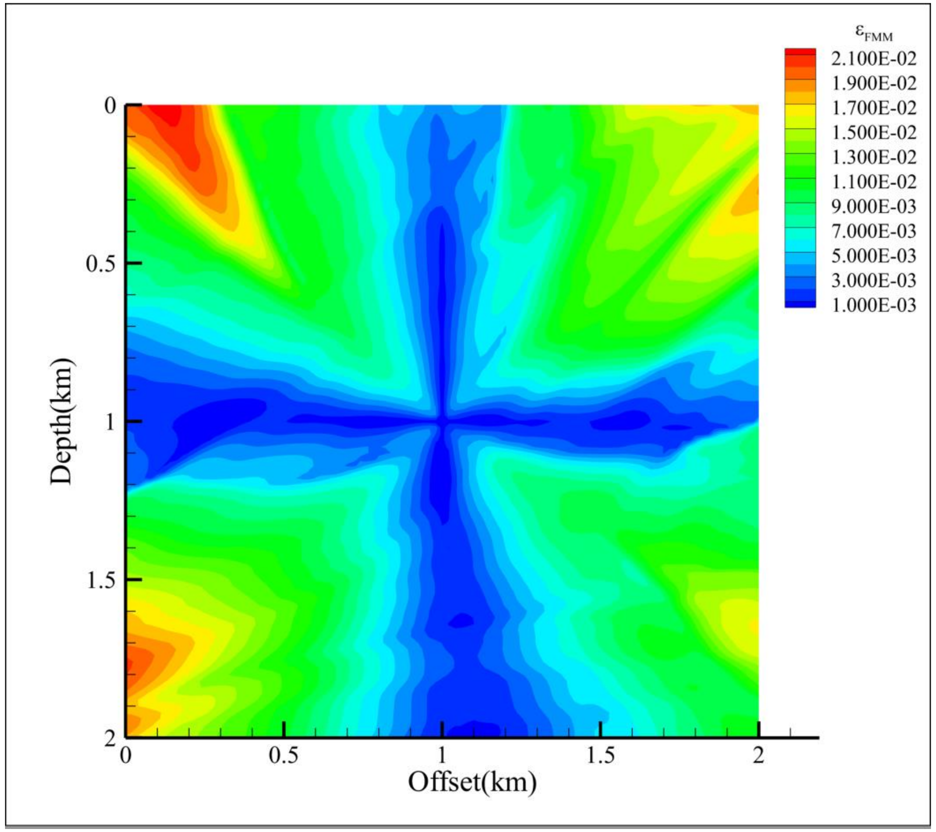

Fast marching method

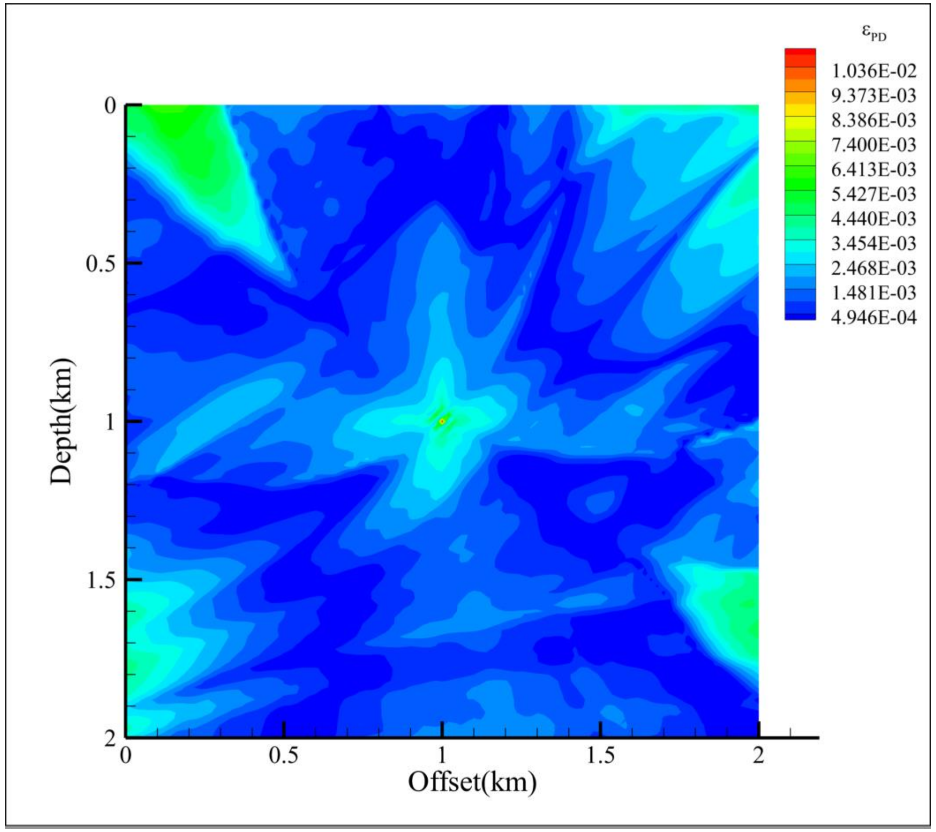

Peridynamics

Bekar et al. ,2022, "Solving the Eikonal equation for compressional and shear waves in anisotropic media using peridynamic differential operator," Geophysical Journal International, Vol. 229, pp. 1942–1963,

PDDO for Euler equations

$$\frac{\partial \mathbf{Q}}{\partial t}+\frac{\partial \mathbf{F}}{\partial x}=0 \quad \text{for} \quad 0\le x\le 10$$

- **Conservation of mass, momentum and energy**
- **Challenging nonlinear equation**

$$\mathbf{Q}=\begin{bmatrix}\rho\\ \rho u\\ E\end{bmatrix} \qquad \mathbf{F}=\begin{bmatrix}\rho\\ \rho u^2+p\\ (E+p)u\end{bmatrix}$$

$$E=\rho e+\frac{1}{2}\rho u^2$$

$$p=(\gamma-1)\rho e$$

ρ - density

u - velocity

p - pressure

E - total energy per unit volume

e - internal energy per unit mass

$\gamma=1.4$

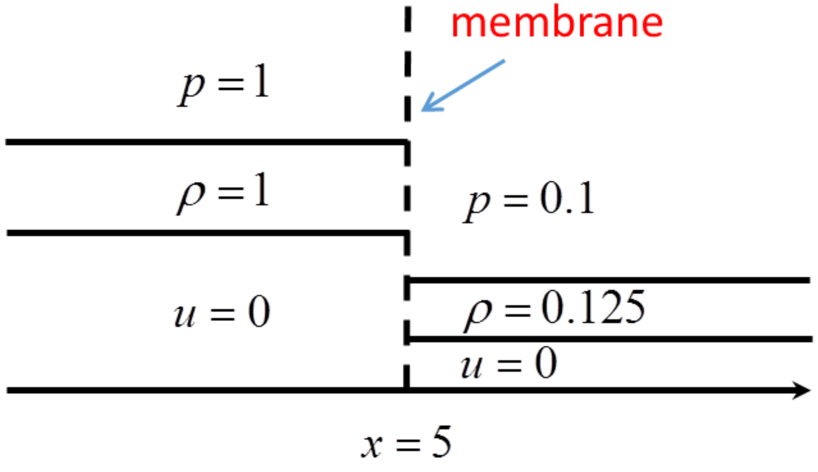

Initial conditions for Sod's shock tube

Sod, G. A. (1978). A survey of several finite difference methods for systems of nonlinear hyperbolic conservation laws. Journal of Computational Physics., 27, 1-31

Flux vector splitting method

$$\frac{\partial \mathbf{Q}}{\partial t}+\frac{\partial \mathbf{F}}{\partial x}=0$$

$$\mathbf{F}=\mathbf{F}^{+}+\mathbf{F}^{-}$$

$$\mathbf{F}^{+}=\frac{\rho}{4c}(u+c)^{2}\begin{bmatrix}1\\ \dfrac{(\gamma-1)u+2c}{\gamma}\\ \dfrac{\left[(\gamma-1)u+2c\right]^{2}}{2\left(\gamma^{2}-1\right)}\end{bmatrix}$$

$$\mathbf{F}^{-}=-\frac{\rho}{4c}(u-c)^{2}\begin{bmatrix}1\\ \dfrac{(\gamma-1)u-2c}{\gamma}\\ \dfrac{\left[2c-(\gamma-1)u\right]^{2}}{2\left(\gamma^{2}-1\right)}\end{bmatrix}$$

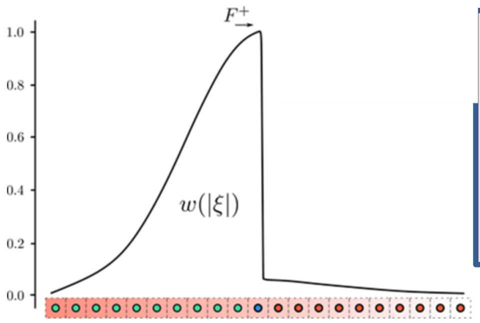

$$w\left(|\xi|,\kappa^{\pm};\delta\right)=\kappa^{\pm}e^{-4\left(|\xi|/\delta\right)^{2}}$$

$$F^{+}\rightarrow\kappa^{+}=\begin{cases}0.1 & \text{if} \quad \xi<0\\ 1.0 & \text{else} \quad \xi\geq 0\end{cases}$$

$$F^{-}\rightarrow\kappa^{-}=\begin{cases}1.0 & \text{if} \quad \xi<0\\ 0.1 & \text{else} \quad \xi\geq 0\end{cases}$$

PD differentiation

$$\frac{\partial}{\partial x}\left(\mathbf{F}^{+}+\mathbf{F}^{-}\right)=\sum_{j=1}^{N_{(k)}}\mathbf{F}^{+}_{(k)(j)}\,{}^{+}g_{1}^{1}(\xi_{1(k)(j)})A_{(j)}+\sum_{j=1}^{N_{(k)}}\mathbf{F}^{-}_{(k)(j)}\,{}^{-}g_{1}^{1}(\xi_{1(k)(j)})\ell_{(j)}$$

Euler's first order explicit time integration

$$\mathbf{Q}_{k}^{t+\Delta t}=\mathbf{Q}_{k}^{t}-\sum_{j=1}^{N_{(k)}}\mathbf{F}^{+}_{(k)(j)}\,{}^{+}g_{1}^{1}(\xi_{1(k)(j)})A_{(j)}-\sum_{j=1}^{N_{(k)}}\mathbf{F}^{-}_{(k)(j)}\,{}^{-}g_{1}^{1}(\xi_{1(k)(j)})\ell_{(j)}$$

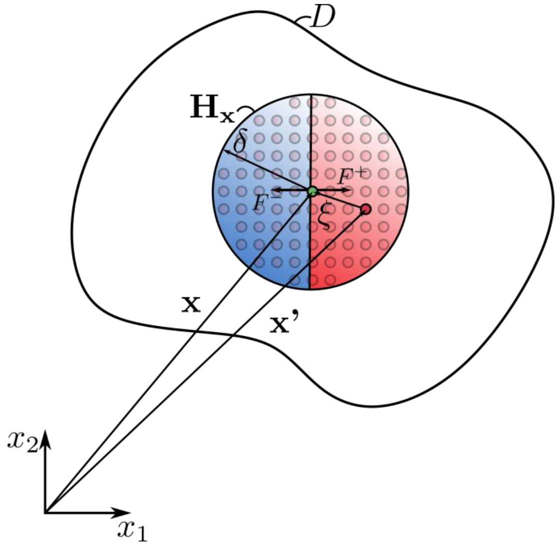

$$\Delta=0.01\text{ m}$$
$$\delta=2\Delta$$
$$\Delta t=0.01s$$
$$K=1001$$

Van Leer, B. "Flux-vector splitting for the Euler equation." Upwind and high-resolution schemes. Springer, Berlin, Heidelberg, 1997. 80-89.

PD solution of Euler equations

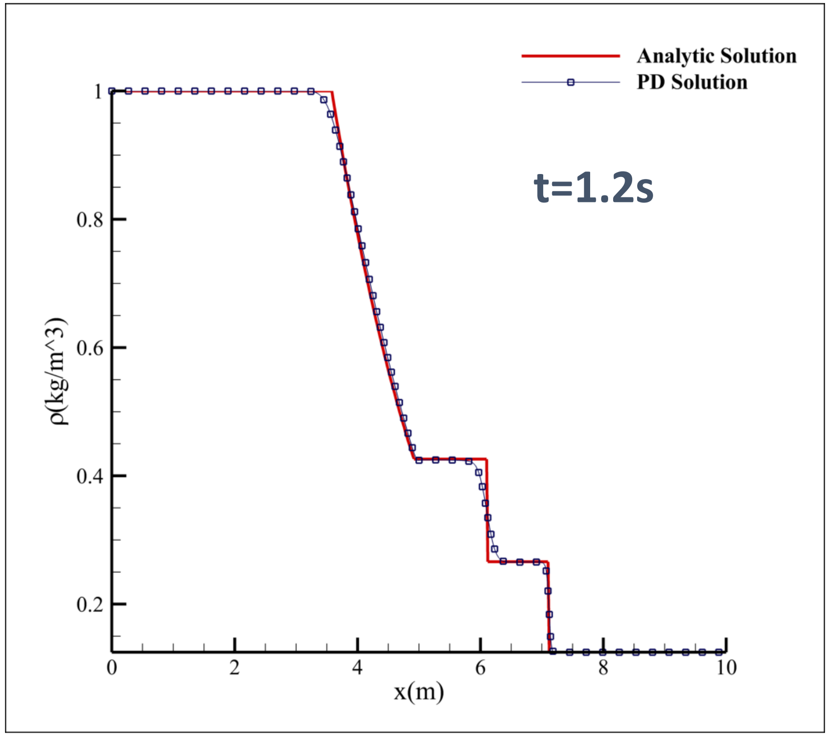

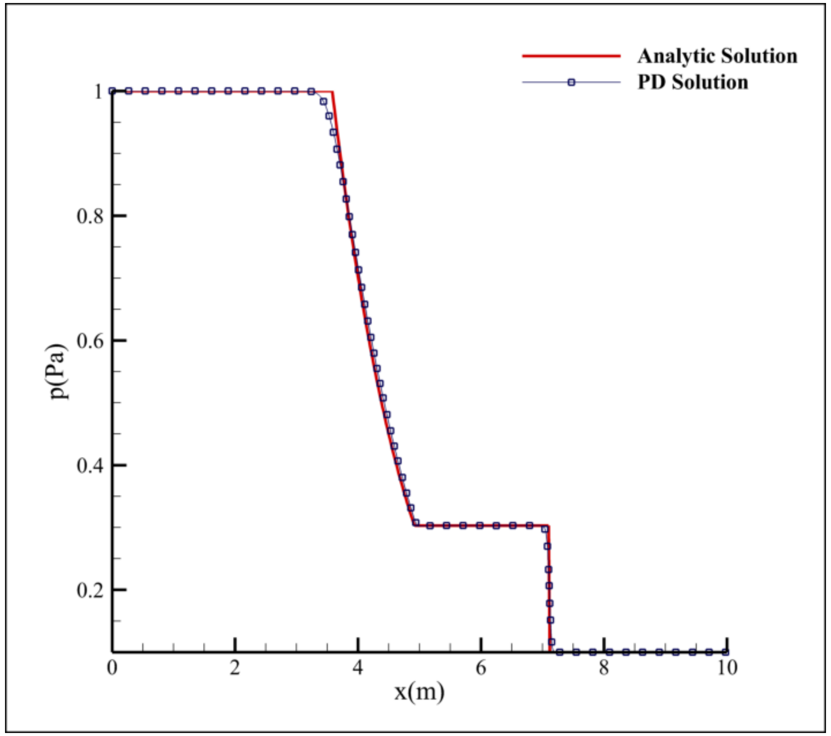

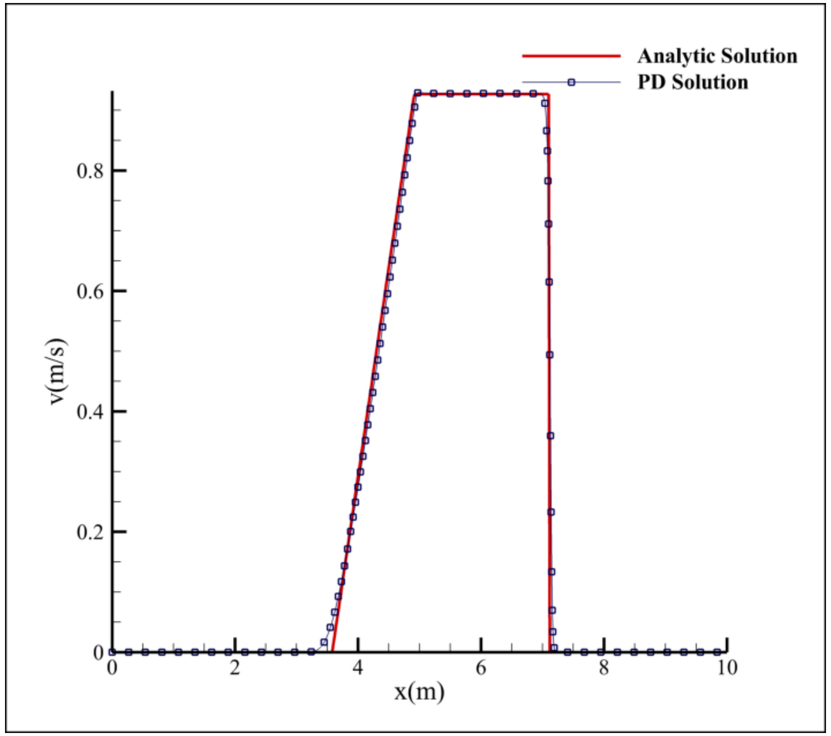

Density

Pressure

Velocity

Close agreement with analytical solution

Captures the shock and rarefaction w/o special treatment

Bekar et al., 2022, "On the solution of hyperbolic equations using the peridynamic differential operator," Computer Methods in Applied Mechanics and Engineering, Vol. 391, 114574

Remarks

- **PDDO enables the solution of different types of Hyperbolic PDEs.**
  - **Weight function enables upwinding in a natural way**
  - **No special treatment is necessary in the solution process**
  - **Same discretization applies regardless of the domain irregularity**
  - **It captures the shocks**
- **Numerical stability is always ensured**

Discovery

- Learning PDEs
- Nonlocal PINN
- Unsupervised learning

Learning partial differential equations

Discover the significant terms in PDEs that describe a particular phenomena based on the measured data

$$\frac{\partial u(\mathbf{x},t)}{\partial t} + \mathcal{L}(u) = 0 \qquad \mathbf{x} \in \Omega \quad \text{and} \quad 0 < t < T$$

$$\mathcal{B}(u) = 0 \qquad \mathbf{x} \in \partial\Omega$$

$$u(\mathbf{x},0) = u_0(\mathbf{x}) \qquad \mathbf{x} \in \Omega$$

- **Determination of** $\boxed{\mathcal{L}(u)}$

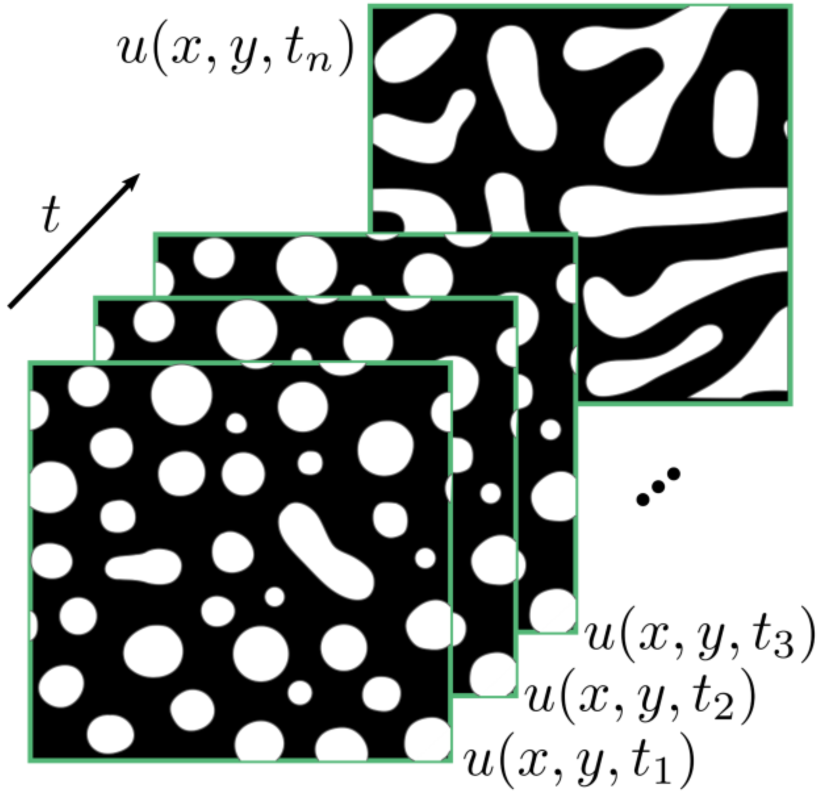

Bekar, A.C. and Madenci, E., 2021, "Peridynamics enabled learning partial differential equations," Journal of Computational Physics, Vol. 434, 110193

H. Schaeffer, Learning partial differential equations via data discovery and sparse optimization, Proc. R. Soc. A. 473 (2017) 20160446

Approach

Feature matrix

$$\mathbf{F}_u(t)=\begin{bmatrix} 1 & u(x_1,t) & u^2(x_1,t) & u_x(x_1,t) & u_x^2(x_1,t) & \cdots & u_{xx}(x_1,t) & u_{xx}^2(x_1,t) & \cdots \\ \vdots & \vdots & \vdots & \vdots & \vdots & \vdots & \vdots & \vdots & \vdots \\ 1 & u(x_j,t) & u^2(x_j,t) & u_x(x_j,t) & u_x^2(x_j,t) & \cdots & u_{xx}(x_j,t) & u_{xx}^2(x_j,t) & \cdots \\ \vdots & \vdots & \vdots & \vdots & \vdots & \vdots & \vdots & \vdots & \vdots \\ 1 & u(x_K,t) & u^2(x_K,t) & u\ (x_K,t) & u_x^2(x_K,t) & \cdots & u_{xx}(x_K,t) & u_{xx}^2(x_K,t) & \cdots \end{bmatrix}$$

Construct a candidate space

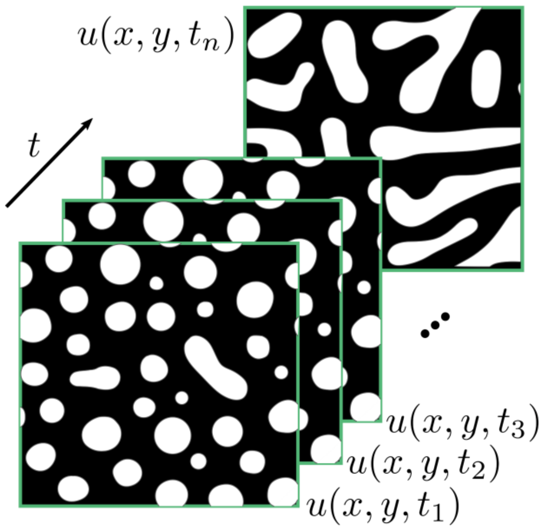

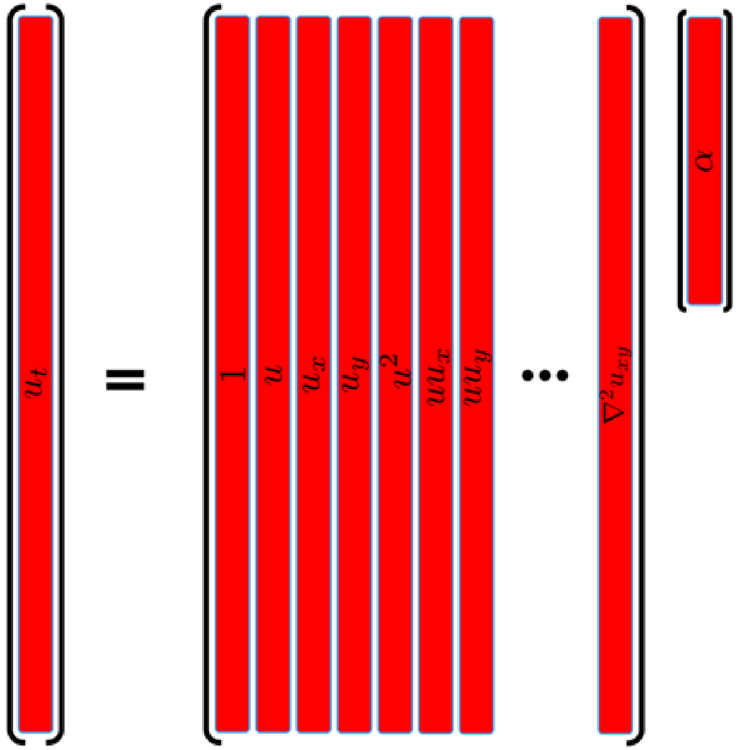

$$\mathbf{V}(t_j)=\mathbf{F}_u(t_j)\boldsymbol{\alpha} \quad \text{for } j=1,\ldots..,S$$

Velocity vector

$$\mathbf{V}(t)=\begin{Bmatrix} u_t(x_1,t) \\ \vdots \\ u_t(x_j,t) \\ \vdots \\ u_t(x_K,t) \end{Bmatrix} \qquad \boldsymbol{\alpha}=\begin{Bmatrix} \alpha_1 \\ \vdots \\ \alpha_j \\ \vdots \\ \alpha_M \end{Bmatrix}$$

Coefficient vector

LSM for determining coefficient vector

$$\min_{\boldsymbol{\alpha}}\left(\frac{1}{2}\sum_{k=1}^{M}\left\|\mathbf{V}(t_k)-\mathbf{F}_u(t_k)\boldsymbol{\alpha}\right\|_2^2+\lambda\left\|\boldsymbol{\alpha}\right\|_1\right) \quad \text{with } \lambda>0$$

$$\left(\sum_{k=1}^{M}\mathbf{F}_u^T(t_k)\mathbf{F}_u(t_k)\right)\boldsymbol{\alpha}+\sum_{k=1}^{M}\mathbf{F}_u^T(t_k)\mathbf{V}(t_k))+\lambda\frac{\partial\left\|\boldsymbol{\alpha}\right\|_1}{\partial\boldsymbol{\alpha}}=0$$

Regression problem with over-fitting

Optimization with a sparse solution

H. Schaeffer, Learning partial differential equations via data discovery and sparse optimization, Proc. R. Soc. A. 473 (2017) 20160446

Learning algorithm

Training data set

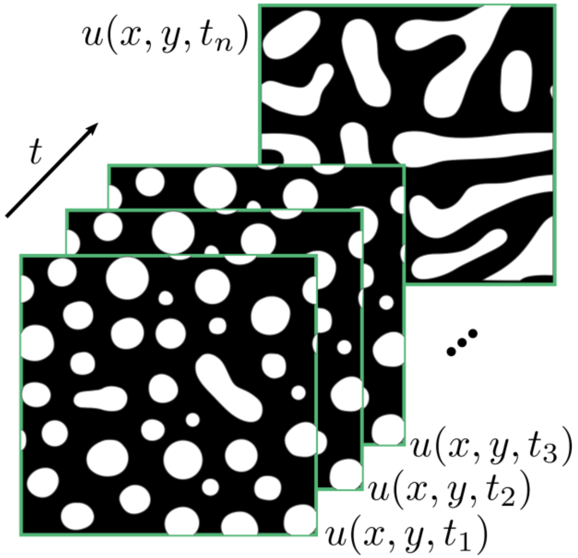

Candidate space construction

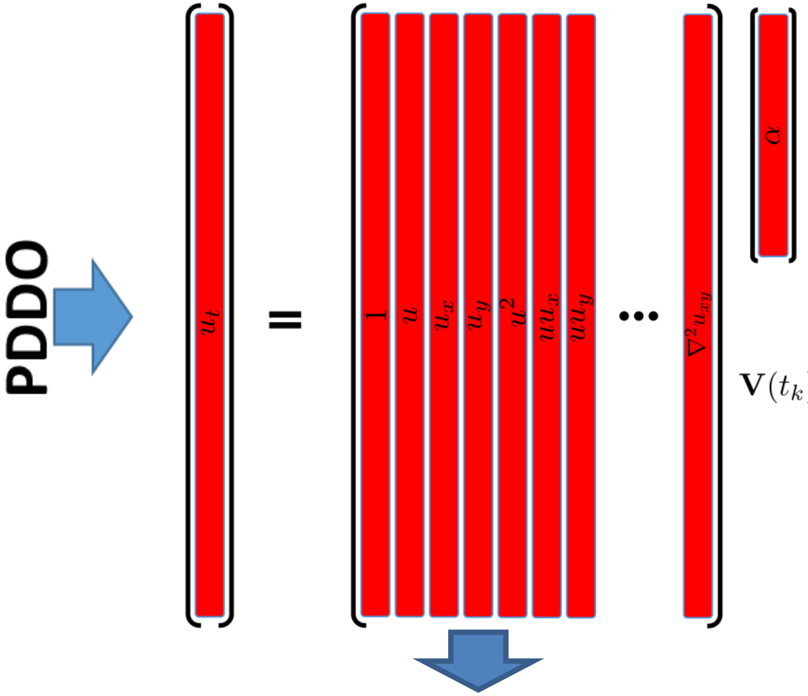

$\mathbf{V}(t_k) = \mathbf{F}_u(t_k)\alpha$

Testing data set

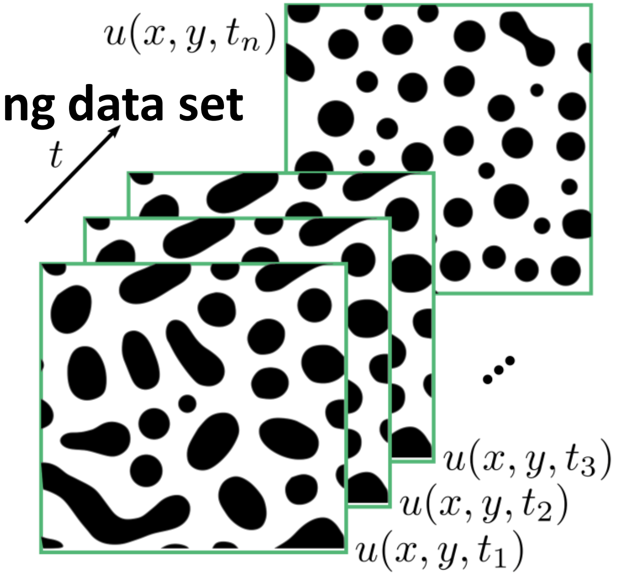

PDDO

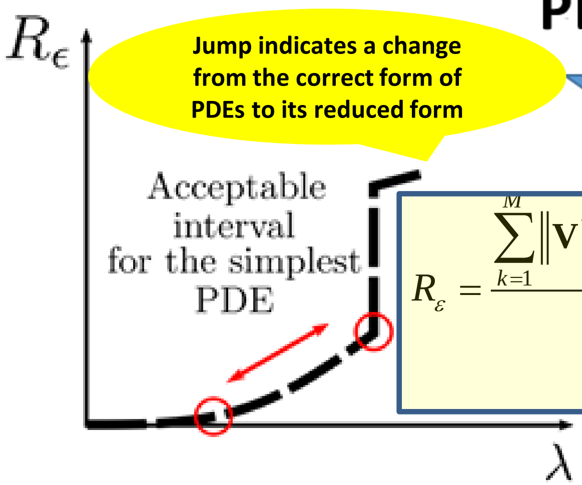

$$R_\varepsilon = \frac{\sum_{k=1}^{M} \left\| \mathbf{V}^{\text{test}}(t_k) - \mathbf{F}_u^{\text{test}}(t_k)\boldsymbol{\alpha}^{\text{training}} \right\|_2^2}{\sum_{k=1}^{M} \left\| \mathbf{V}^{\text{test}}(t_k) \right\|_2^2}$$

Douglas–Rachford optimization

$$\min_{\boldsymbol{\alpha}} \left(\frac{1}{2} \sum_{k=1}^{M} \left\| \mathbf{V}(t_k) - \mathbf{F}_u(t_k)\boldsymbol{\alpha} \right\|_2^2 + \lambda \left\| \boldsymbol{\alpha} \right\|_1 \right) \quad \text{with} \quad \lambda > 0$$

Determine α for different regularization parameter λ

Coefficient α corresponding to smallest acceptable λ identifies the PDE

H. Schaeffer, Learning partial differential equations via data discovery and sparse optimization, Proc. R. Soc. A. 473 (2017) 20160446

Cahn-Hilliard equation

$$u_t = -\frac{1}{2}\nabla^4 u + \nabla^2(u^3 - u) \text{ for } 0 \le x, y \le L_x = L_y = 50\pi$$

Periodic BC

$$u(x=0,y,t) = u(x=L_x,y,t)$$
$$u(x,y=0,t) = u(x,y=L_y,t)$$

Random IC

$$u(x,y,t=0) = \bar{u} + 0.05\,rand(x,y)$$
$$\bar{u} = -0.4, \quad rand(x,y) \in [-1,1]$$

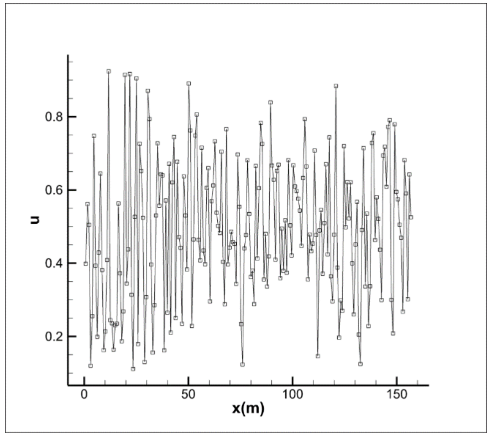

PD solution with ground truth coefficients

$t = 31s$

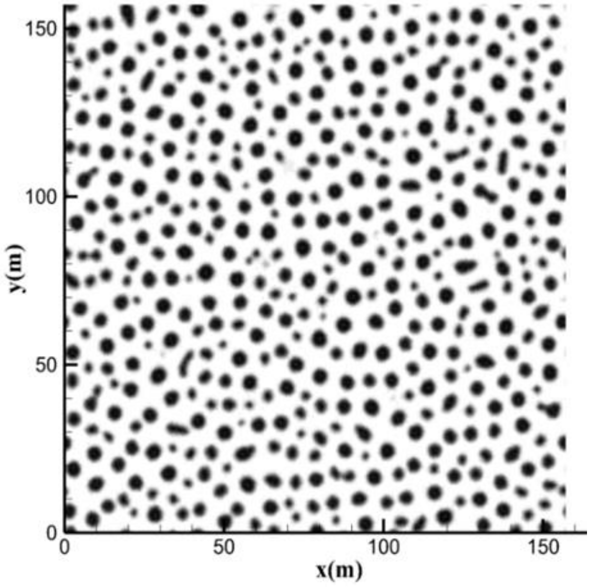

$$\Delta = 0.785 \text{ m}$$
$$\delta = 5\Delta$$
$$\Delta t = 0.01s$$

$$\begin{aligned} u^{t+\Delta t}(\mathbf{x}_{(k)}) = {} & \Delta t\left[\sum_{j=1}^{N_{(k)}} u^{t+\Delta t}(\mathbf{x}_{(j)})^3 g_4^{20}(\xi_{1(k)(j)},\xi_{2(k)(j)})A_j + \sum_{j=1}^{N_{(k)}} u^{t+\Delta t}(\mathbf{x}_{(j)})^3 g_4^{02}(\xi_{1(k)(j)},\xi_{2(k)(j)})A_j\right] \\ & -\frac{1}{2}\Delta t\left[\begin{array}{l}\displaystyle\sum_{j=1}^{N_{(k)}} u^{t+\Delta t}(\mathbf{x}_{(j)}) g_4^{40}(\xi_{1(k)(j)},\xi_{2(k)(j)})A_j + \sum_{j=1}^{N_{(k)}} u^{t+\Delta t}(\mathbf{x}_{(j)}) g_4^{22}(\xi_{1(k)(j)},\xi_{2(k)(j)})A_j \\ \displaystyle + \sum_{j=1}^{N_{(k)}} u^{t+\Delta t}(\mathbf{x}_{(j)}) g_4^{04}(\xi_{1(k)(j)},\xi_{2(k)(j)})A_j \end{array}\right] \\ & -\Delta t\left[\sum_{j=1}^{N_{(k)}} u^{t+\Delta t}(\mathbf{x}_{(j)}) g_4^{20}(\xi_{1(k)(j)},\xi_{2(k)(j)}) + \sum_{j=1}^{N_{(k)}} u^{t+\Delta t}(\mathbf{x}_{(j)}) g_4^{02}(\xi_{1(k)(j)},\xi_{2(k)(j)})A_j\right] + u_k^t \quad \text{for } k = 1,..,K = 201\times 201 \end{aligned}$$

Recovered coefficients – C-H equation

Terms	Noise = %0 ($\lambda = 0.01$)	Noise = %20 ($\lambda = 0.01$)	Noise = %50 ($\lambda = 0.01$)
$\nabla^2 u$	-1.012	-1.012	-1.013
$\nabla^2 u^2$	0	0	0
$\nabla^2 u^3$	1.012	1.012	1.013
$\nabla^2 u^4$	0	0	0
$\nabla^2 u_x$	0	0	0
$\nabla^2 u_y$	0	0	0
$\nabla^2 u_{xx}$	−0.505	−0.505	−0.506
$\nabla^2 u_{yy}$	−0.505	−0.505	−0.506
$\nabla^2 u_{xy}$	0	0	0

$$u_t = -\frac{1}{2}\nabla^4 u + \nabla^2(u^3 - u)$$

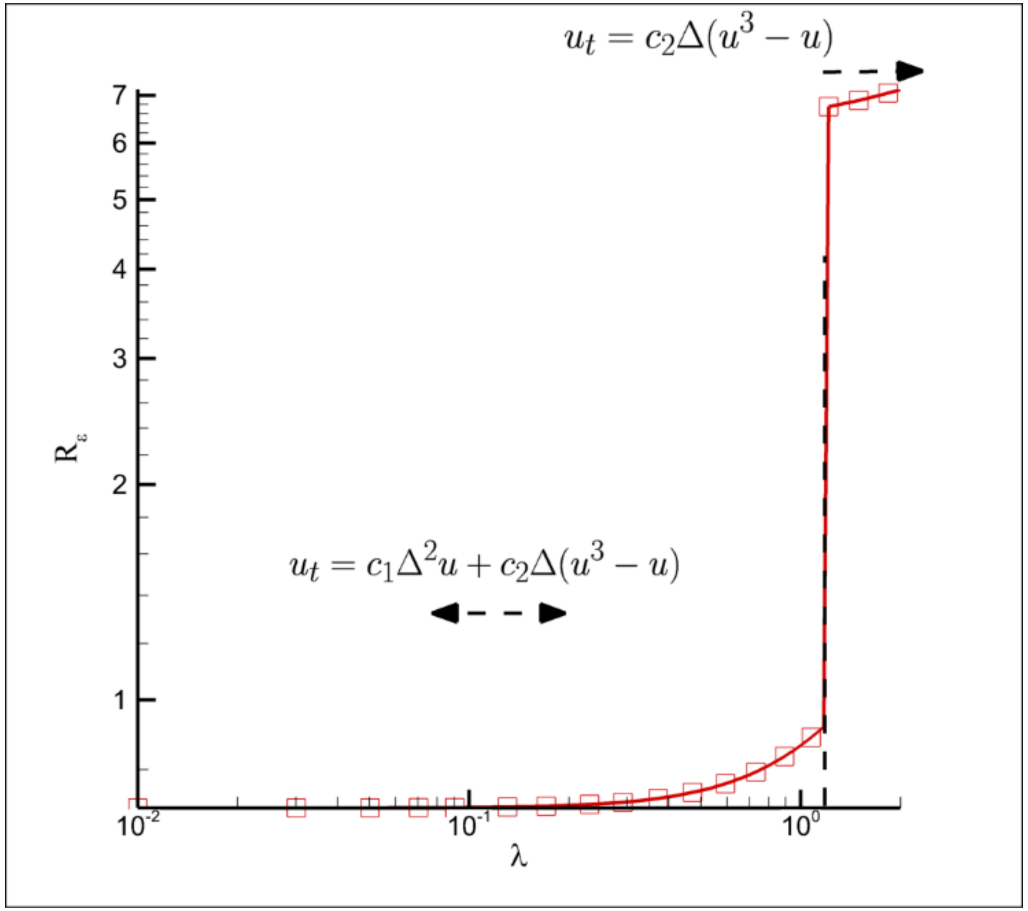

Training data set: 200
Testing data set: 200

Relative error – C-H equation

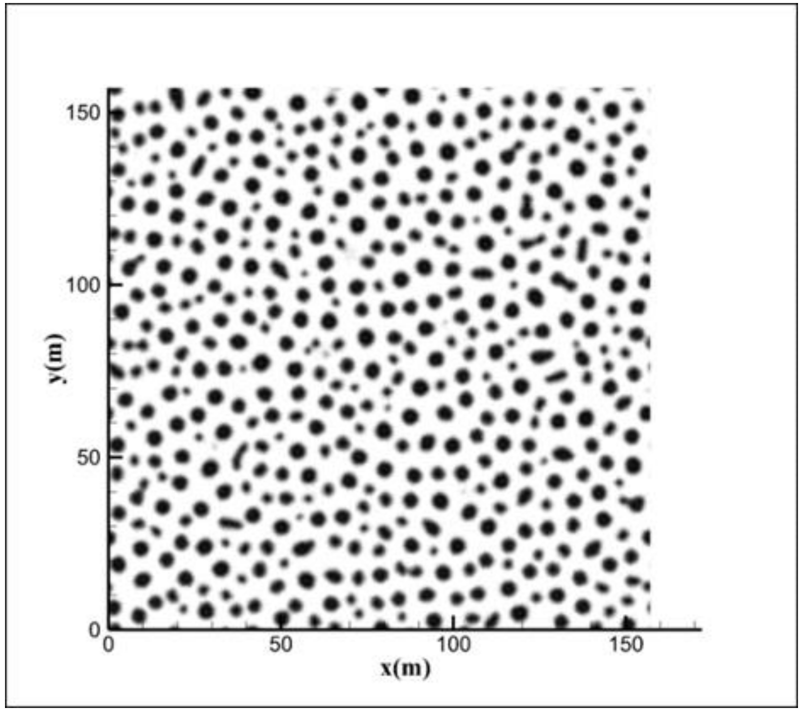

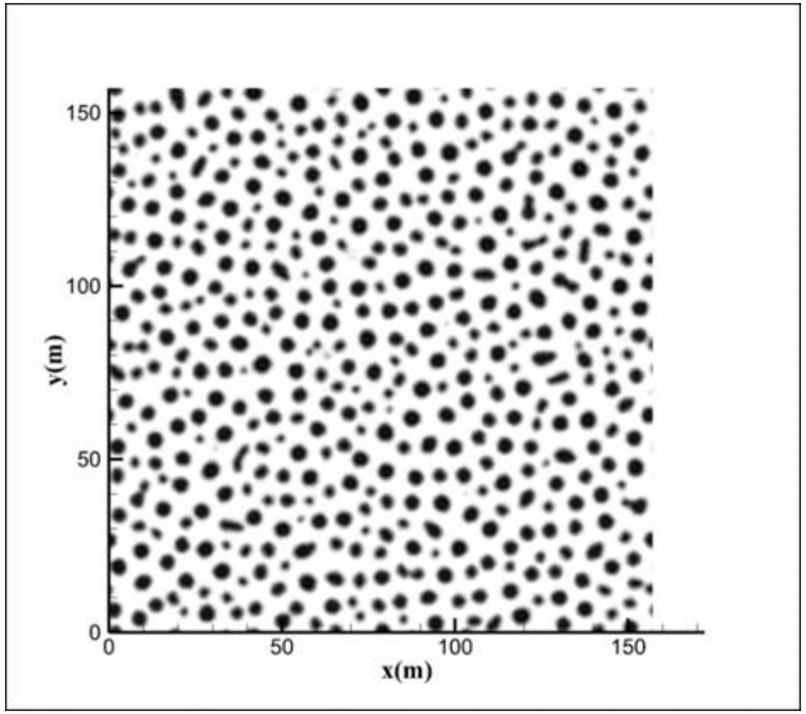

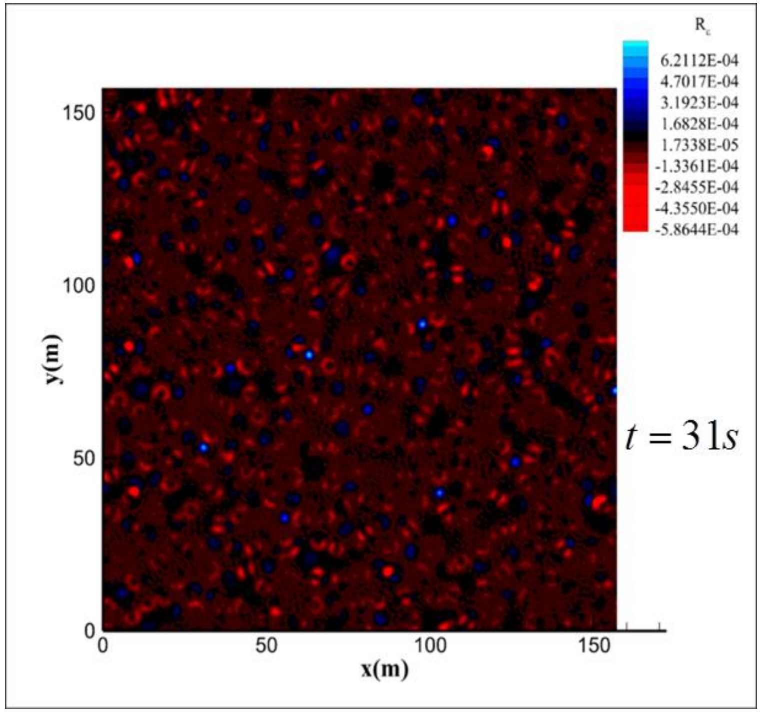

Ground truth coefficients

Recovered coefficients
- % 50 noise

Relative error

Data manipulation

- Data reduction/compression
- Data smoothing
- Data enhancing
- Interpolation
- Regression
- Digital image correlation

Madenci et al. , 2022, “Peridynamics for data estimation, image compression/recovery and model reduction,” Journal of Peridynamics and Nonlocal Modeling, Vol. 4, pp. 159-200

Data reduction/compression

262,144 pixels

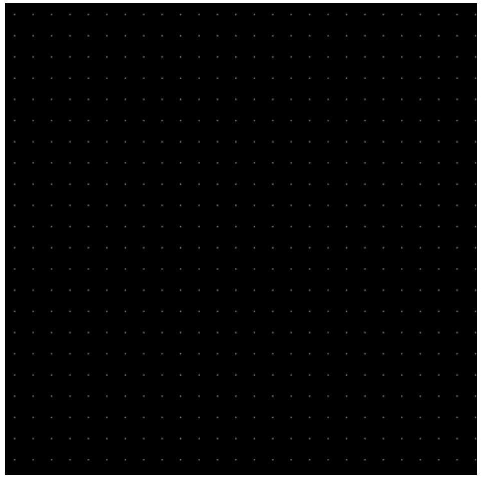

572 pixels

118,518 pixels

Recovered pixels
(error of 9.07%)

Recovered pixels
(error of 0.88%)

Data smoothing

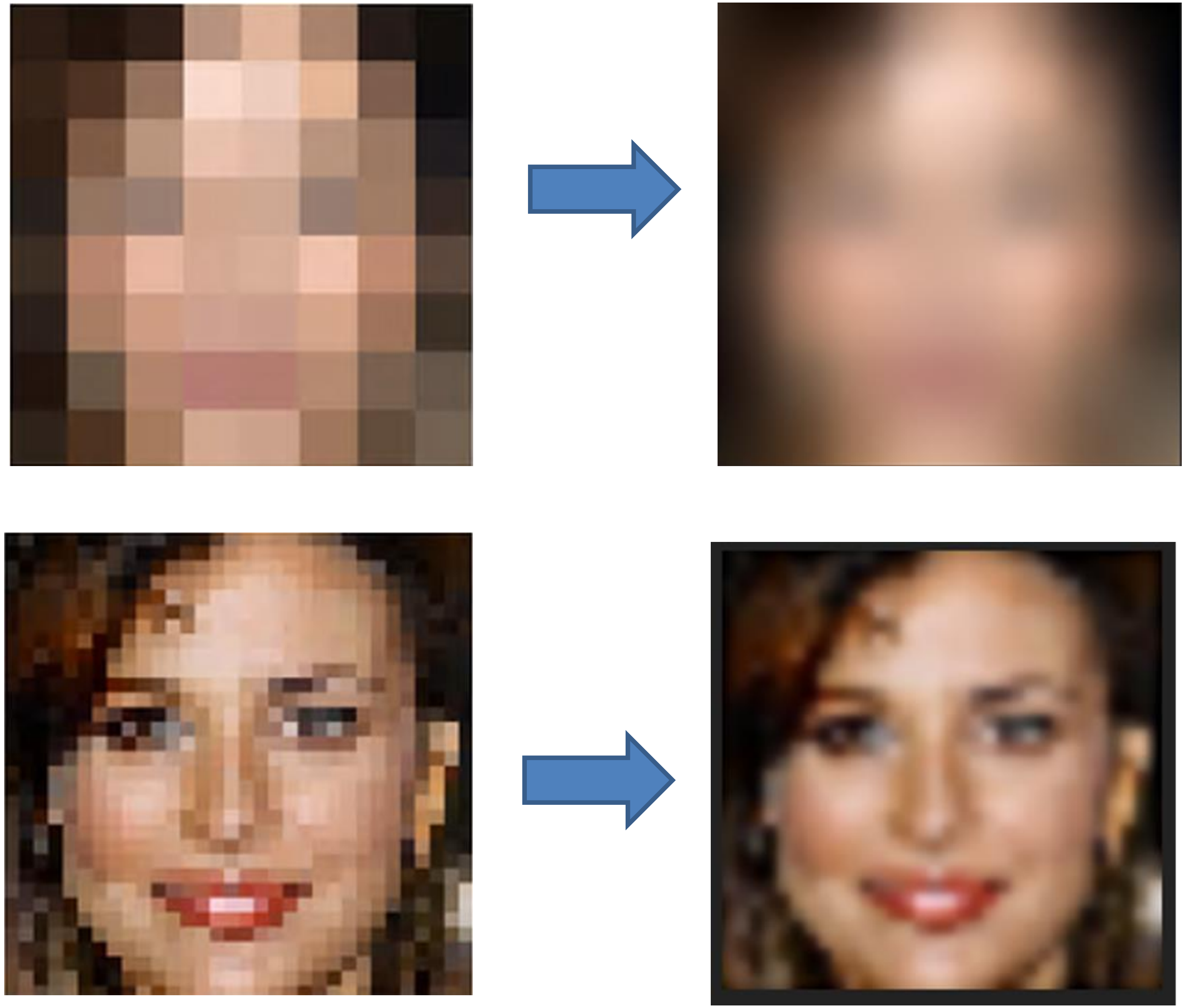

Data enhancing

Original image @ t=0	Enhanced image @ t=100s	Enhanced image @ t=200s
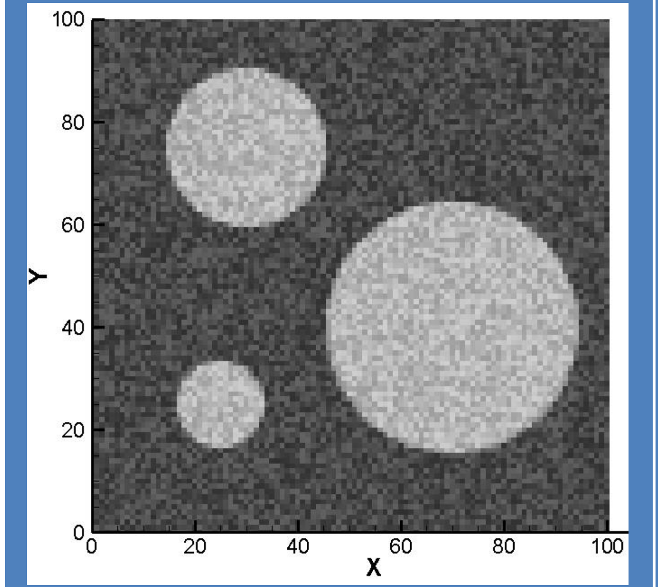	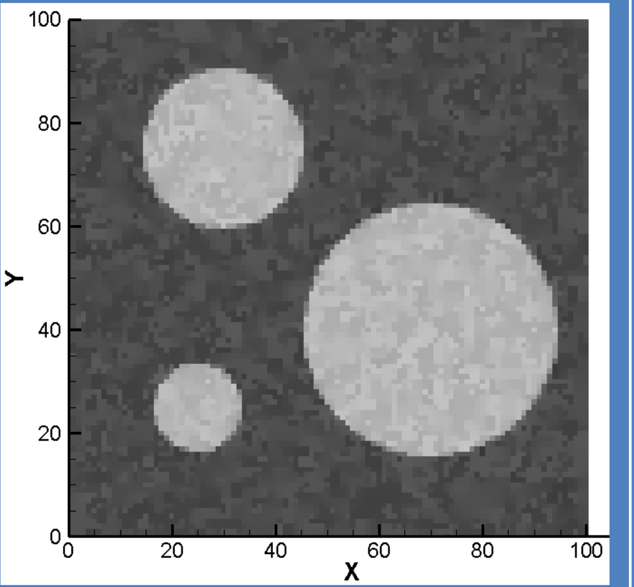	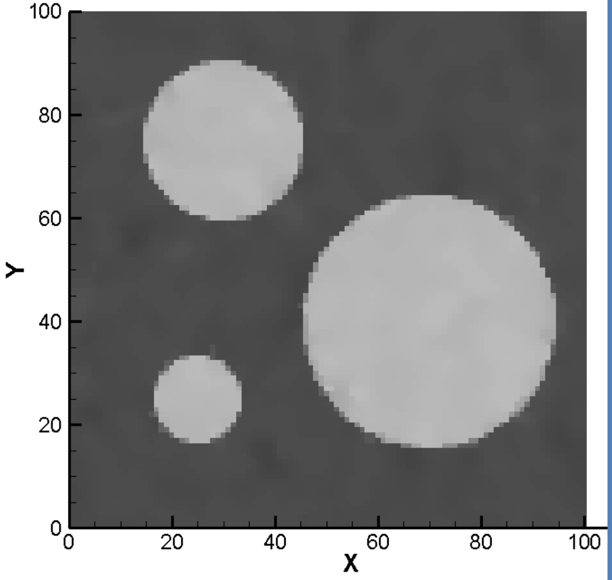

Image processing -DIC

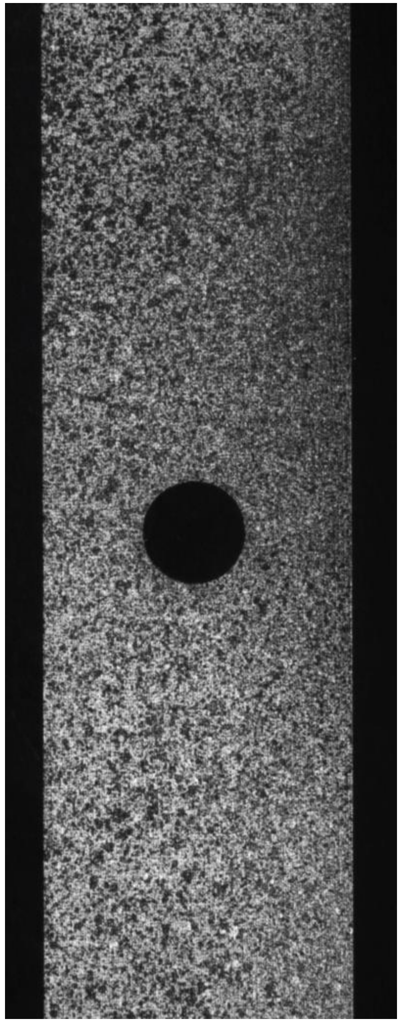

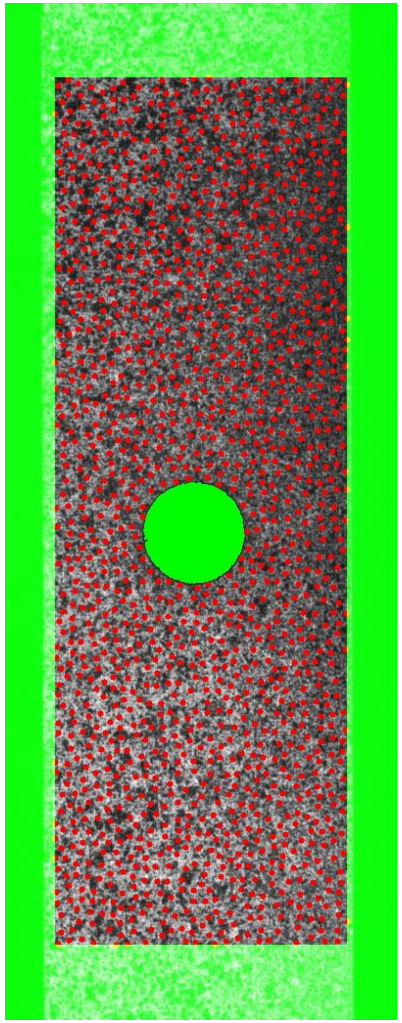

- **DIC Challenge – Sample 12**
  - Experimental Images
    - Bottom constrained, top pulled.
  - Contrast: Good
  - Noise: Low
  - Shift: N/A
  - Time steps (Images): 12
- Tracked points were picked in the following ranges:
  - X : (50, 350)
  - Y : (75, 965)
- Also, a point at (190, 540) was picked to mask the hole.

- Total Points: **1481**
- Minimum Inter-Point Spacing: **10 px**
- The area outside of the tracked points was masked.

Original Images courtesy of The Society for Experimental Mechanics

Madenci et al., 2022, "Peridynamics Enabled Digital Image Correlation for Tracking Crack Paths," Engineering with Computers, https://doi.org/10.1007/s00366-021-01592-4

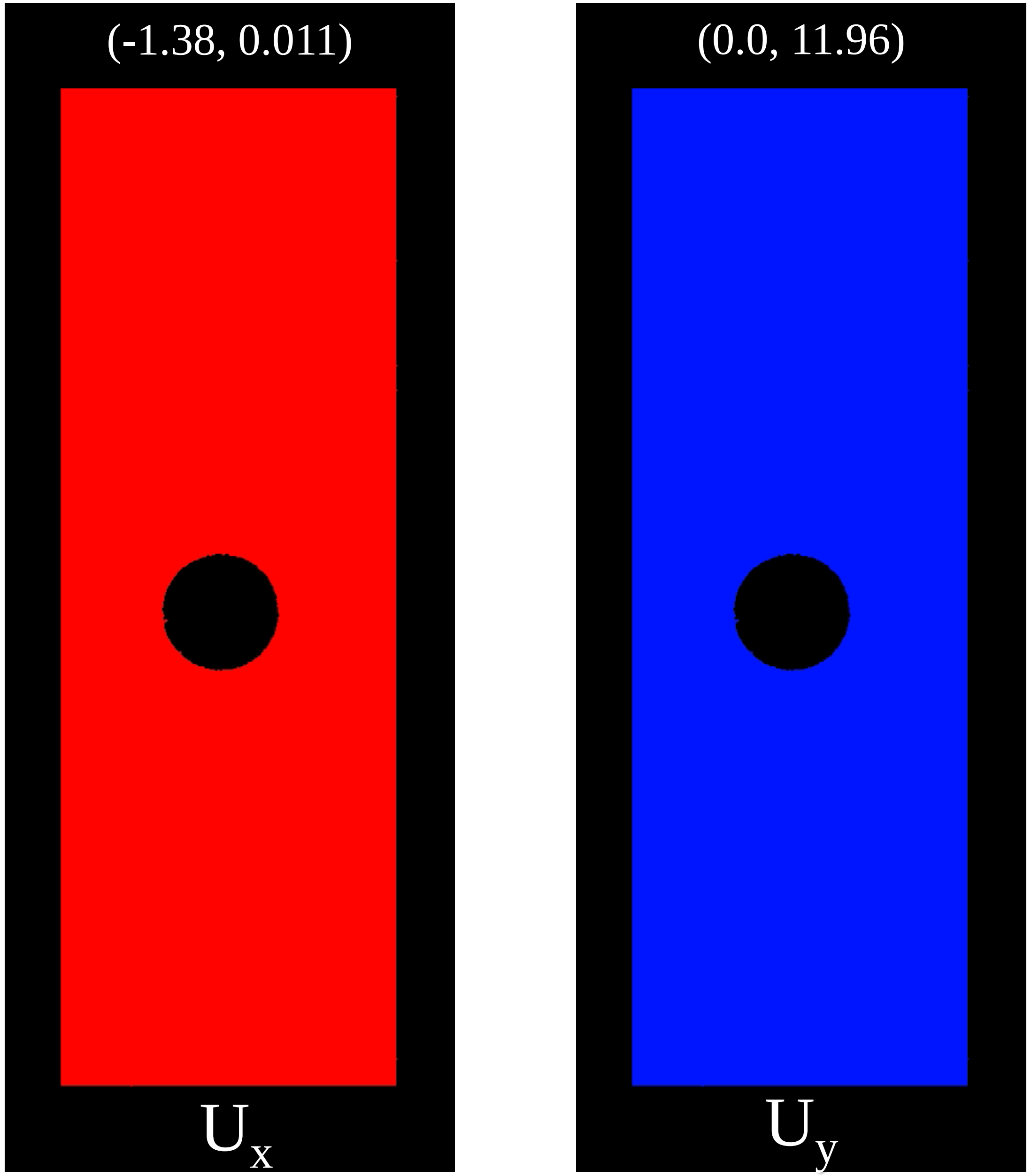
(-1.38, 0.011)
(0.0, 11.96)
U_x
U_y

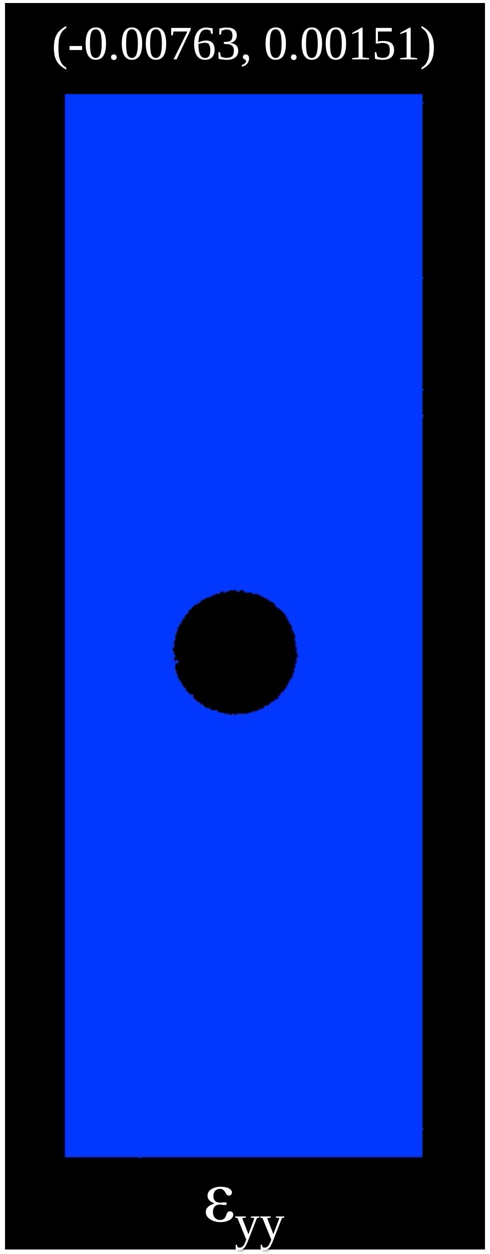

Normal strain – y-direction

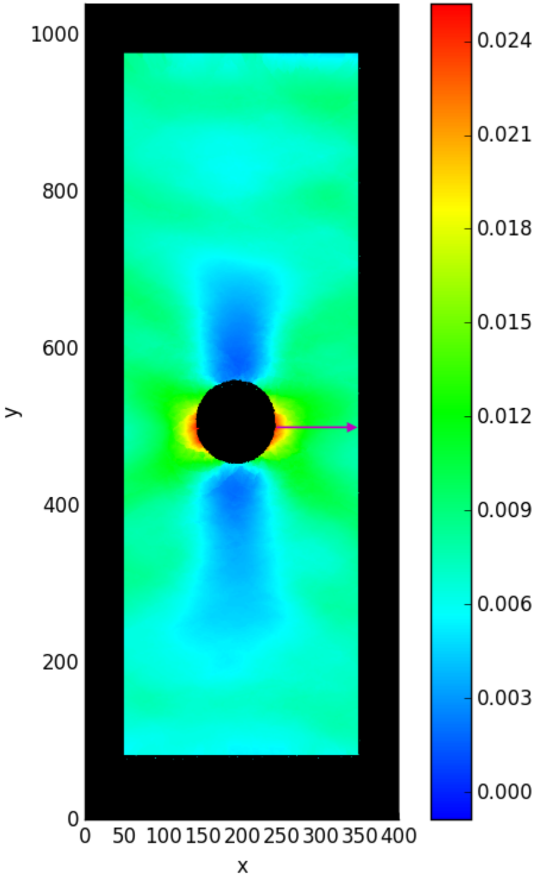

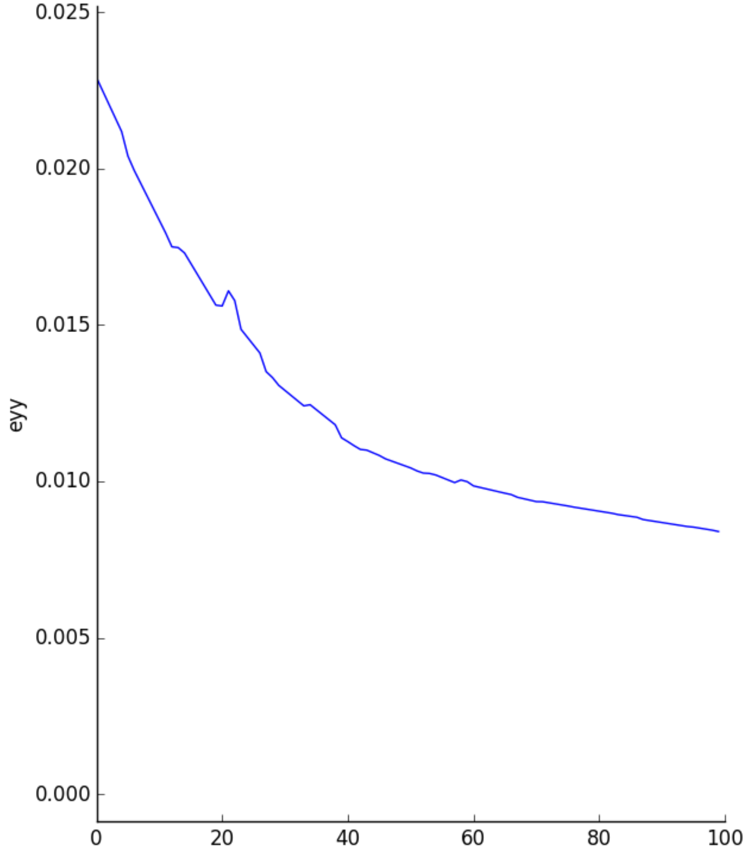

PD-DIC for tracking discontinuous paths

Images of deforming specimen

Track randomly picked points

PDDO for displacement and strain fields

PDDO for strain compatibility parameter

Calculate damage certainty using probability density function

Apply regression model, MARS to damage certainty to obtain crack path

$$s = \frac{\partial^2 \varepsilon_x}{\partial y^2} + \frac{\partial^2 \varepsilon_y}{\partial x^2} - 2\frac{\partial^2 \varepsilon_{xy}}{\partial x \partial y} \begin{cases} = 0 & \text{Medium is continuous} \\ \neq 0 & \text{Medium is discontinuous} \end{cases}$$

PD-DIC for crack detection

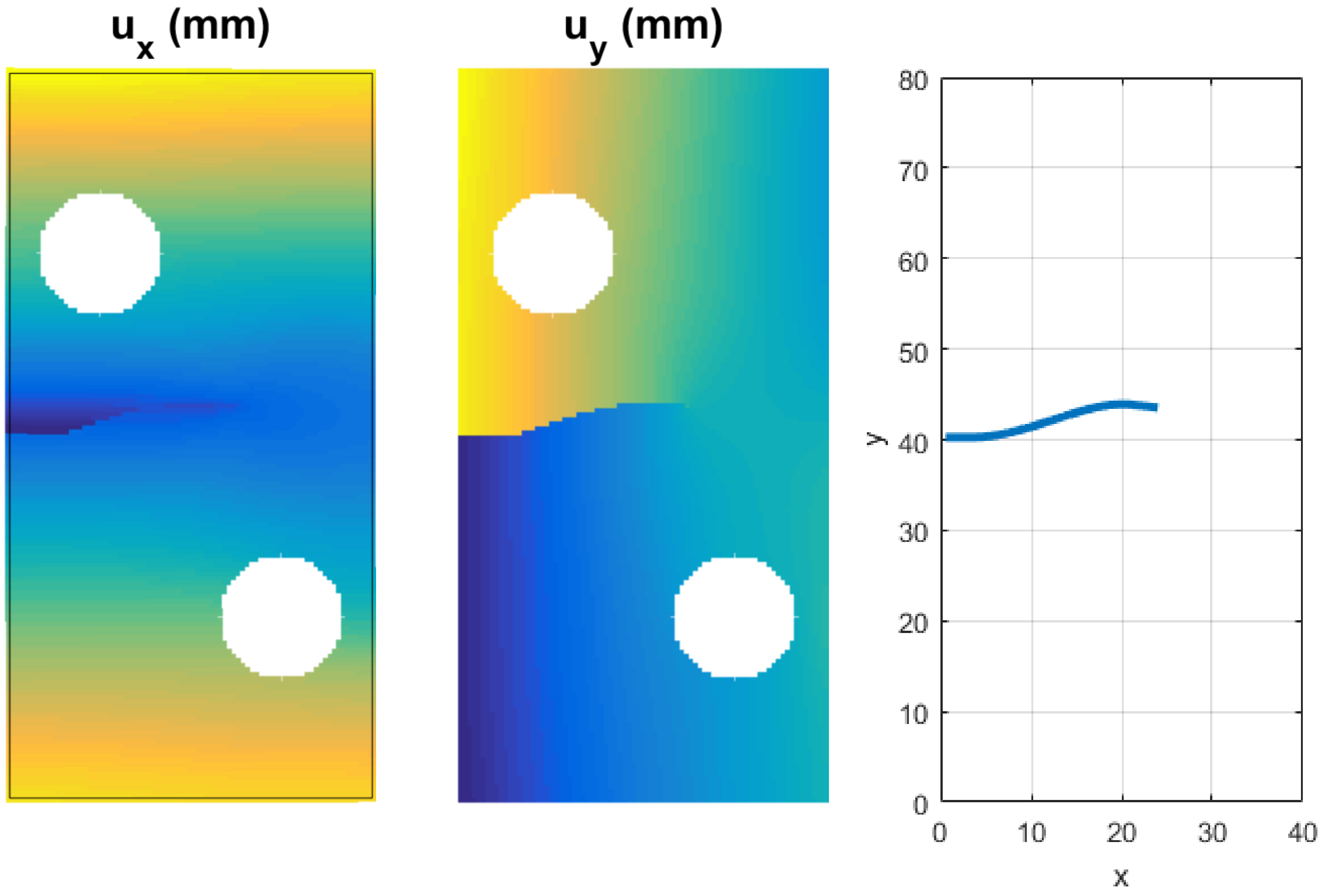

Detected Crack using PD-DIC

PD-DIC for slip band detection

Images from Nickel-based Superalloy 718

Frame 1 u_x

Frame 2 u_y

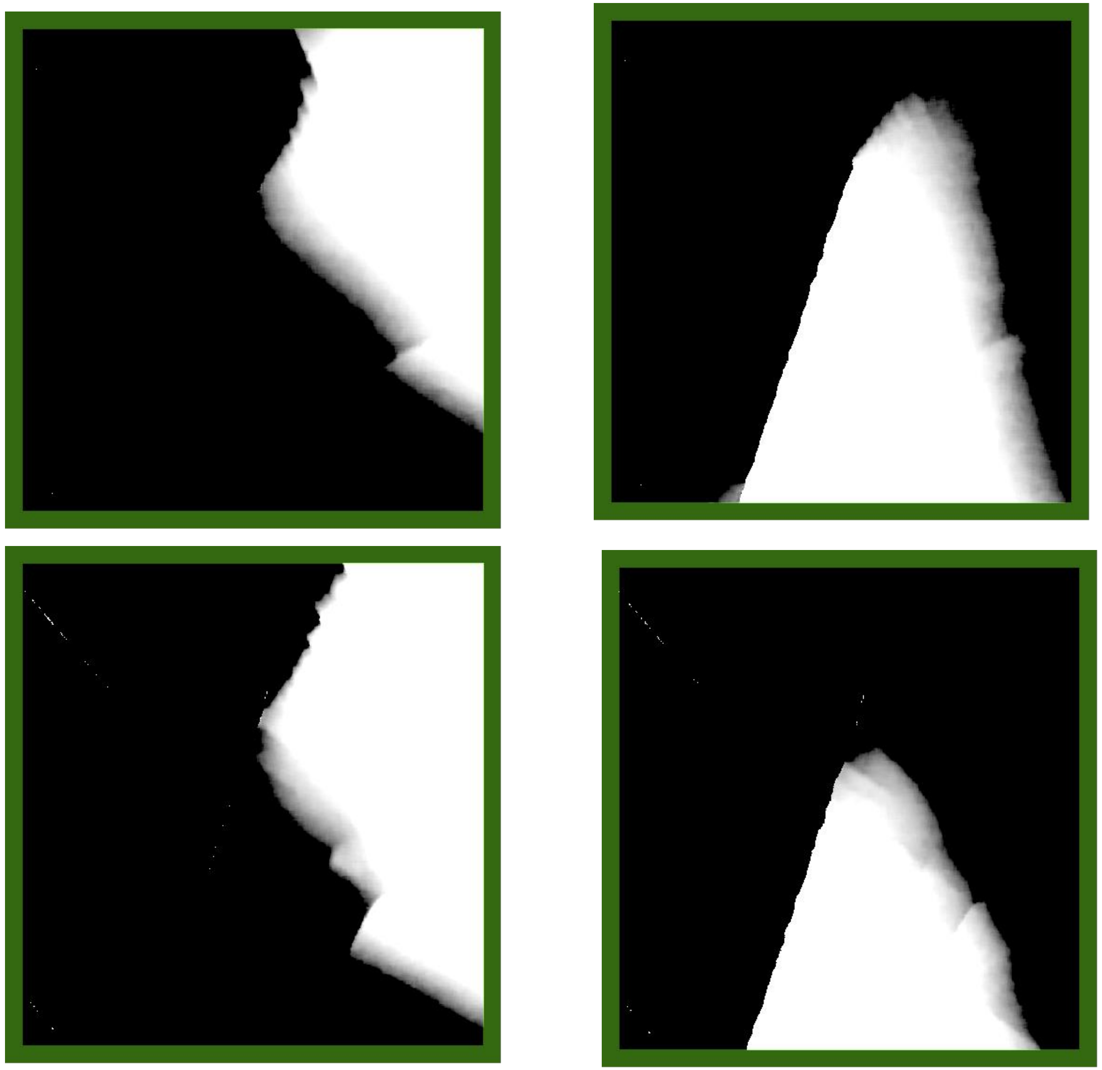

PD-DIC displacement construction from images

Frame 1 u_x

Frame 2 u_y

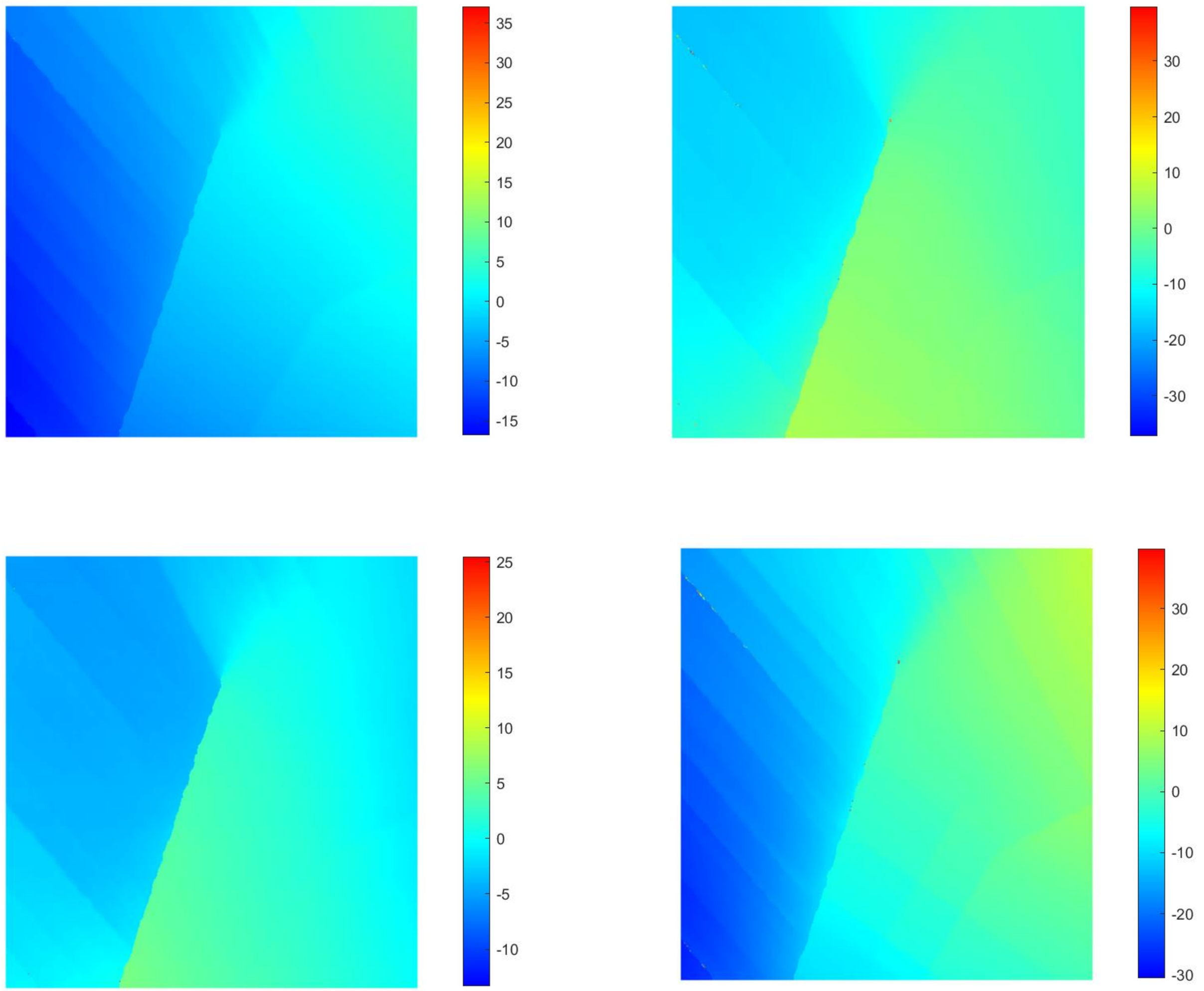

PD-DIC strain field evaluation

Frame 1

Frame 2

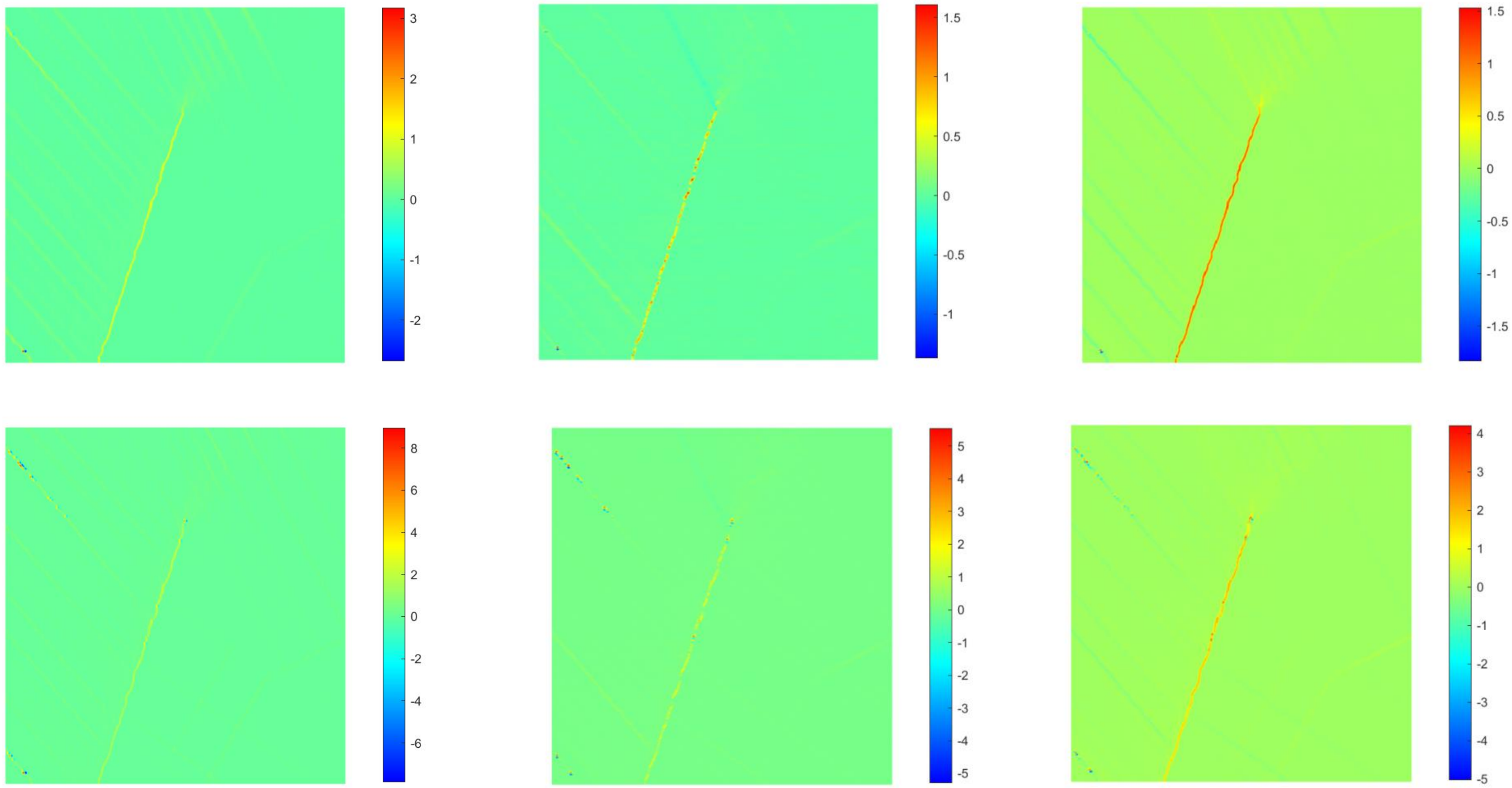

ε_{xx} ε_{yy} ε_{xy}

PD-DIC slip band detection

Frame 1

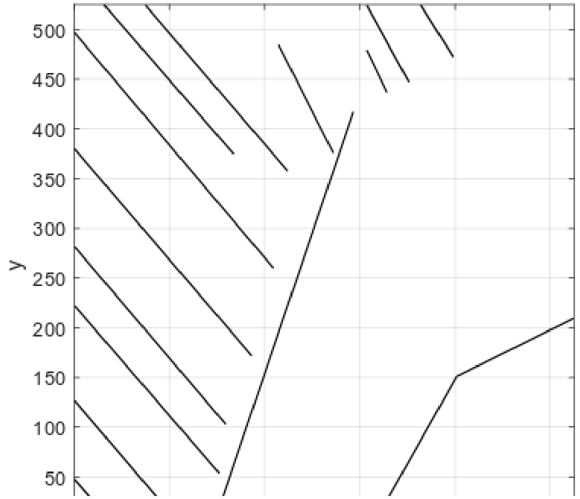

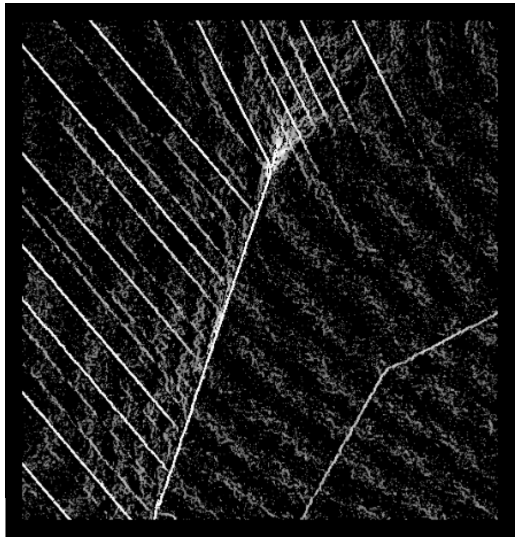

Frame 2

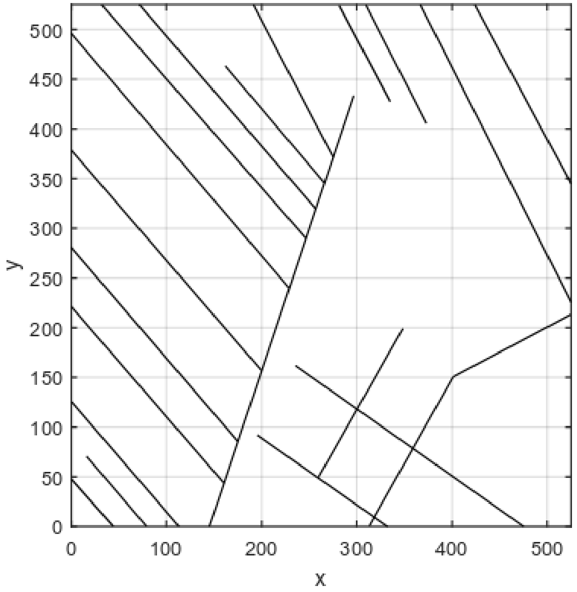

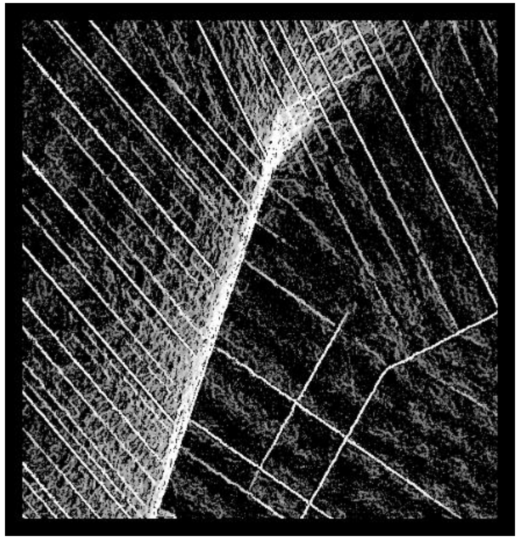

Heaviside DIC

Unlike Heaviside DIC, it provides the specific location of each slip band with beginning and end points.

Final remarks

- The nonlocal Peridynamic Differential Operator (PDDO):
  - allows for accurate solution of field equations in the presence of discontinuities
  - enables upwinding in a natural way through a weight function
  - handles discontinuities without any special treatments in a natural manner
  - enables the evaluation of derivatives of any order in a multi-dimensional space
  - captures cracking as part of the solution
  - size effect in multi-scale material design
  - provides a unified approach to transferring information within a set of discrete data and among data sets.